

---

## SUPPORTING INFORMATION: UNRAVELING THE MOLECULAR MAGIC: AI EXPLAINS THE FORMATION OF THE MOST STRETCHABLE HYDROGEL

---

**Shahriar Hojjati Emmami**

Department of Biomedical Engineering  
Amirkabir University of Technology

**Ali Pilehvar Meibody**

Department of Applied Science and Technology  
Polytechnic University of Turin

**Lobat Tayebi**

Department of Developmental  
Sciences  
Marquette University

**Mohammadamin Tavakoli**

Department of Computing and  
Mathematical Sciences  
California Institute of Technology

**Pierre Baldi**

Department of Computer Science  
University of California, Irvine

### S1 Classification of Hydrogels

An alternative conceptualization of hydrogels underscores their capacity for absorbing water and retaining a substantial portion thereof within their structure, without undergoing dissolution in aqueous environments[1]. The primary limitation of hydrogels derived from a single polymer resides in their suboptimal mechanical performance and extensibility. For instance, when an alginate hydrogel is stretched to approximately 1.2 times its original length, it is susceptible to rupture[1]. Hydrogel classification ( see Fig. 1 based on specific attributes has been made feasible by introducing interpenetrating polymer network (IPN) hydrogels and other strategies aimed at augmenting their mechanical characteristics. Hydrogels, as the name suggests, are composed of a singular monomer unit forming a network, and these networks can be structured in various configurations. Consequently, hydrogels can be dichotomized into two categories predicated on the chemical or physical nature of their crosslink junctions. Chemically crosslinked networks possess enduring junctions, whereas physical networks feature transient junctions stemming from phenomena such as polymer chain entanglements or physical interactions, including ionic interactions, hydrogen bonds, or hydrophobic interactions[2]. Hydrogels can be further classified into three categories based on their polymeric composition[3]. Their preparation method yields several notable classes of hydrogels: (a) Homopolymeric hydrogels, constituted by polymer networks derived from a single monomer species, serve as the fundamental structural unit of any polymer network[4]. Depending on the monomer's inherent characteristics and the polymerization technique employed, homopolymers may exhibit a crosslinked skeletal structure. (b) Co-polymeric hydrogels encompass two or more distinct monomer species, at least one of which is hydrophilic, arranged in a random, block, or alternating configuration along the polymer network chain[5]. (c) Interpenetrating Polymeric Hydrogel (IPN), a pivotal category of hydrogels, involves two distinct crosslinked synthetic and/or natural polymer components coexisting within a network structure[6]. This approach is used to have multiple functions instead of using one network with one property.

In semi-IPN hydrogels, one component is crosslinked, while the other remains non-crosslinked. In hydrogel synthesis, the entrapment of a linear polymer in a matrix can yield a semi-interpenetrating network (IPN) hydrogel, which subsequently can be transformed into a fully IPN hydrogel by selectively crosslinking the linear polymer chains[7]. IPN represents a versatile polymer system amenable to various classifications[8]. Depending on the synthesis chemistry employed, IPN hydrogels can be categorized as (a) Simultaneous IPN, in which both networks' precursors are mixed and independently synthesized through non-interfering pathways such as chain and stepwise polymerization[9, 10, 11]. (b) Sequential IPN, in which a single-network hydrogel swells within a solution that contains a mixture of monomers, initiators, and activators, either with or without a crosslinker. (c) The presence of crosslinker results in a full IPN, while its absence leads to a network featuring linear polymers embedded within the primary network (semi-IPN)[9, 10, 12].

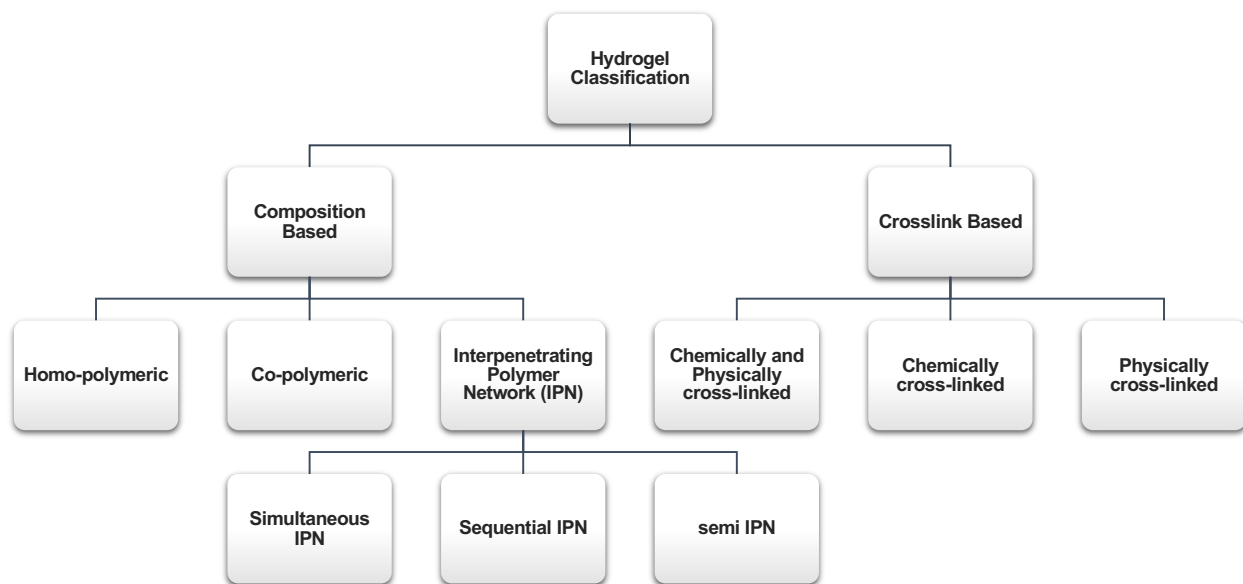


Figure 1: Hydrogel classification based on composition and crosslink nature.

Despite their numerous advantages and improvements in mechanical properties, hydrogels are recognized for their limited stretchability and mechanical strength, constraining their application range. When an IPN network is prepared, it can possess two chemical crosslinks, one of which acts as a sacrificial bond, or two independent crosslinks, one of which is physical and capable of reversibility. This article introduces novel methodologies for fabricating ultra-stretchable hydrogels incorporating linear polymer chains into polymeric networks. To attain heightened mechanical performance and stretchability, our objective is to harness the attributes of linear chains within a polymeric network, thereby achieving an unprecedented level of stretchability.

## S2 AI for Reaction Prediction

### S2.1 Radical Reaction Predictor

For all experiments, we use a specific version of the radical reaction predictor introduced in [13]. We use the contrastive learning model presented in [13] with an atomic descriptor of length one. This model is trained on the entire dataset of RMechDB [14]. Even though the RMechDB dataset is dominated by atmospheric data, the reaction predictor is highly generalizable to other radical domains such as polymerization.

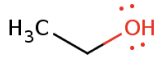
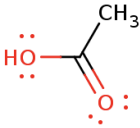
We follow the exact procedure of pathway search described in [13], with the use of different starting materials, branching factors (also referred to as selection factors), depth, and reaction contexts. The selection of these parameters is described in the following sections.

### S2.2 How to Use RMechRP

The Radical Mechanistic Reaction Predictor (RMechRP) is a web-based platform accessible at <https://deepchem.ics.uci.edu/rmechrp/>, designed for the prediction and mechanistic interpretation of radical-mediated reactions. The interface provides two major functionalities: (i) single-step prediction, and (ii) pathway prediction. In the single-step prediction mode, users can predict the outcome and mechanism of an individual radical reaction. As shown in Fig. 2, users may enter the reactants (in this example ethanol and acetic acid) and reaction conditions directly into the web interface. Upon submission, the trained AI models identify potential reactive sites and rank all feasible reactions according to their predicted likelihood. Input reactants are provided in SMILES format, and reaction conditions can be selected from common solvents such as water, acetic acid, and others. Additional parameters allow users to define

RMechRP
Documentation
RMechRP Article
Contact Us

Single Step Predictor

Enter SMILES string of the reactants:\*

Parameters:

298K - Water
Select the reaction conditions.

5
Specify the number of reactive atoms to be considered for the reaction.

0.5
Only atoms with score above this number will be considered as reactive atoms.

20
Number of reactions to be displayed.

Drfp
The model for the ranker.

Predict

Figure 2: Single-step prediction interface of the RMechRP webserver. Users can enter reactants in SMILES format, specify reaction conditions and parameters, and obtain ranked predictions of plausible radical reaction products.

the number of reactive atoms to be considered, the minimum reactivity score threshold (only atoms above this score are treated as reactive), and the number of reactions to be displayed in the output. Furthermore, users may select between two ranking models, DRFP or RxnFP, to prioritize predicted reactions based on molecular fingerprints. Once the prediction is initiated, the interface returns a ranked list of plausible reaction products and their corresponding mechanistic rationales.

### S2.3 Pathway Prediction

In the pathway prediction mode, users can predict complete mechanistic pathways starting from specific reactants and proceeding toward target molecules. As illustrated in Fig. 2, this mode requires inputting the reactants and target molecules (as SMILES strings or molecular masses separated by commas), along with the desired reaction conditions. Several additional parameters are available to control the search process, including the reaction depth (extent of pathway expansion), branching factor (number of reactions considered at each level), minimum reaction score for pathway inclusion, and the reaction context, such as the solvent or medium (e.g., water, acetic acid, etc.). Users can further constrain the model to specific reaction types (for instance, all reactions or only radical reactions) and optionally enforce chemical rule-based filters. After submission, the AI model performs an iterative, constrained search to identify feasible mechanistic routes from reactants to the target molecule. Additional details on the model architecture, training procedure, and computational framework are provided in Tavakoli *et al.* [13].

[RMechRP](#)
[Documentation](#)
[RMechRP Article](#)
[Contact Us](#)

Radical Pathway Search

Enter in the reactant and target molecules with reaction conditions below. On submission, trained reaction prediction models will perform a constrained search for the target molecule starting from the reactants. Please note that the maximum runtime for the pathway search is 15 minutes.

Reactants:\*

Target molecules (a list of SMILES strings or masses, separated by commas):\*

Reaction context

Parameters:

3

How deep the search tree must be expanded.

5

How many reactions must be considered at each level.

298K - Water

Reactions condition.

-20.0

Minimum score of a reaction to be considered in the pathway expansion.

All

The type of reactions for each prediction.

Yes

Chemistry rules applied to the list of products.

Predict

Figure 3: Pathway prediction interface of the RMechRP webserver. Users can enter reactants and target molecules, specify reaction conditions and search parameters, and obtain automatically generated mechanistic pathways from reactants to the target molecule.

### S3 Pre-setting Before Run

Before starting the experimental procedures as elucidated in the methodology section, it is imperative to establish certain requisite settings. These settings, crucial to the experiment’s accurate execution, pertain predominantly to the reactants, serving as the fundamental core of the pre-setting parameters. The first important parameter is the reactants, which must be adjusted before being run. Subsequently, these reactants have the potential to engage in chemical reactions with one another. However, it becomes imperative to ascertain the depth to which these reactions are pursued. The question arises: how profound an exploration of the reaction depths should be undertaken? Moreover, within each depth, the reactants can undergo multifarious reactions, prompting the need to discern and prioritize the most probable products—a facet encapsulated within the ambit of selectivity. It is also essential to underscore the context parameters’ significance. The term “context” denotes the specific composition that must be incorporated into each reaction or the depth to which such a composition should extend. The final data format is presented in SMILE notation, characterized by distinct paragraphs delineating the possible products. Each paragraph signifies the distinct number of reactions required to yield these products. Certain paragraphs may exhibit duplications, which have been eliminated to enhance clarity and comprehensibility. In light of the above considerations, it becomes evident that the pre-setting parameters, encompassing reactants, depth, selectivity at various depths, and context, play an indispensable role in shaping the experimentation course. The ensuing sections explore two pivotal questions that merit elucidation: The first query asks whether the monomer should serve exclusively as a reactant or whether it can also be reintroduced into the reaction

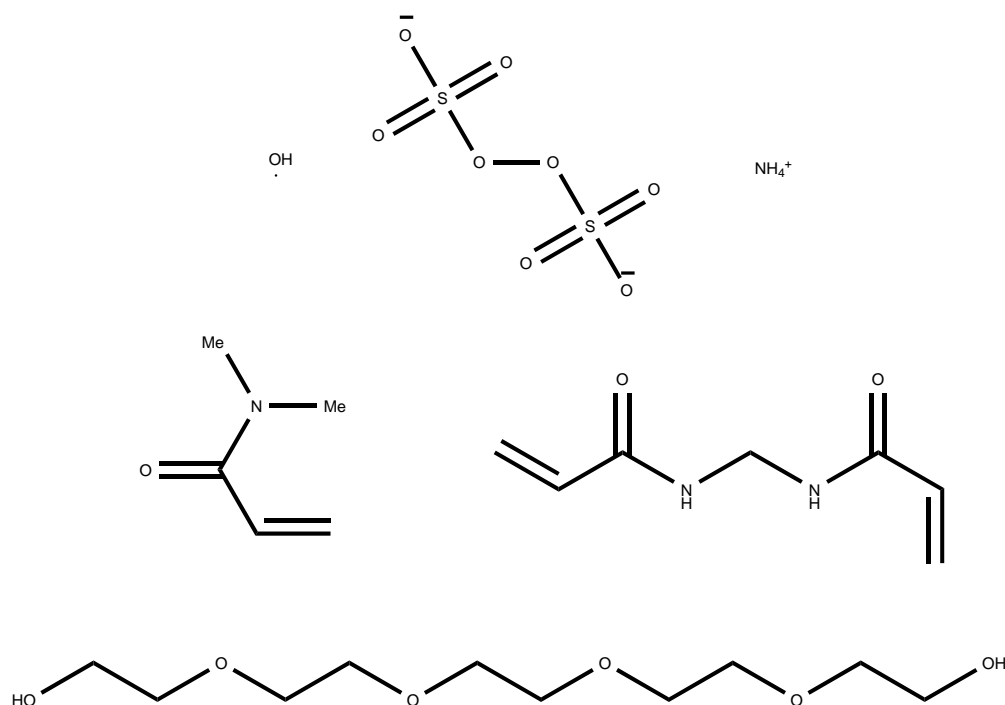


Figure 4: The initial reactants, comprising Hydroxyl Radical, Ammonium Persulfate, N, N- Dimethylacrylamide, N, N'-Methylenebisacrylamide, and a limited quantity of Polyethylene Oxide (constrained to five units due to system limitations). The study encompasses three iterative depths, evaluating all predicted products and highlighting the eight most promising reactions for further consideration.

as part of the context, thereby mirroring real-world scenarios. The second inquiry addresses the role of water in the experimental framework—specifically, whether it should be considered as a reactant or, conversely, as part of the contextual parameters.

### S3.1 Effect of Adding Monomer as Context

We conducted two experimental runs employing N, N-dimethylacrylamide, N, N'- Methylenebisacrylamide, and ammonium persulfate as our primary reactants, each explored to a depth of three levels with a selectivity factor of eight, as illustrated in Fig. 4. Both runs share a commonality in their initial step, where a monomer serves as the first reactant. However, the key distinction between these two runs lies in their context parameter. In the first run, the monomer is not added back, whereas in the second run, the monomer is added back to the next two levels. In practical, real-world experimentation, a system comprises a multitude of monomers. In such a scenario, radical attacks are not limited to a single monomer; rather, they propagate the chain by incorporating other monomers. However, in our experimental context, the absence of an additional monomer leads to a unique situation where only the initial monomer undergoes activation, as depicted in the accompanying figure. Due to the absence of additional monomers, this monomer rearranges itself to maximize the use of its radical electrons.

#### S3.1.1 Monomer as Reactant

In the first run, we conducted experiments using the aforementioned set of reactants without adding the monomer back at each depth. Among the numerous reactions performed, we have selected and investigated the most significant ones, as elaborated in Figures 5-8.

#### S3.1.2 Monomer as Reactant and Context

As established in the preceding section, it is evident that following the initiation step, in which the initiator radical interacts with the monomer, the chain's subsequent growth depends on re-adding the monomer to the system. This phenomenon is commonly referred to as the system's "context setting." In the present scenario, all experimental parameters remain consistent with those elucidated in the previous section, except for one crucial distinction—monomer

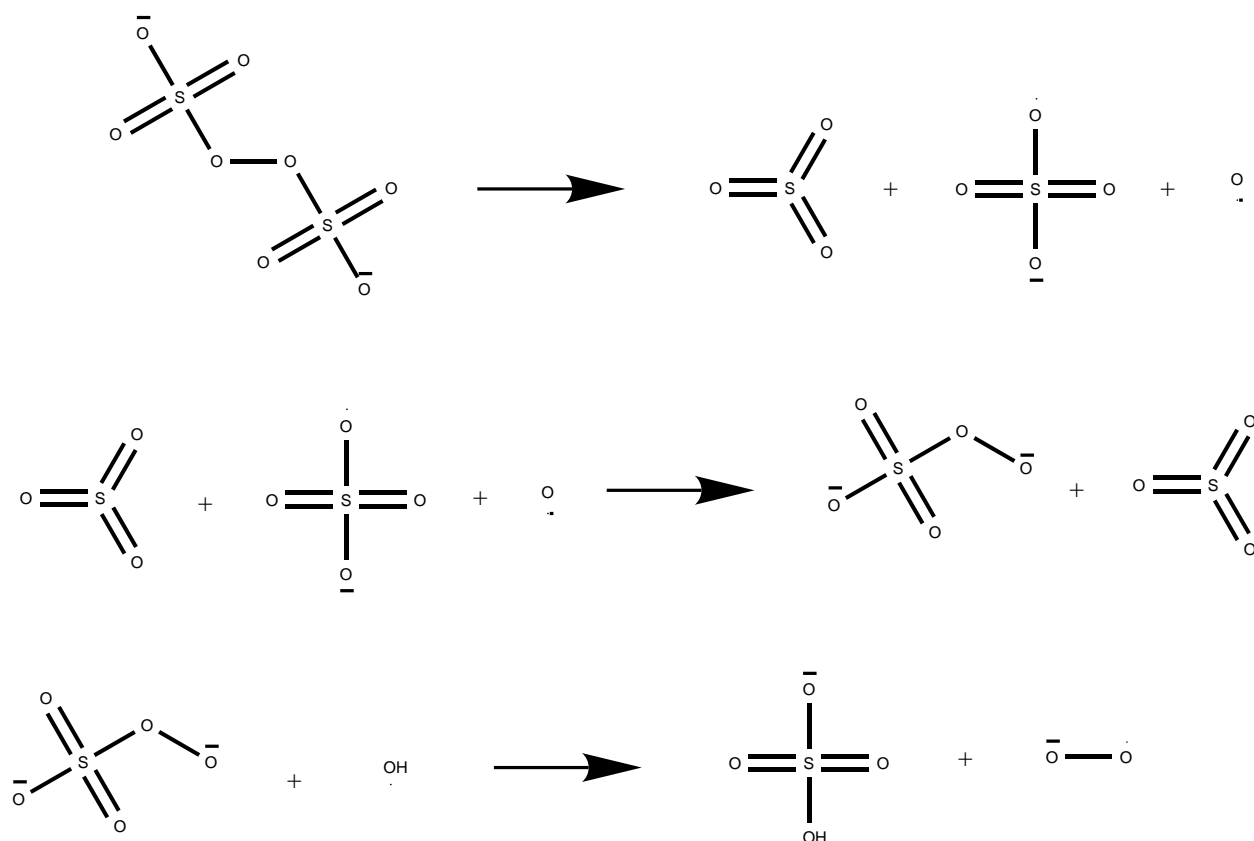


Figure 5: In cases like the one illustrated in this prediction pathway, the initial decomposition of Ammonium Persulfate leads to the formation of reactive intermediates. Due to their high reactivity, these intermediates subsequently engage with other species, ultimately giving rise to stable initiator radicals. Such pathways are potentially applicable across a broad spectrum of systems.

reintegration as a contextual element. Under these conditions, it becomes apparent that the activation of one monomer can facilitate the addition of another monomer, thereby providing the necessary substrate for chain growth, as depicted below. Among the myriad reactions predicted by the system, we have selected specific cases for detailed examination, as illustrated in Figures 9-11. These selected cases are intended to offer a deeper understanding of the system's functionality and the impact of certain factors on presetting parameters. Consequently, to emulate real-world conditions more faithfully, we have opted to utilize the monomer as both a reactant and a context parameter.

### S3.2 Water Condition

We conducted a total of three experimental runs, each encompassing three levels of depth and exhibiting a selectivity factor of 8. The reactants employed remained consistent with those presented in Fig. 4. In the first run, the reactants remained unchanged; notably, water was not included as part of the reactant composition, but rather, it was used as a contextual element, as illustrated in Fig. 12. The second run introduced water as a reactant without subsequent reintegration, as depicted in Fig. 13. The final run also incorporated water as a reactant, but it was re-added as a contextual component, as visualized in Fig. 14. Building on the insights gained from the preceding section, which considered the results of reintroducing monomers in all cases, we have thoroughly analyzed these three scenarios and their corresponding reactions. This meticulous examination found that there exist no significant discernible differences among these cases. Consequently, we have decided to include water as a reactant in the main and final runs, omitting the re-addition of water as a reactant for the sake of computational efficiency.

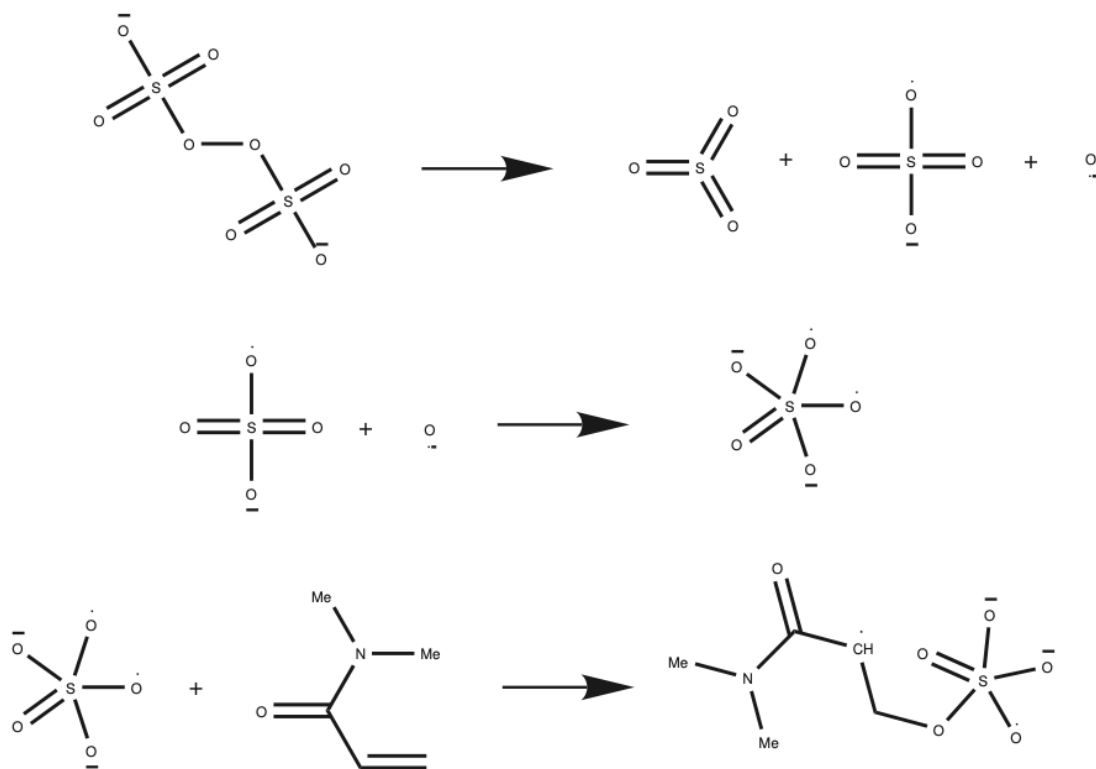


Figure 6: In an alternate scenario, Ammonium Persulfate may undergo decomposition, resulting in the generation of radicals. After a rearrangement process leading to the formation of a stable radical species, the desired radical may initiate a reaction with a monomer. This activation process readies the monomer for subsequent steps in the reaction sequence.

## S4 Main Run

Following the determination of the pre-run setting parameters, it has been unequivocally established that the context parameter bears significant importance. In this regard, it has become evident that the monomer must be added back as a context parameter at each depth, thus playing a crucial role in the system setup. Furthermore, it has been ascertained that water, when used as a contextual element, does not exert any discernible effects on the predictor outcomes. For the primary run, conducted with these established parameters, our initial inquiry focuses on the initiation step: specifically, the decomposition of APS (ammonium persulfate). Within this context, our primary objective is to explore the various reactions that the modeling system can predict. This entails selecting the most plausible radicals produced during the decomposition of ammonium persulfate in conjunction with our primary reactants: namely, the monomer and crosslinkers. Such an approach enables us to deduce the most probable final molecular structures. It is important that our investigation of the decomposition process incorporates two scenarios: one in the presence of water within the reactants and another without water. This comparative analysis underscores the significance of water's inclusion in these reactions, shedding light on its potential impact.

### S4.1 Decomposition of APS

#### S4.1.1 Decomposition of APS with Water

The decomposition of APS, as documented in the existing literature, remains somewhat opaque, with certain products such as sulfate radical anion[15, 16], hydroxyl radical[17], hydroxyl ion[18], Peroxymonosulfate[19], bisulfate[20, 21] and superoxide anion[22] being reported. In certain instances, various products are documented across different sources, yet it remains elusive precisely how this initiator's activation of monomer molecules initiates and catalyzes growth. Our first step, which constitutes the initiation phase, employed an artificial intelligence predictor to predict APS decomposition, as visually depicted in Figures 15-26. The experimental parameters used ammonium persulfate and

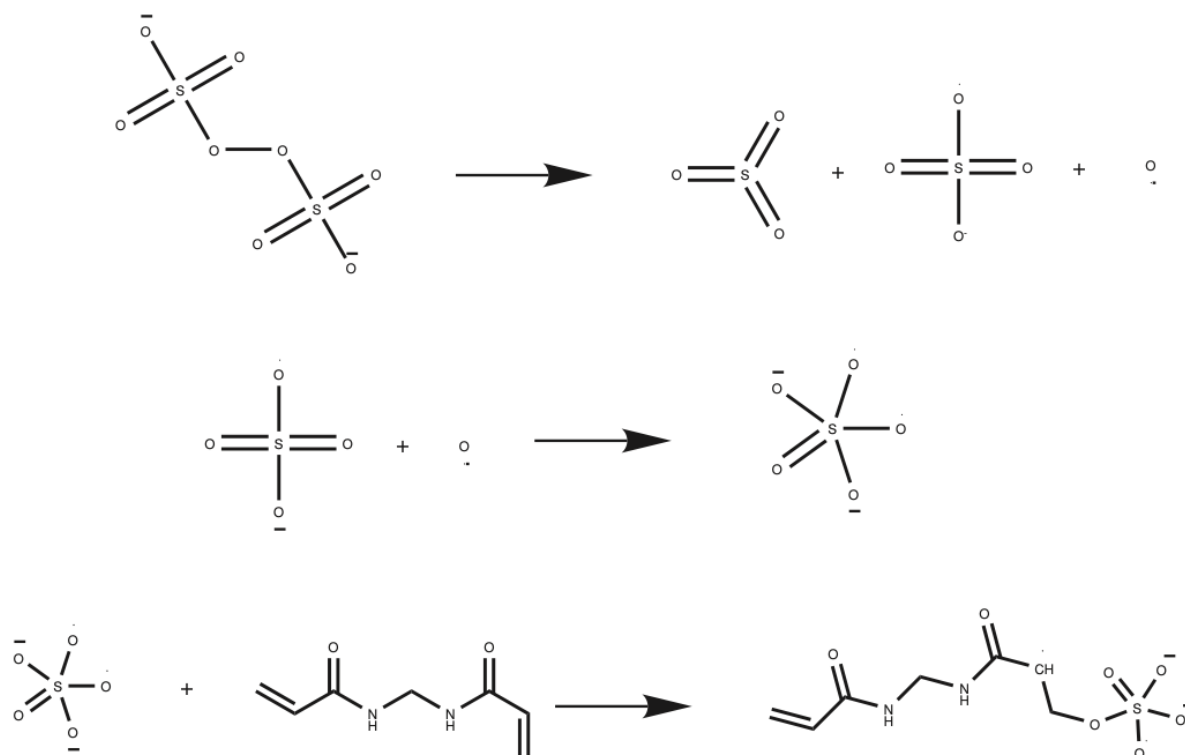


Figure 7: According to predictions, within the spectrum of the most likely reactions, stable radicals originating from the decomposition of Ammonium Persulfate possess the capacity to activate the crosslinker, priming it for the gelation process.

water, and the experimentation extended to a depth of three levels. Notably, selectivity factors of (2, 2, 3) were applied in each respective depth. It is pertinent that water was not added back as a contextual component. The adjustment of selectivity values aimed to prioritize the most probable outcomes, subsequently eliminating any duplicated structures. Ultimately, this process identified the 12 most prominent products. In accordance with findings in the existing literature, all products are documented. However, it has been reported that compounds such as sulfate radical anion ( $\text{SO}_4^{\cdot-}$ ) and hydroxyl radical play pivotal roles in the subsequent growth stage[17, 23, 24, 25]. All the data pertaining to both this section and the subsequent section (SI Section 3.1.2) are comprehensively documented. Please be aware that the order of reactions and products presented here does not imply ranking; rather, it signifies that these represent the most plausible outcomes based on the applied selectivity and depth parameters, considering all conceivable interactions and reactions among the reactants.

#### S4.1.2 Decomposition of APS Without Water (Water as Context)

We further explored the decomposition of ammonium persulfate, this time in the absence of water, and subsequently reintroduced water as a contextual element. This exploration was undertaken to elucidate water's potential impact, a departure from our previous investigation in SI Section 3.1.1. The experimental parameters were held constant, mirroring those outlined in SI Section 3.1.1, with the exception that the reactants did not include water. Instead, water was added back exclusively as a contextual component. A representative sample of the 12 most probable products is presented in Fig. 27. Our findings lead us to conclude that the presence of water plays a significant role, potentially exerting an influence in certain scenarios, perhaps in relation to the presence of hydroxyl radicals and hydroxide ions.

#### S4.2 Run with All Decomposition Products

Building on the findings from the previous sections (SI Sections 3.1.1 and 3.1.2), which predicted various products such as sulfate radical anion ( $\text{SO}_4^{\cdot-}$ ), bisulfate, sulfuric acid, hydroxyl radical, hydroxyl, sulfur trioxide, stable and unstable peroxymonosulfate structures, sulfate dianion, peroxide, superoxide anion, and bisulfate, it is noteworthy that in real-world scenarios, all these decompositions can potentially coexist for a very brief period. Among these



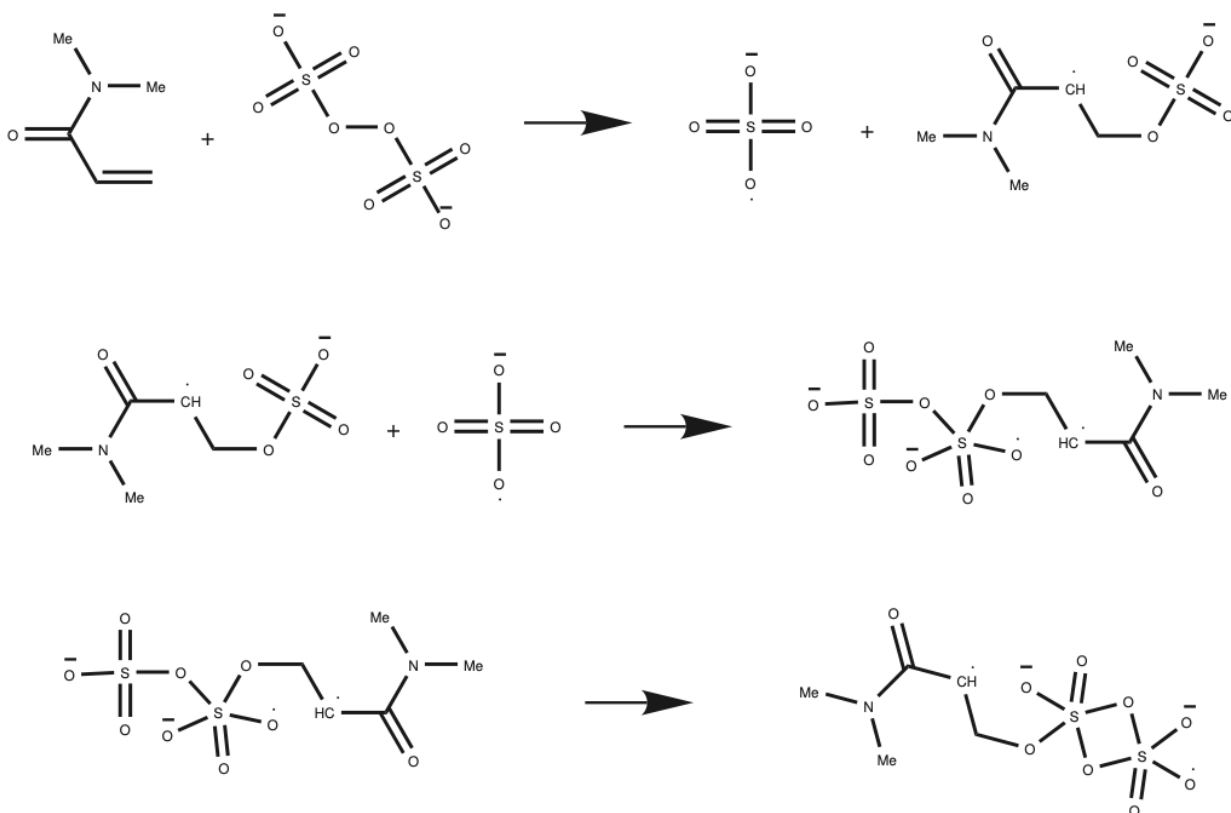


Figure 8: In some cases, the reaction begins with the initiator's direct attack on the monomer, while in contrast, other scenarios involve an initial rearrangement step leading to a more stable product before monomer interaction. Notably, when no additional monomer is present in the context, these reactions may self-rearrange until reaching their final stages.

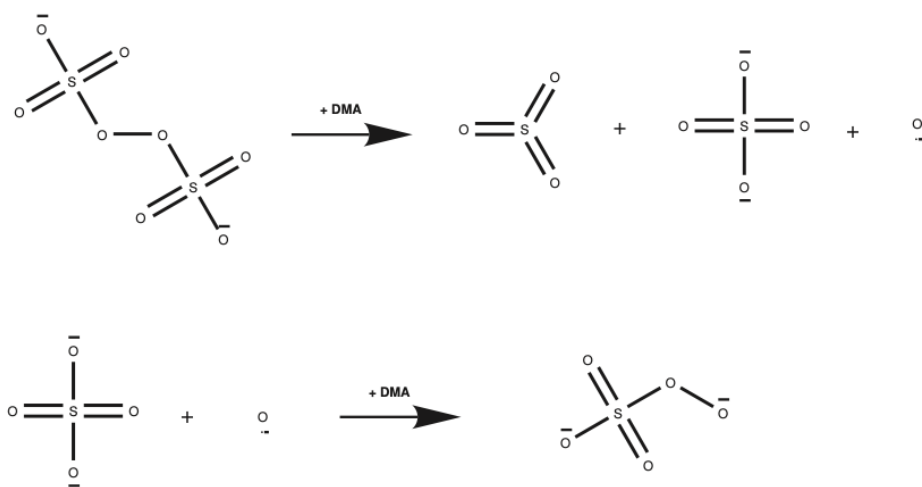


Figure 9: Highlighting a consistent observation across all cases, the addition of monomer does not interfere with or alter the decomposition of Ammonium Persulfate (APS). This consistent behavior is a favorable aspect of the reaction process.

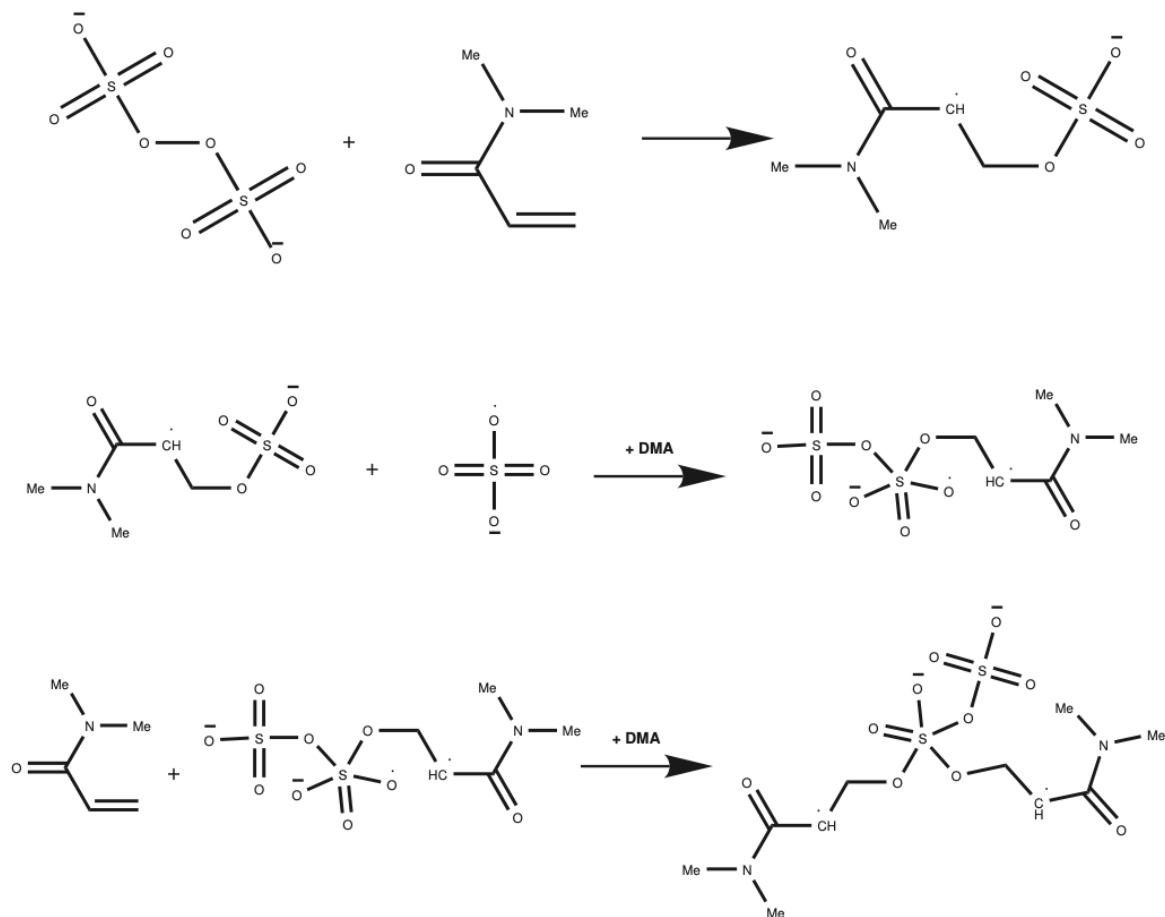


Figure 10: In scenarios following the activation of a monomer, the presence of an adjacent monomer serves as a contextual element, creating an opportunity for chain growth through dimer formation. In these reactions, it is postulated that the dimer, composed of two monomers, symbolizes the inception of a polymer chain.

species, sulfate radical anion (SO<sub>4</sub>•<sup>-</sup>), hydroxyl radical, and bisulfate are considered to play pivotal roles in subsequent reactions and steps, as documented in the literature[21, 23, 25]. Hence, in this section, we performed three benchmark experiments. All runs used ammonium, water, hydroxyl radical, bisulfate, and sulfate radical anion (SO<sub>4</sub>•<sup>-</sup>) as reactants. Each benchmark entails different primary reactants: In the first run, our monomer (N, N-Dimethylacrylamide) served as the primary reactant, as illustrated in Fig. 28. The second run employed our crosslinker as the primary reactant, as depicted in Fig. 30. In the third run, our polymer (polyethylene oxide) was the primary reactant, as showcased in Fig. 32. The first run explored these processes to a depth of 4 levels, selecting only 2 reactions at each depth. An example of this is presented in Fig. 29. In the second and third runs, we investigated to a depth of 3 levels. In the former, we selected 2 paths from all possible paths, as shown in Fig. 31, and in the latter, we chose 3 paths at each depth, as demonstrated in Fig. 33. All runs included the initiator radicals as contextual elements and reintroduced them at each depth. It is important that in all cases, it was observed that the initiator radicals' high reactivity rendered these settings impractical. Due to their propensity for rapid rearrangement, interaction, and mutual reaction, the initiator radicals failed to initiate reactions with the monomer or other components. While it was anticipated that activation of the monomer or crosslinkers would occur at the second or third depth, the initiator radicals' reactivity necessitated a more prolonged period, potentially extending to the sixth or seventh depth for their rearrangement. Such prolonged rearrangement would substantially increase computational costs, rendering these settings infeasible.

### S4.3 Run with Desired Initiators

Due to the complexities highlighted in the preceding section, we have encountered difficulties in incorporating all potential initiator radicals into our reactions. To address this challenge, we have devised two distinct strategies. The

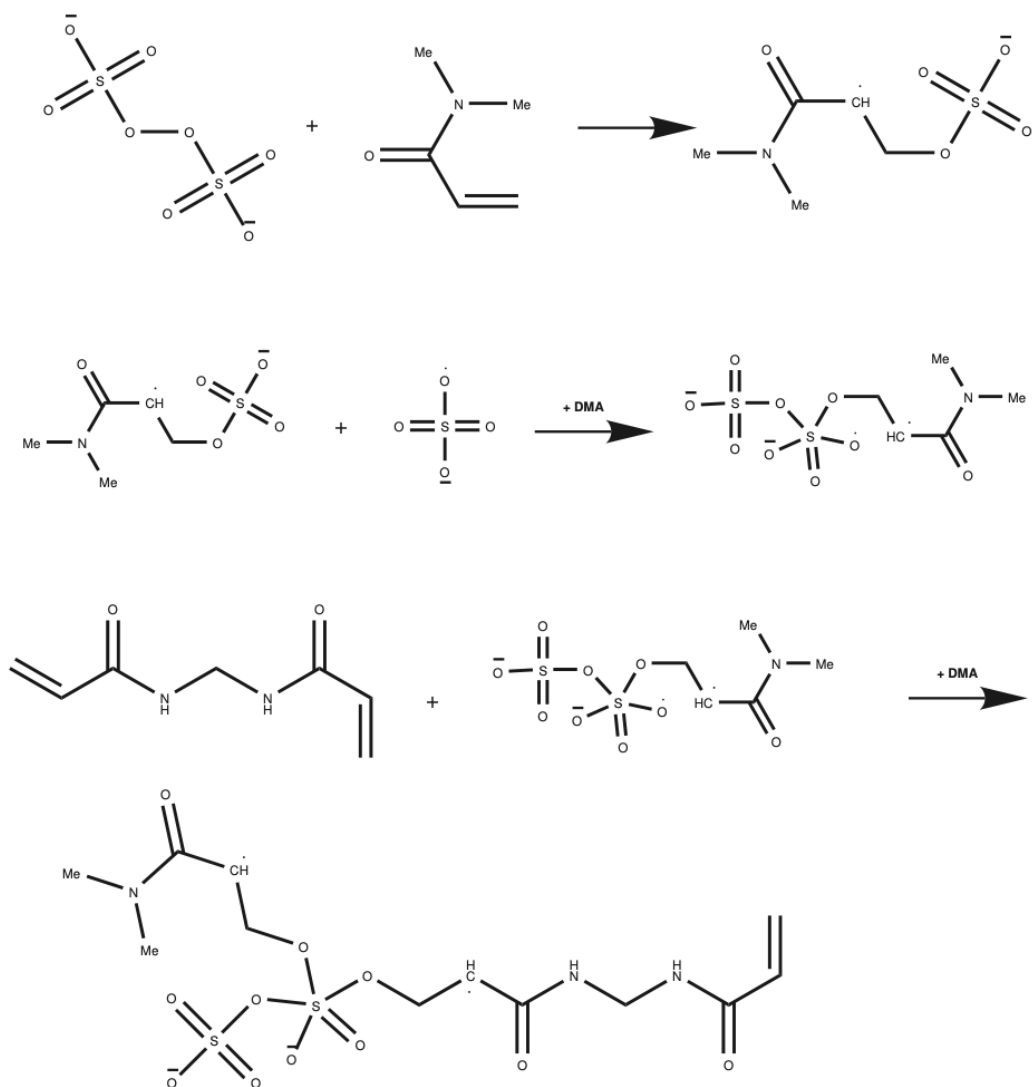


Figure 11: A key observation demonstrates that even in the presence of another monomer, the initially activated monomer retains the capacity to engage with a crosslinker, facilitating their linkage and setting the stage for subsequent reactions.

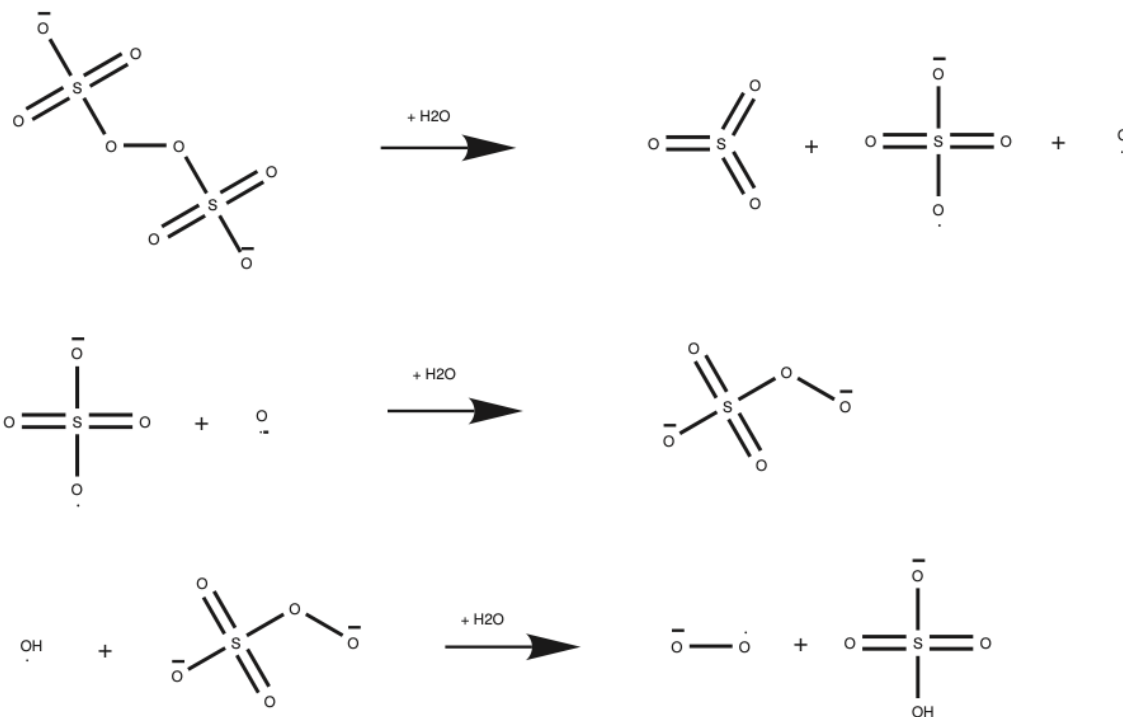


Figure 12: In this scenario, water serves as a contextual component rather than a reactant. The process begins with the decomposition of APS, followed by interactions with monomers or other reactants. Importantly, throughout these reactions, water does not exert any influence on monomers, initiators, or initiator radicals.

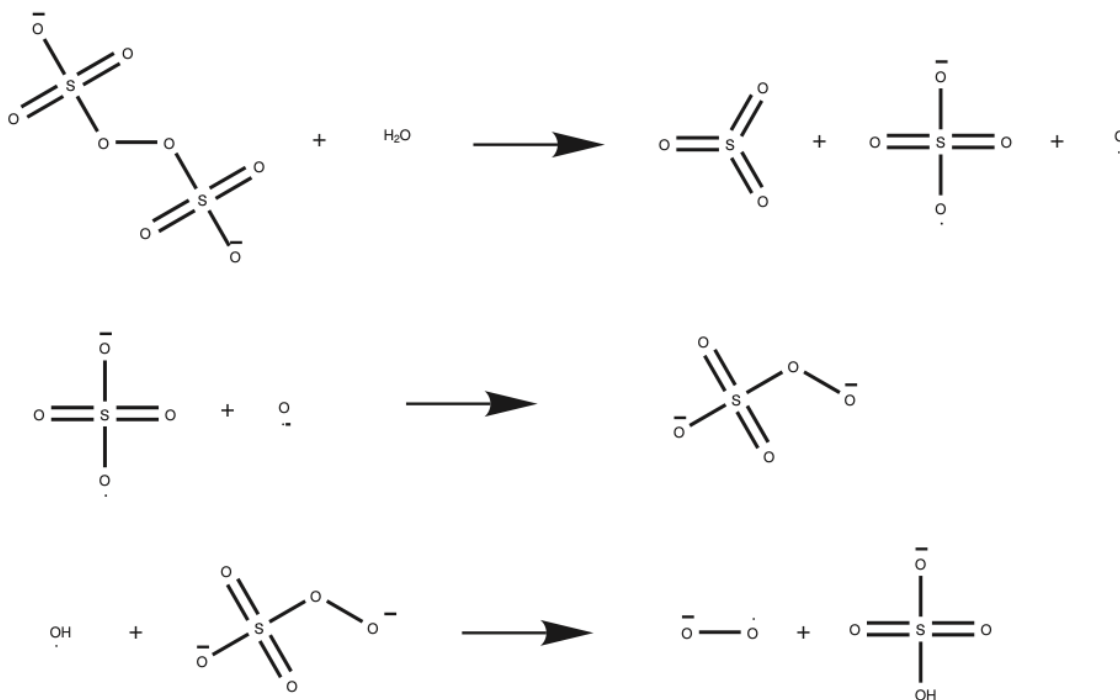


Figure 13: In this scenario, water serves as a reactant. The study explores the influence of water, revealing that its presence has no discernible effect on monomers or APS decomposition.

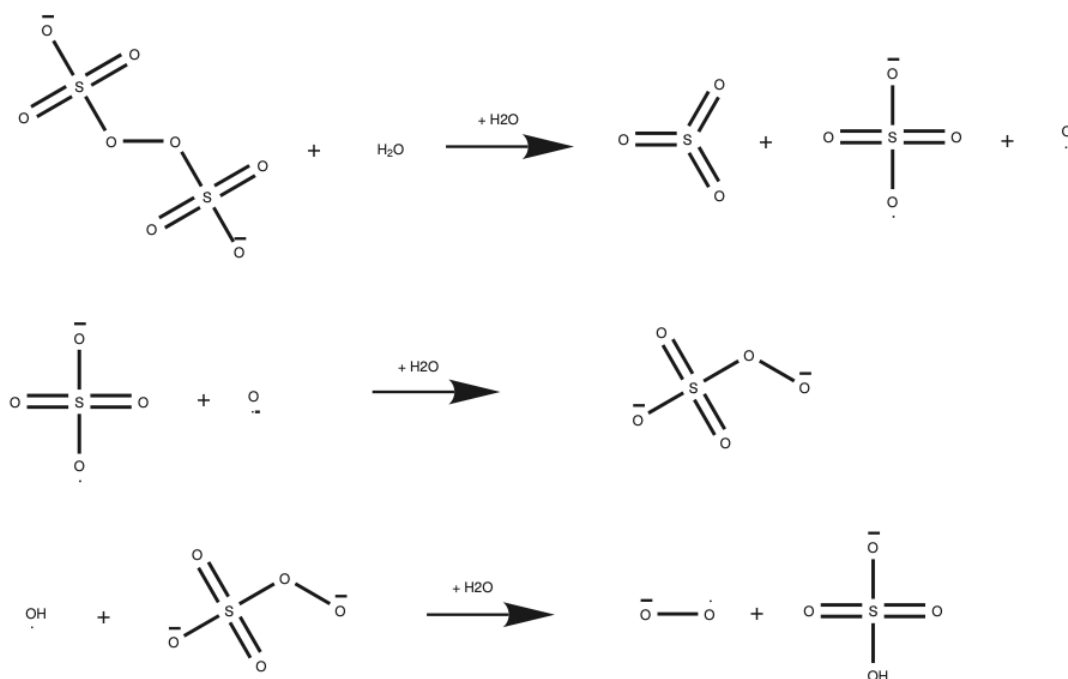


Figure 14: In this case, water serves dual roles as both a reactant and a contextual component. Importantly, it is observed that whether a reaction involves water as a reactant or a contextual component, there is no discernible distinction in the outcomes. Additionally, in specific instances where initiator radicals seek to obtain hydrogen (H) from  $\text{H}_2\text{O}$ , it is evident that they can do so equivalently from either the contextual or reactant water, with no distinguishable differences in behavior.

first approach employs ammonium persulfate as the initial reactant. This strategy is grounded in selecting the most probable initiator decomposition products based on the initial reaction's selectivity. While this approach permits us to explore a broad spectrum of potential mechanisms, it has two notable drawbacks. First, the limited number of steps allocated for initiator decomposition—typically two or three—can substantially escalate computational costs. Second, it generates an abundance of products, rendering subsequent analysis a formidable task. The multitude of products complicates our ability to discern which ones are more likely to occur in the real-world context. The second approach was adopted to mitigate the challenges faced in the first approach. In this method, we investigate all the products from the first approach, selecting one of them as the primary reactant. This strategy effectively reduces the sample space, enabling us to obtain a specific number of products with decreasing selectivity at each depth. This streamlined approach aids in determining the final molecular structures with greater clarity and precision.

### S4.3.1 Run with Ammonium Persulfate

Our first approach restricted our reactants to N, N-Dimethylacrylamide, N, N'-Methylenebisacrylamide, ammonium persulfate, polyethylene oxide (represented by a two-unit polymer segment), and water. Our contextual parameter, N, N-Dimethylacrylamide, served as the monomer, and it remained in use until the seventh depth, as depicted in Fig. 35. We conducted investigations up to the eighth depth, applying a selectivity factor of 2 at each depth. Notably, at the final depth, to observe which reactions might occur in the absence of monomer, we intentionally did not reintroduce monomer, thus shedding light on potential termination mechanisms. In this approach, the initial two depths emphasize APS decomposition. We have categorized all 188 possible mechanisms into four distinct groups based on the activation centers, denoted as A, B, C, and D. The investigation of these four groups is documented in Figures 36 and 37, which provide an example for Group A (Figures 38 and 39), illustrating one example from Group B (Figures 40-43), showcasing two examples from Group C, and finally, presenting an example from Group D (Figures 44 and 45).

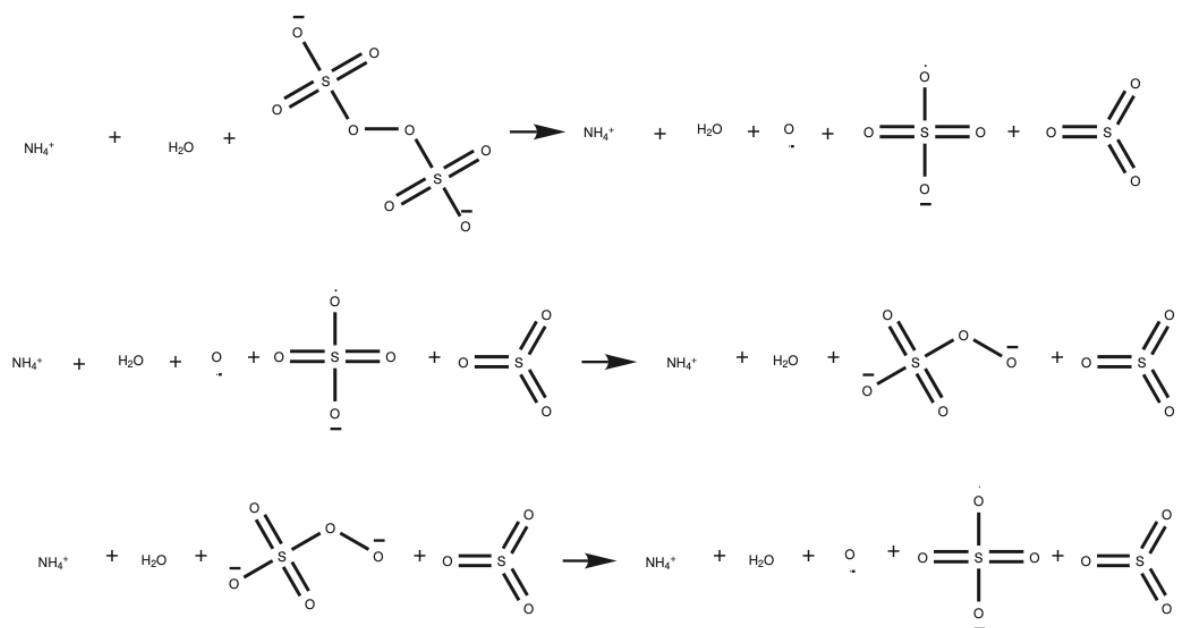


Figure 15: This figure provides valuable mechanistic insights into ammonium persulfate (APS) decomposition. Initially, APS decomposes into the sulfate radical anion ( $\text{SO}_4^{\cdot-}$ ) along with sulfur trioxide and the oxygen radical anion, which may represent an unstable form of oxygen. The figure shows that at this mechanistic level, in a subsequent reaction, the oxygen radical anion has the potential to re-engage with sulfate radical anion ( $\text{SO}_4^{\cdot-}$ ) to form Peroxymonosulfate. Upon further examination at subsequent depths, this cycle continues, with the transformation oscillating between the formation of sulfate radical anion ( $\text{SO}_4^{\cdot-}$ ) and Peroxymonosulfate. This mechanism highlights a dynamic tradeoff between these two radical species.

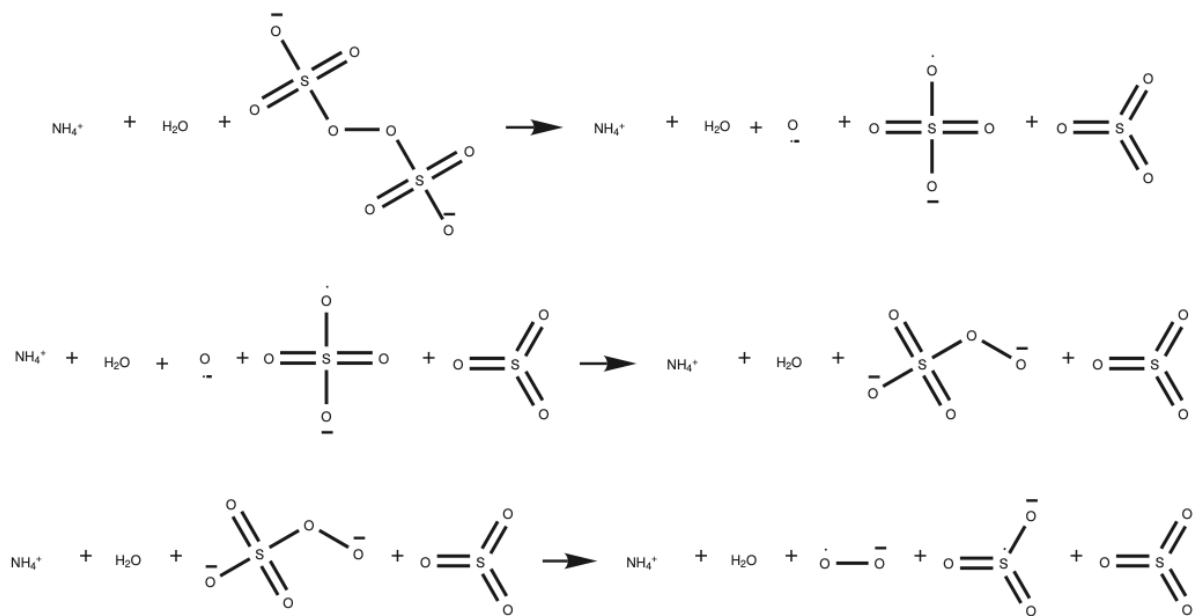


Figure 16: This diagram mirrors the decomposition mechanism observed in Fig. 15, involving two primary reactions. However, in this case, the final step reveals that Peroxymonosulfate can undergo further decomposition, forming the sulfite radical and the superoxide anion.

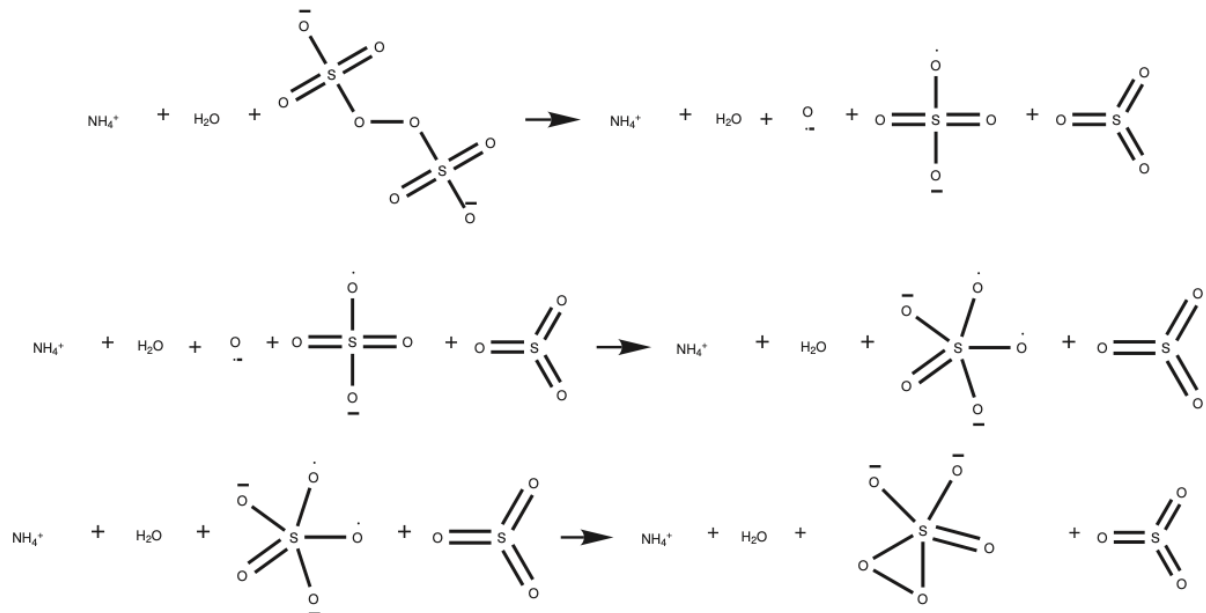


Figure 17: A reactive pathway in which the sulfate radical anion ( $\text{SO}_4^{\bullet-}$ ) engages with the oxygen radical anion ( $\text{O}^-$ ) in the second reaction. This interaction leads to the formation of a rare species,  $\text{SO}_5$ , which subsequently undergoes further structural transformation into even more distinctive configurations.

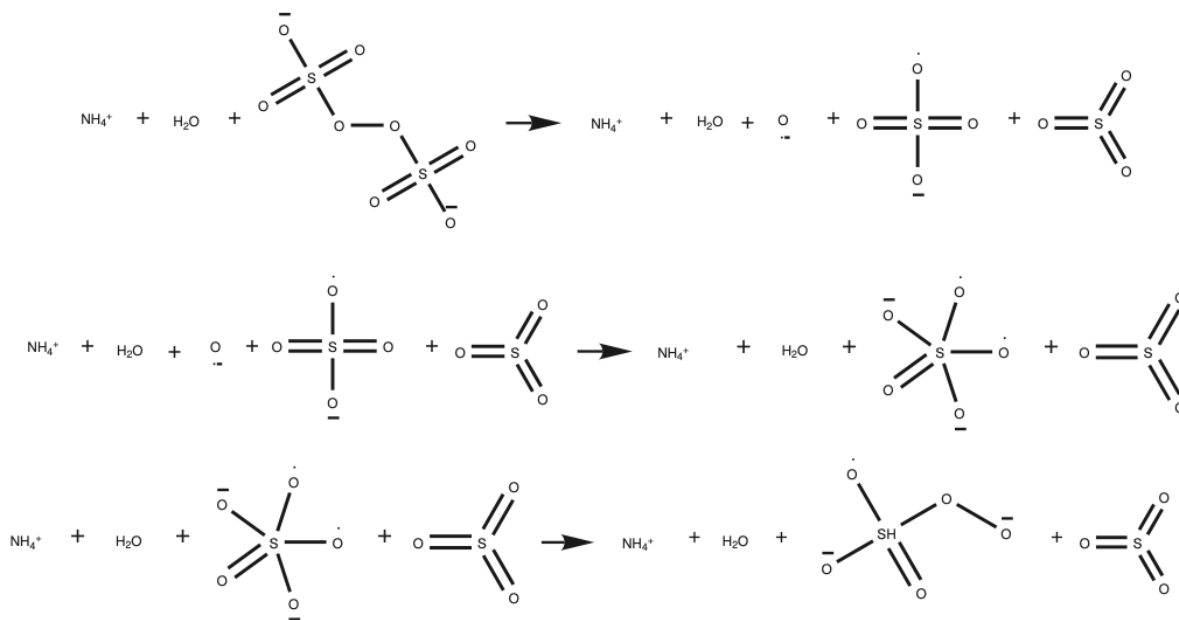


Figure 18: In this decomposition pathway, as the progression advances toward the formation of the rare  $\text{SO}_5$  species, predictions may encounter challenges when dealing with the inherently unstable structure of  $\text{SO}_5$ .

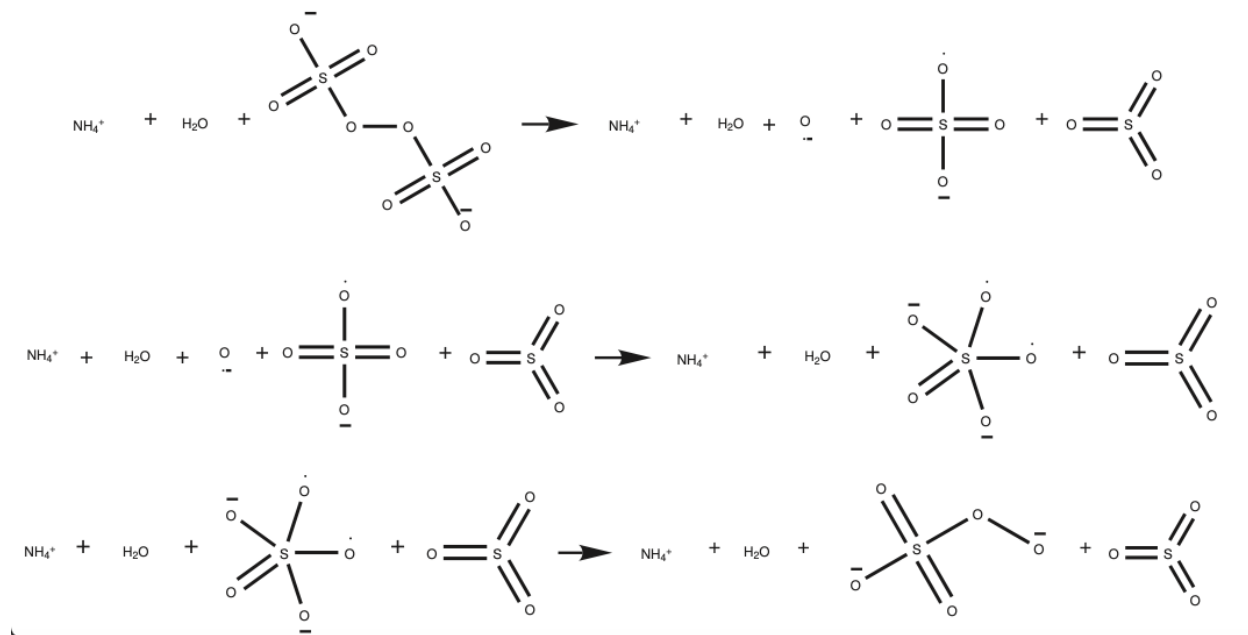


Figure 19: In certain instances, it is possible for the rare and unstable SO5 species to undergo a conversion process, returning to the Peroxymonosulfate state.

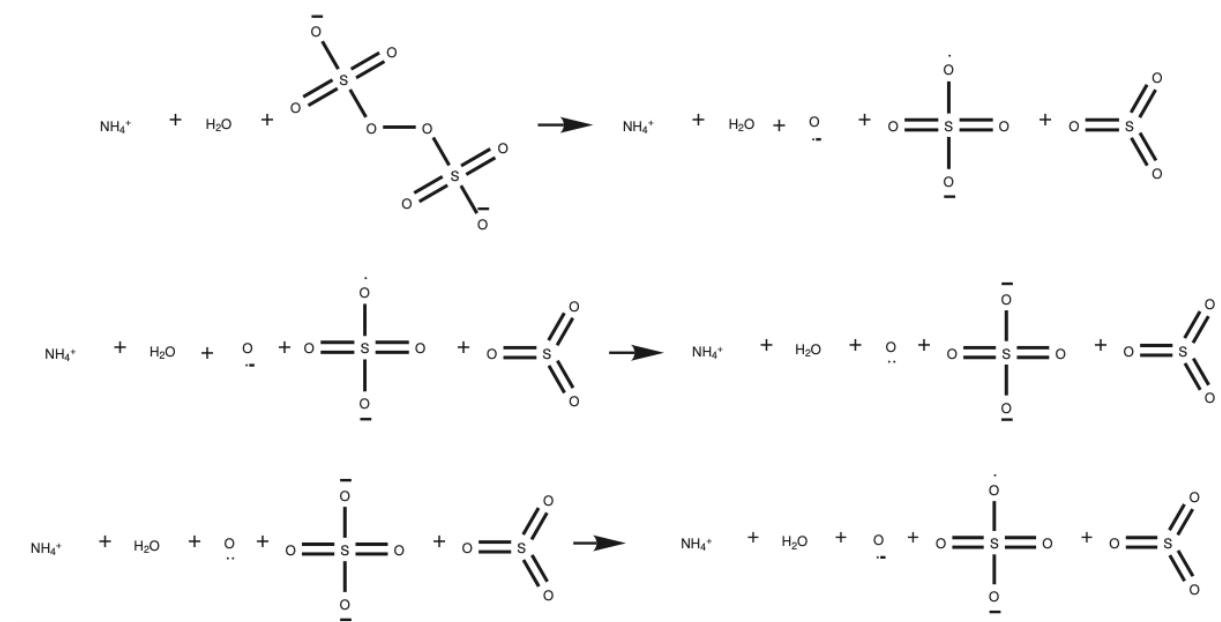


Figure 20: A transformation pathway in which the sulfate radical anion undergoes conversion to the sulfate dianion, eventually combining with oxygen(-2) to generate a sulfate radical anion (SO4<sup>-•</sup>) again.



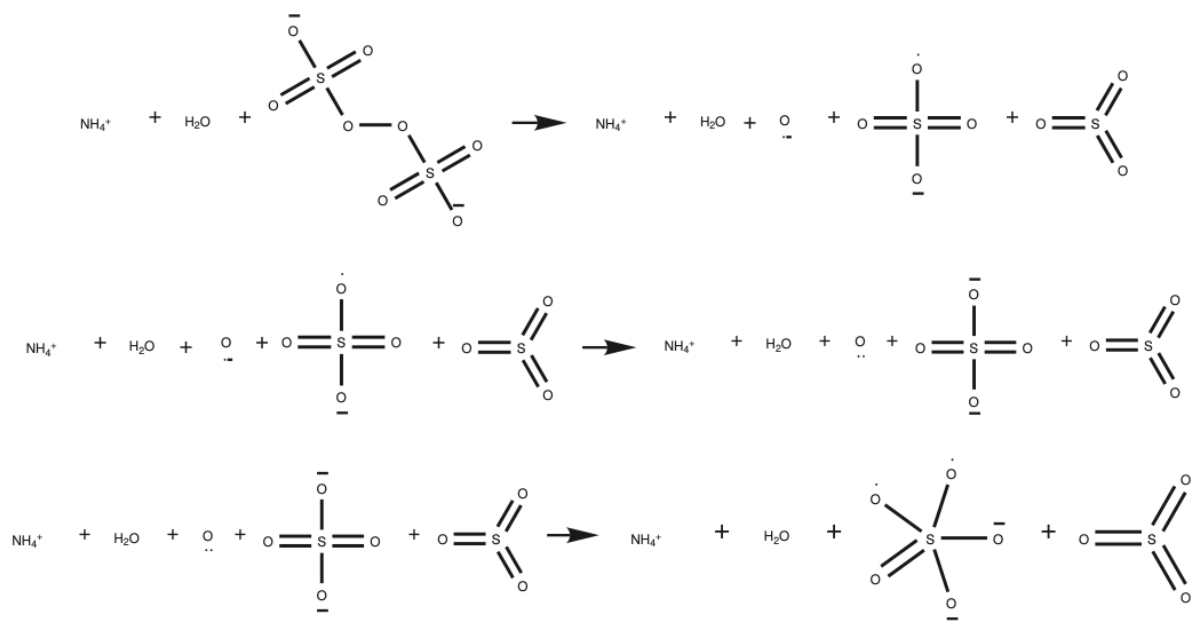


Figure 21: Occasionally, upon further progression beyond the standard steps, the prevalent sulfate radical anion (SO<sub>4</sub>·-) is found to convert into the rare SO<sub>5</sub> species, involving an additional, nonessential step in the reaction pathway.

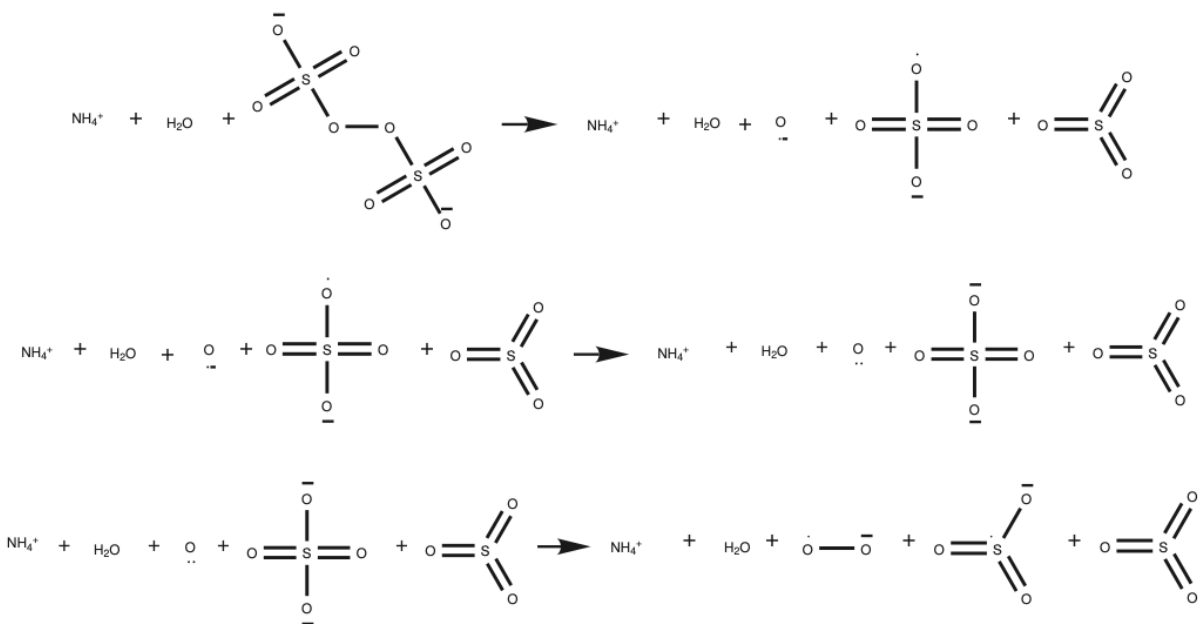


Figure 22: Produced SO<sub>3</sub> anion radical and oxygen and peroxide.

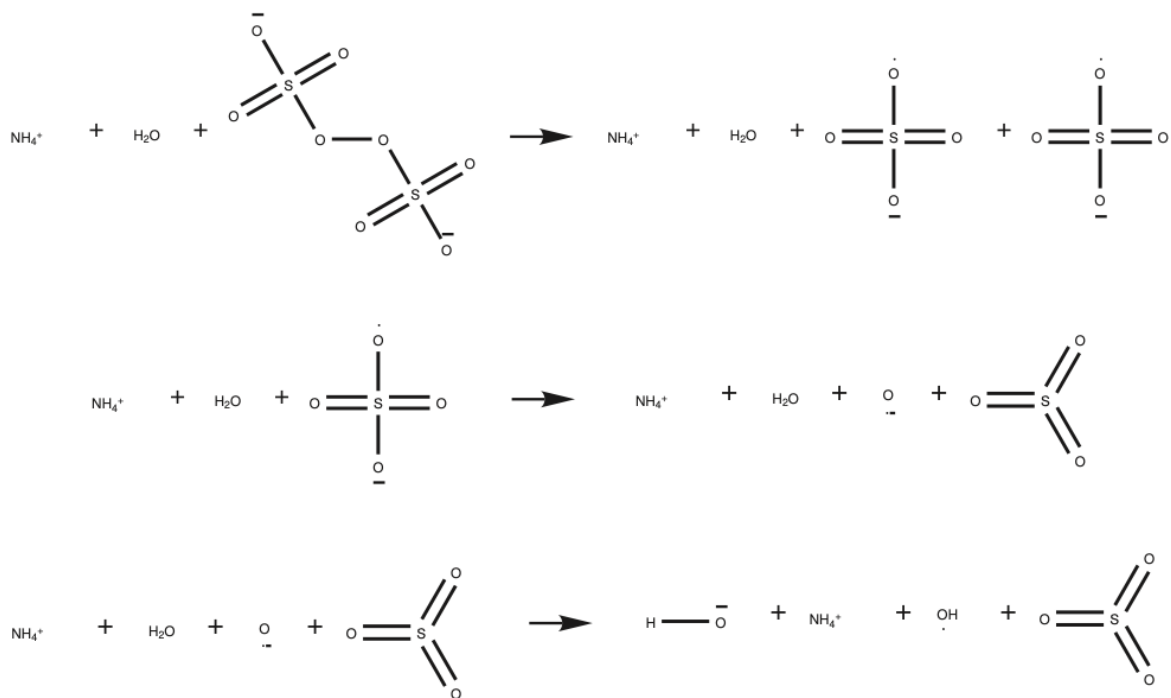


Figure 23: A distinct decomposition pathway for ammonium persulfate, unlike the preceding reactions. In this scenario, ammonium persulfate decomposes into two sulfate radical anions ( $\text{SO}_4^{\bullet-}$ ), emphasizing that the initial reaction yields sulfate radical anion ( $\text{SO}_4^{\bullet-}$ ). Of notable significance is water's role in this decomposition process. Here, the oxygen radical anion can interact with water, forming both hydroxyl radicals and hydroxide ions in the final stages.

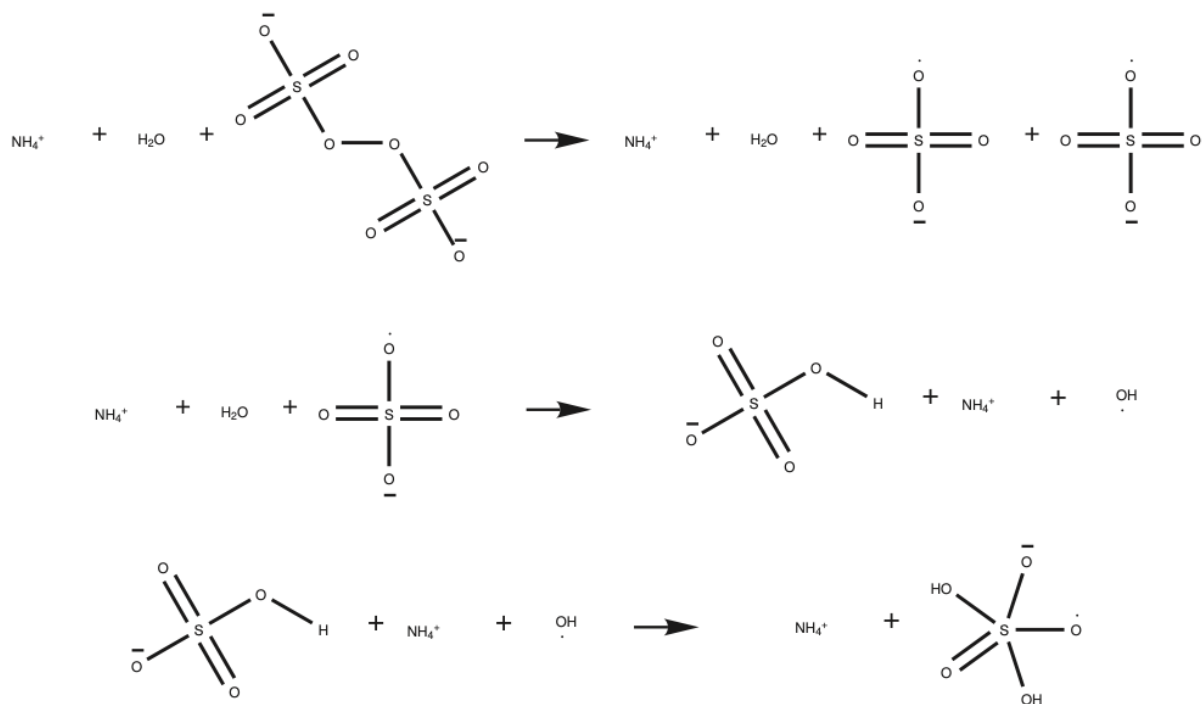


Figure 24: A reaction pathway where water and sulfate radical anion ( $\text{SO}_4^{\bullet-}$ ) react to produce hydroxyl radicals and hydrogen sulfate ions. The final stages of this sequence give rise to a further decomposition event, generating a rare  $\text{h}_2\text{so}_5$  anion radical.

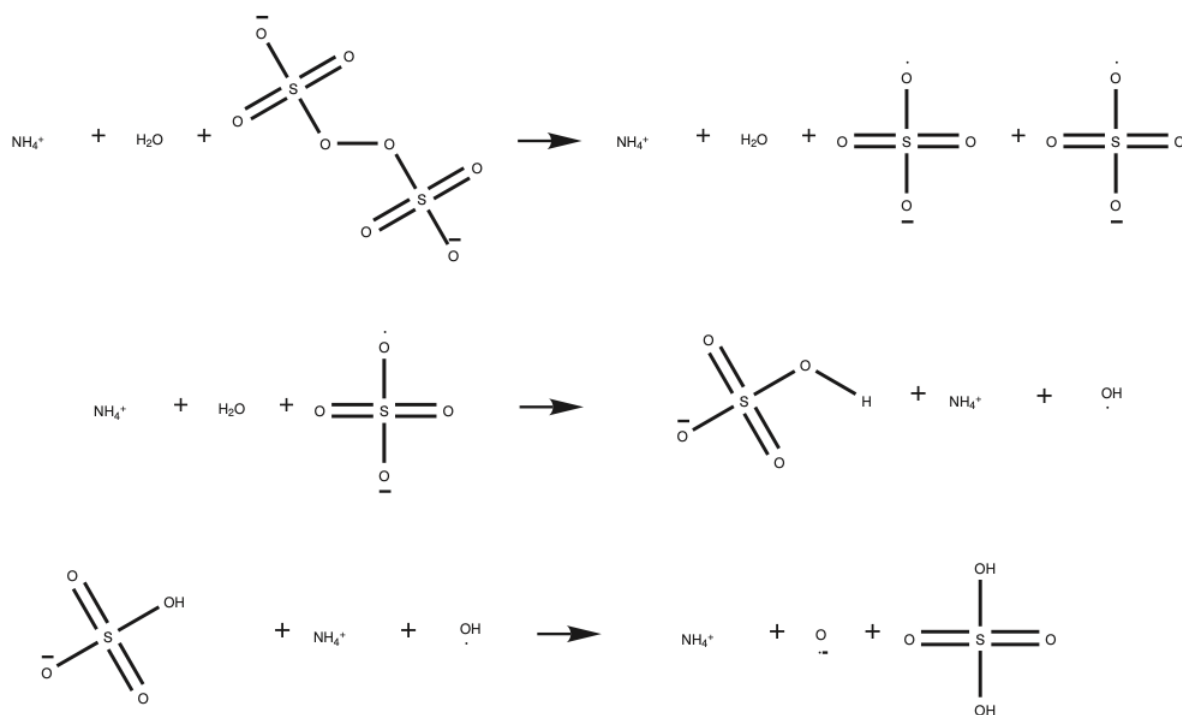


Figure 25: As the reaction sequence continues, hydrogen sulfate ions interact with hydroxyl radicals to produce sulfuric acid. This accumulation of sulfuric acid can subsequently influence the surrounding water's acidity, potentially affecting various chemical reactions.

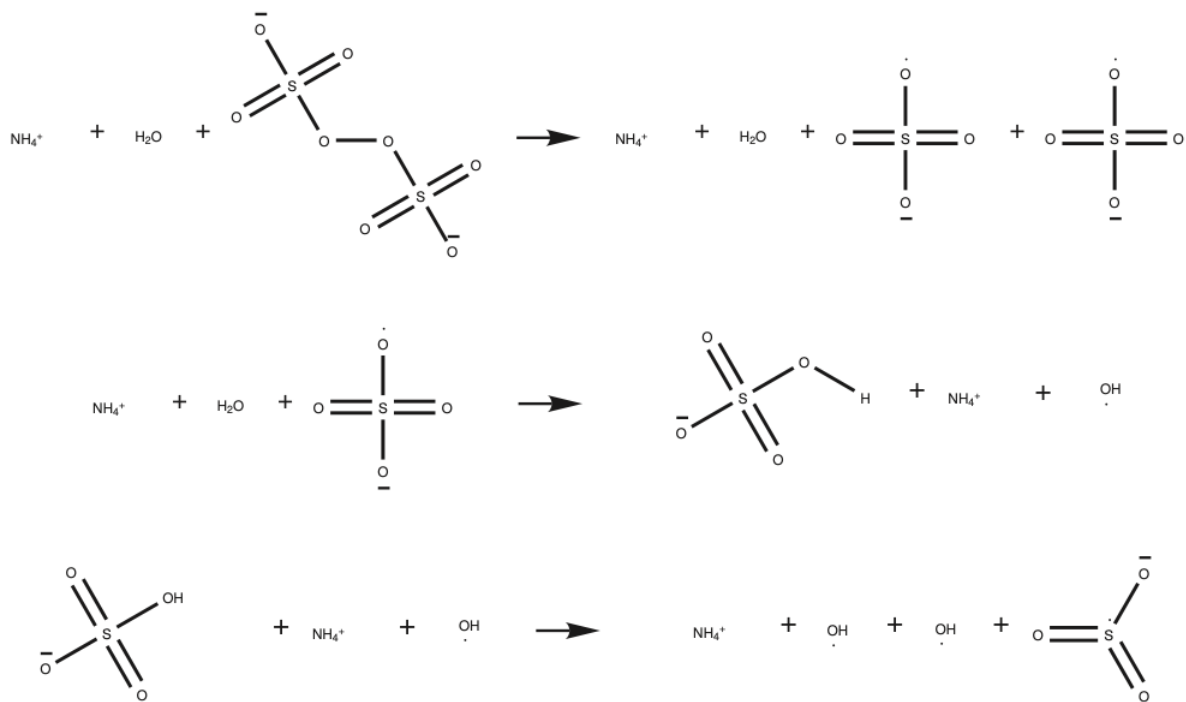


Figure 26: Under certain conditions, the interaction between hydrogen sulfate ions and hydroxyl radicals can lead to the production of double hydroxyl radicals and sulfate anion radicals. This observation underscores the potential significance of hydroxyl radicals' presence, consistent with findings reported in the existing literature.

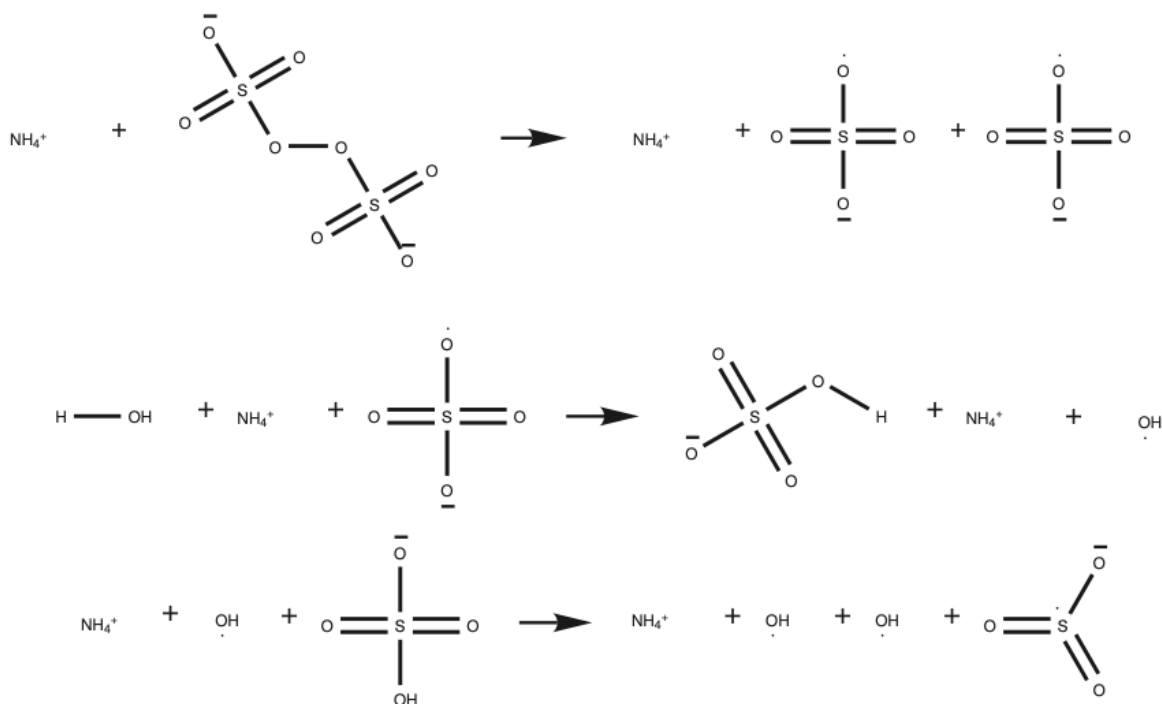


Figure 27: This figure demonstrates that whether water is considered a reactant or a contextual component, the desired product can obtain hydrogen from water in both scenarios. In this case, the sulfate radical anion ( $\text{SO}_4^{\cdot-}$ ) acquires hydrogen from water, which is added either as a reactant or context. This observation suggests that while it is essential for water to be present as a reactant due to the importance of these hydrogen-transfer reactions, its inclusion as context yields comparable results. This approach is adopted to optimize computational efficiency, as the choice between reactant and context does not significantly affect the outcome.

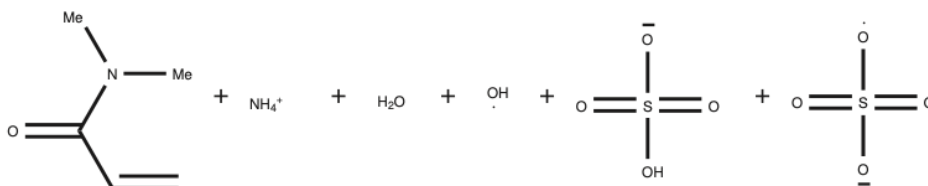


Figure 28: The primary reactants employed in the first run include N, N- Dimethylacrylamide, ammonium, hydroxyl radical, bisulfate, and sulfate radical anion.

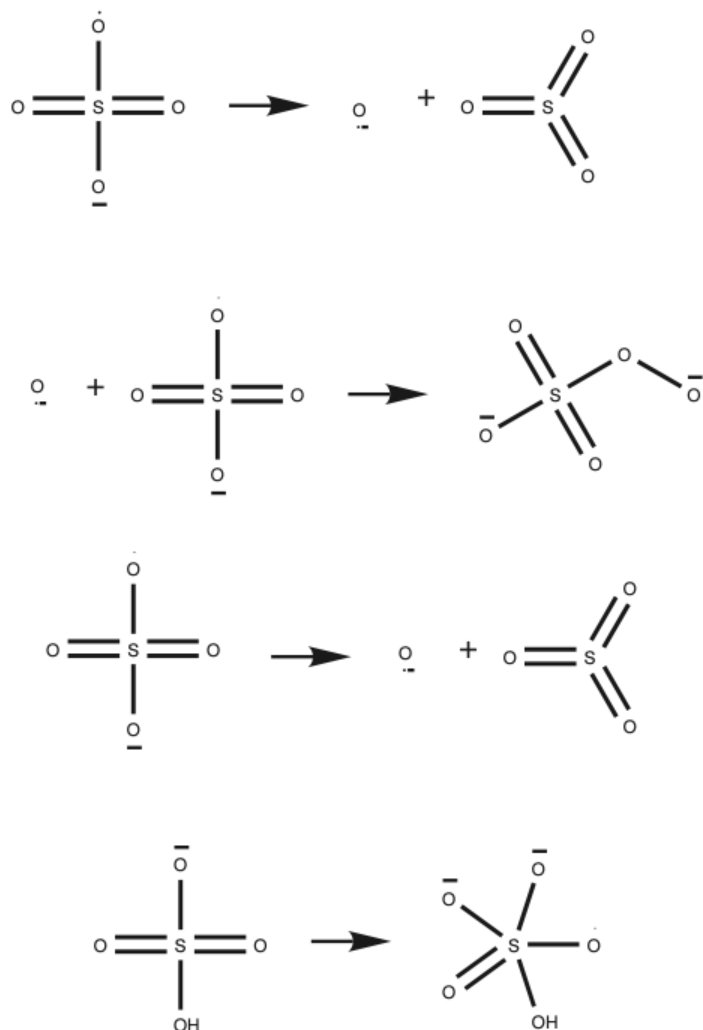


Figure 29: In a significant aspect of the reaction dynamics, the sulfate radical anion ( $\text{SO}_4^{\cdot-}$ ) undergoes rearrangement, yielding an unstable oxygen radical anion. This highly reactive species subsequently interacts with other sulfate radical anions ( $\text{SO}_4^{\cdot-}$ ), ultimately forming peroxydisulfate. Notably, this sequence of reactions is primarily consumed by the rearrangement of initiator radicals due to their high reactivity and accessibility to other molecules. Consequently, these initiator radicals have only limited opportunities to engage with the monomers present in the reactant, leading to an emphasis on rearrangement.

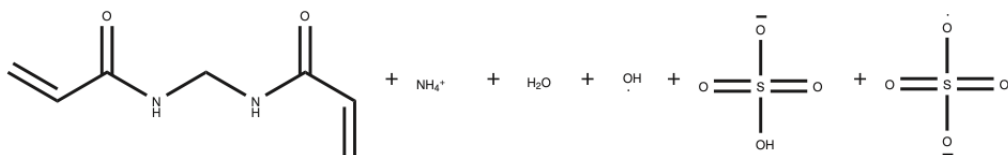


Figure 30: The reactants employed in the second run consist of N, N'-Methylenebisacrylamide, ammonium, hydroxyl radical, bisulfate, and sulfate radical anion.

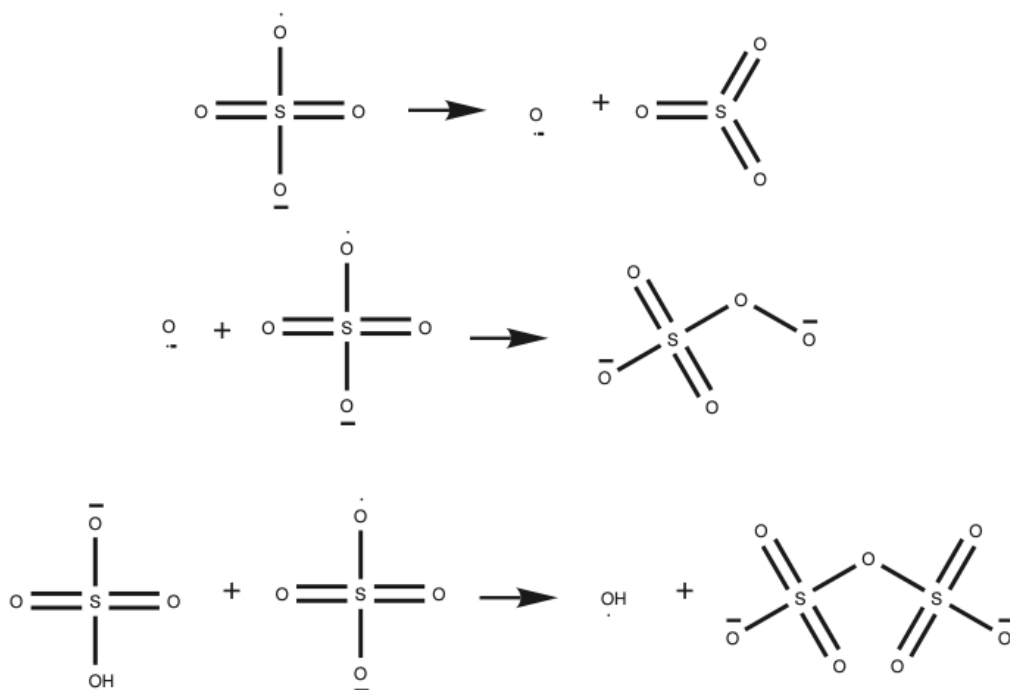


Figure 31: In a pattern similar to previous reactions, certain steps in the decomposition of Ammonium Persulfate (APS) recur. These recurring steps, along with reactions between some intermediates, may lead to APS regeneration. Consequently, this impedes the opportunity for crosslinker attack, potentially hindering the mimicry of real-world reactions.

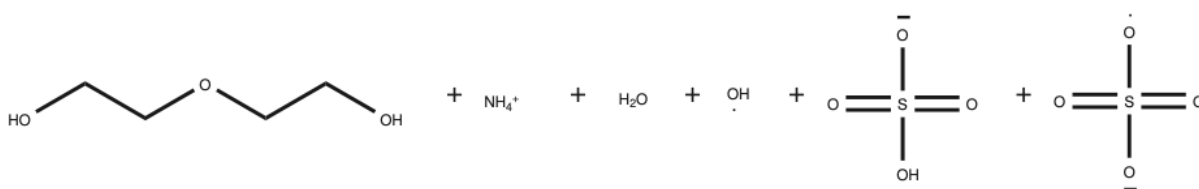


Figure 32: The third run uses the reactants Polyethylene Oxide (PEO), ammonium, hydroxyl radical, bisulfate, and sulfate radical anion. Notably, for computational efficiency, only two units of PEO are considered to emphasize distinctions between monomers and polymers.

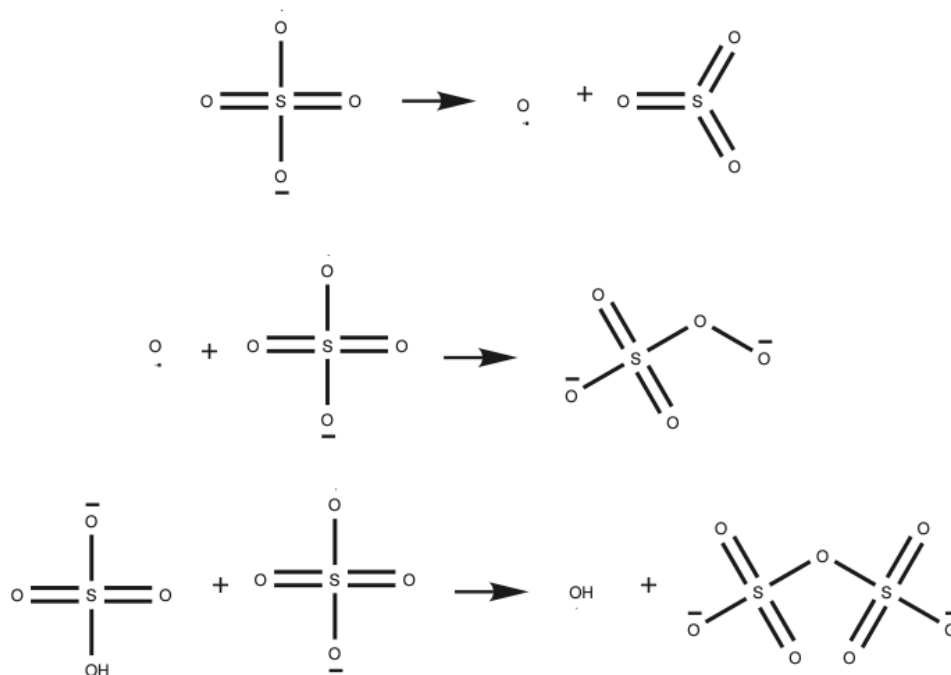


Figure 33: A recurring sequence of crosslinker related reactions leads to a constrained opportunity for Polyethylene Oxide (PEO) to actively participate in the reactions.

### S4.3.2 Most Possible Products of the Main Run

The four previous groups have primarily demonstrated the validity of mechanisms pertaining to polymerization, encompassing aspects such as the decomposition of APS, radical initiation, monomer radical generation, chain growth, and crosslinking. These investigations were instrumental in analyzing the effects of APS decomposition and validating the polymerization processes. However, our central objective, as previously mentioned, revolves around our second approach, which aims to reduce selectivity and depth to identify the most probable structures within the four identified groups. This endeavor specifically focuses on sulfate radical anion (SO<sub>4</sub>•-), a species well documented in numerous literature sources and thus regarded as a potential key player[19, 26]. In this section, our experimental system incorporates the reactants as outlined in Fig. 48. These runs explored the system down to the fourth depth, reintroducing the monomer up to the final step. Our selectivity was set at 2, and after eliminating redundant structures, we identified a total of 11 structures as the most probable candidate products. These 11 structures are illustrated in Figures 49-59. It is important to reiterate that the order in which these 11 mechanisms are presented does not denote any ranking. Instead, the order signifies that all 11 products are considered equally plausible among the entire spectrum of mechanisms that could potentially occur.

## S5 Further Investigation and Running

In all but one of the mechanisms and runs conducted thus far, we observed that PEO (polyethylene oxide) appeared not to play a substantial role and did not actively participate in the reactions. However, in real-world experiments, we utilized PEO as one of our reactants, detecting its presence through peaks in the FTIR (Fourier-transform infrared) spectra. Furthermore, our experimental data indicated that PEO was indeed incorporated into the final hydrogel structure. This raises the question of how PEO is integrated into the hydrogel network. To address this query, we conducted an in-depth analysis of all initiator radicals and observed that following sulfate radical anion (SO<sub>4</sub>•-), hydroxyl radicals exhibited the highest likelihood of occurrence, both in accordance with existing literature and as predicted by our modeling system in the decomposition section[27]. Notably, some literature sources have attributed a pivotal role to hydroxyl radicals in the activation and initiation steps involving monomers[24, 25]. In this context, we sought to

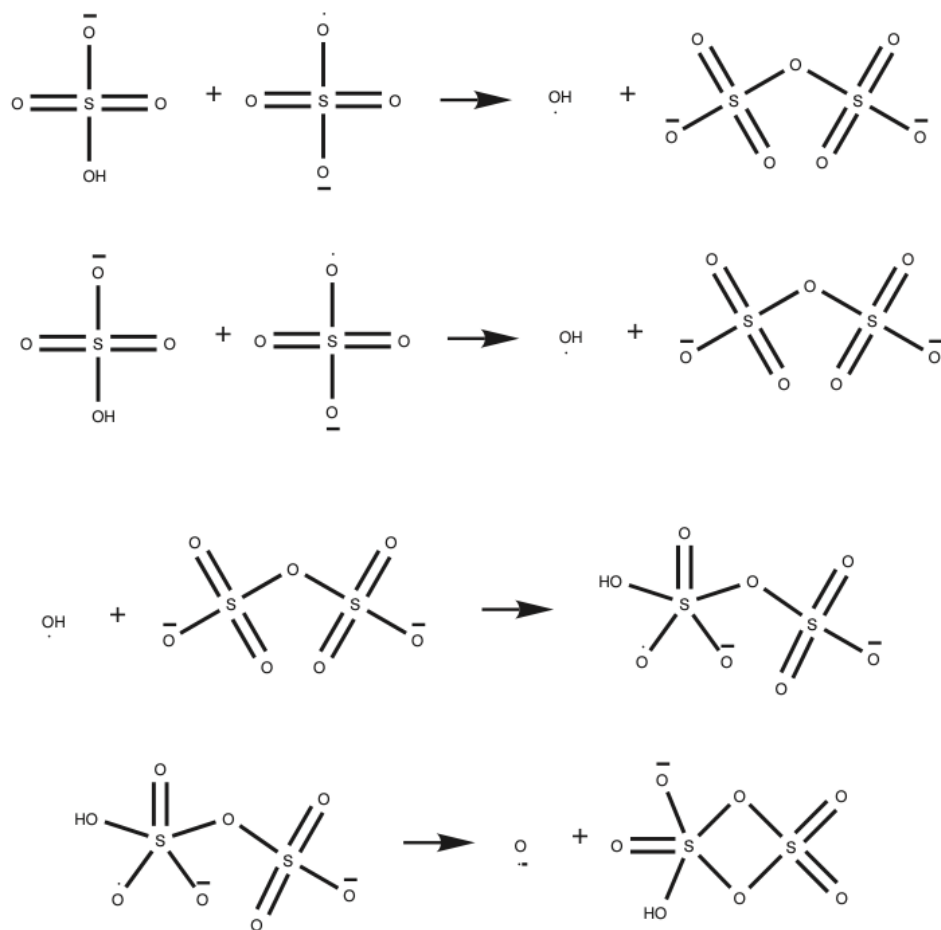


Figure 34: Having other initiator radicals as contextual components can lead to heightened complexity in certain instances across all three runs, necessitating additional computational steps and depths to observe monomer growth. As selectivity becomes a pivotal factor, complexity can escalate exponentially, increasing the number of potential final structures. This increase in complexity may pose challenges in terms of analysis and other aspects of the study.

elucidate hydroxyl radicals' potential impact on the polymerization process. This exploration is pivotal as it may lead to a paradigm shift in our understanding of hydrogel formation.

### S5.1 The Role and Effect of Hydroxyl Groups

In this section, we specifically examined the influence of hydroxyl radicals. For this purpose, we ran experiments utilizing hydroxyl radicals as initiators, along with PEO, N, N-Dimethylacrylamide as the monomer, and N, N'-Methylenebisacrylamide as the crosslinker, as outlined in Fig. 60. Within this framework, we conducted supplementary runs, using our monomer as the contextual parameter and reintroducing it at each depth. Our investigations extended to a depth of 4 levels, with 3 selectivity options considered at each depth. Select cases and results are shown in Figures 61-64.

### S5.2 Effect of PEO Chain Size

We are acutely aware that our use of a restricted number of PEO units responds to a combination of both system constraints and, notably, computational cost considerations. Our strategy consolidates all pertinent factors into a single, unified unit, wherein we conceptualize a dimer—comprising two monomers—as emblematic of the polymer itself[28]. This reduction to a mere pair of numerical values is motivated by our methodology's inherent intricacies. In delineating the fundamental mechanisms governing PEO, we discern a pair of predominant pathways. Initially, PEO exhibits a



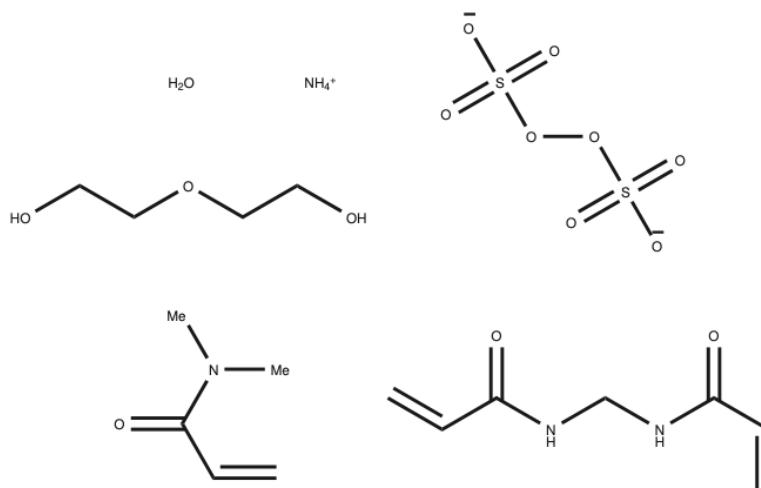


Figure 35: The initial reactants common to all reactions include water, utilized as a conditioning agent, Ammonium Persulfate as the initiator, Polyethylene Oxide (PEO) as polymer, N, N-Dimethylacrylamide as a monomer, and N, N'-Methylenebisacrylamide as the crosslinker.

propensity to relinquish hydrogen atoms from its terminal groups. Subsequently, due to the presence of radicals along the chain, a propitious confluence occurs, resulting in the amalgamation of these radicals into the ultimate molecular architecture. It is indispensable to acknowledge that in the physical realm, as the chain elongates, adopting a random coil configuration, it restricts terminal end group accessibility and becomes resistant to attachment or incursion by other molecular constituents. Our approach executed three distinct runs, each featuring varying lengths of PEO chains. Specifically, one run featured a short chain consisting of a mere two units, another employed a medium chain comprising three units, and the third incorporated a long chain encompassing five units, as shown in Fig. 65. Intriguingly, all three chains exhibited the attachment of OH radicals, a phenomenon cogently depicted in the first reactions of Figures 66-68. This observation underscores the pivotal role played by the sulfate radical anion (SO<sub>4</sub><sup>•-</sup>), along with other components, which manifest significantly higher reactivity relative to hydroxyl radicals, and the literature reports that the first reactions in initiation steps belong to the sulfate radical anion (SO<sub>4</sub><sup>•-</sup>) and that the hydroxyl radical emerges after a long time at the end of reaction[29]. Consequently, toward the culmination of polymerization, it becomes feasible to incorporate PEO. This elucidates why, in our prior run, PEO's participation in reactions was seemingly hindered, primarily due to these radicals' heightened reactivity. Moreover, it becomes evident that as we progress through the runs, each characterized by an increasing computational depth, the potential for PEO to be incorporated into the reaction mix increases. Furthermore, our investigation explores the fascinating dynamics of chain sessions[30], as visually expounded in the next steps of these figures. Remarkably, these chain sessions manifest predominantly in the long chain, where they are much more likely to occur. The predictive system anticipates and integrates the effects of chain size, offering invaluable insights into the intricacies of these molecular interactions.

## S6 The Final Step

Upon the culmination of our exhaustive series of runs, we can deduce that the initiator disintegrates, yielding various radicals such as the sulfate radical anion (SO<sub>4</sub><sup>•-</sup>) and other species, including hydroxyl radicals. Our postulation centers on the SO<sub>4</sub> radical anion's capacity to initiate polymerization and subsequently engage in gelation with a crosslinking agent. The ultimate structural configuration emerging from this complex interplay is meticulously presented as our final outcome, chosen from among 11 distinct possible structures. Additionally, we scrutinize the superoxide anion, another radical generated through APS decomposition. In the initial stages, we facilitate its interaction with water, and then introduce our aforementioned final structure. This conjuncture is meticulously documented in Figures 69-72.

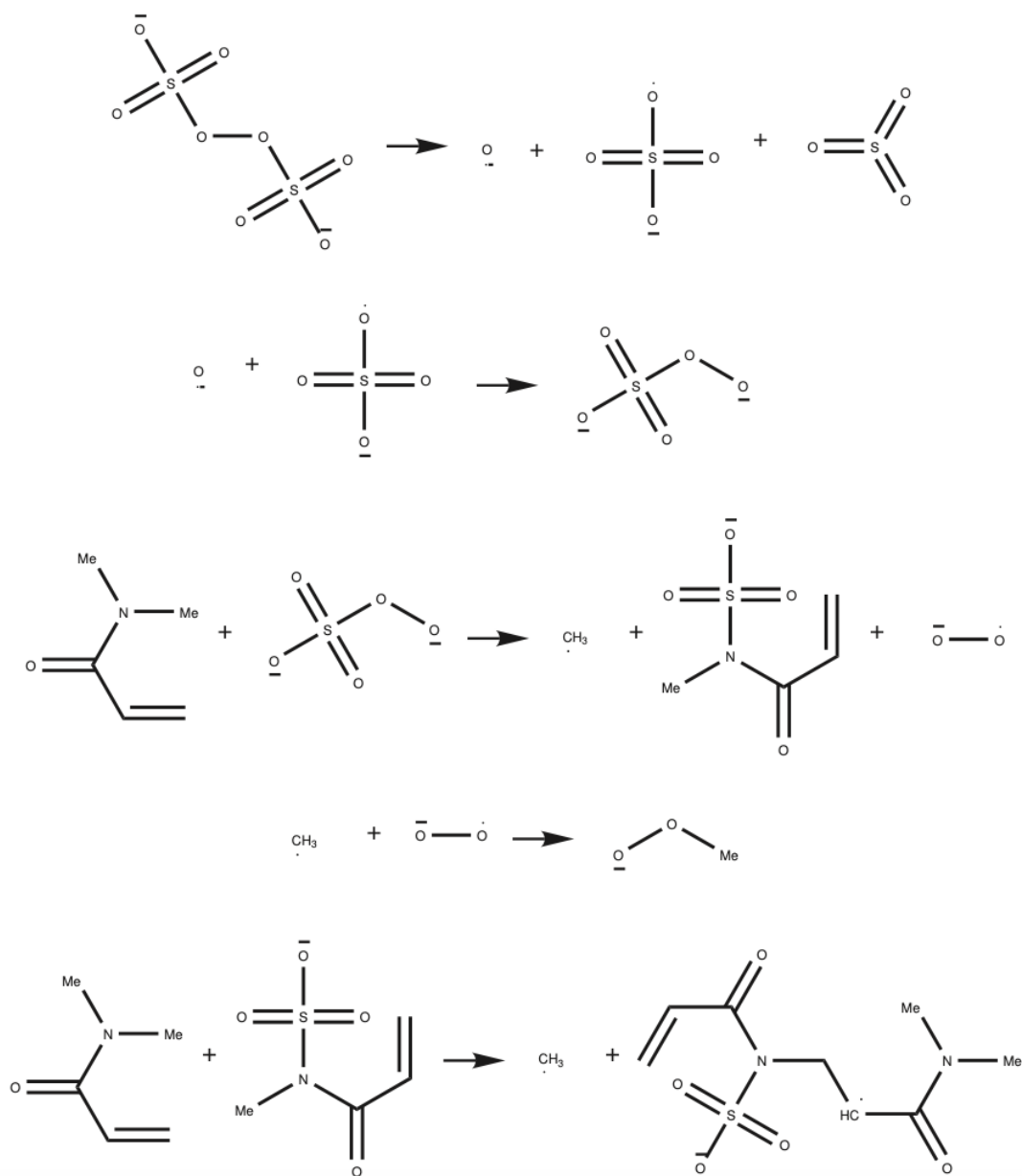


Figure 36: In all mechanisms within Group A, these reactions commence with the decomposition of Ammonium Persulfate (APS) into Sulfur trioxide, sulfate radical anion ( $\text{SO}_4^{\cdot-}$ ), and oxygen radical anion. These species subsequently combine to form Peroxymonosulfate. Notably, this peroxymonosulfate initiator deviates from real-world behavior, as it initiates reactions by attacking the methyl group of monomers, a phenomenon unlikely to occur in reality.

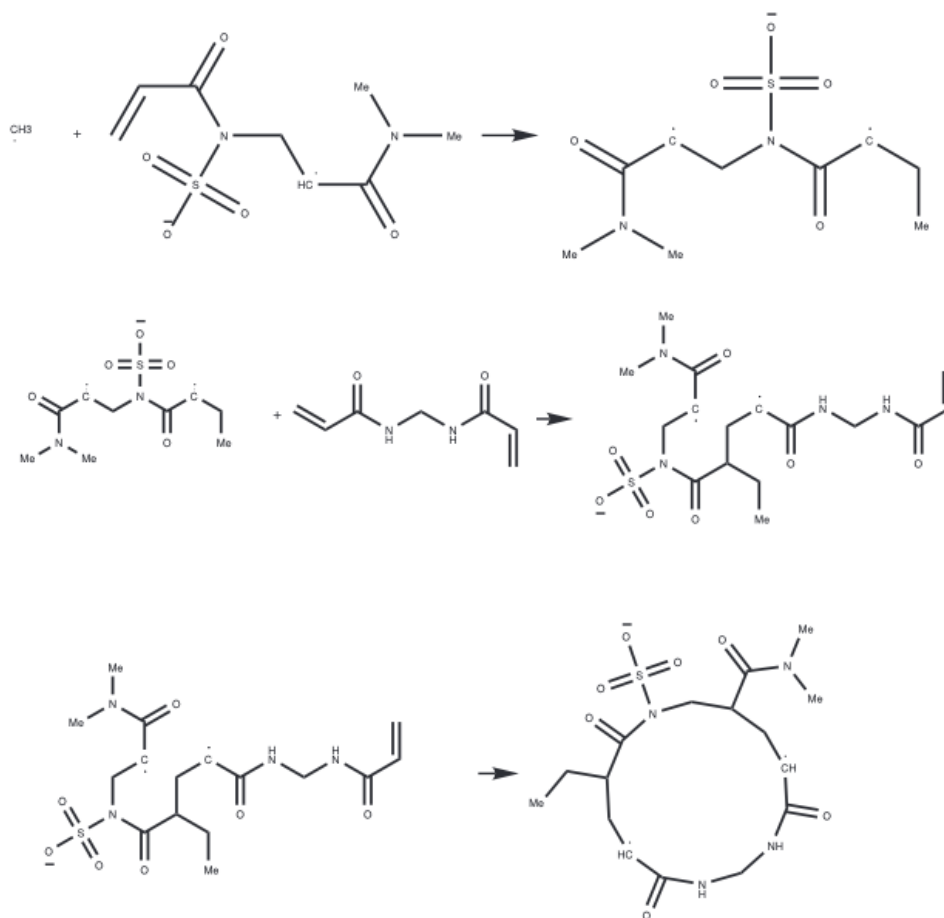


Figure 37: In the final stages of the previous example's reactions, two monomers come together, allowing the crosslinker to establish connections. Notably, in the absence of adding more monomer units to the system, a unique situation arises where two radicals reside within a single structure, potentially suggesting insight into ring-like termination mechanisms, although such events may be uncommon in practice.

## S7 Additional Experimental Test

### S7.1 Relaxation Time

A relaxation test was performed at 150 mm displacement for 20 hours and as seen in Fig. 73, Force gradually and steadily increases to 0.2 N and is dissimilar from typical solid materials' stress relaxation curves. As the time increases, it also decreases in stress-bearing capacity[32, 33, 34]. Water removal from PDMA hydrogel enhances mechanical properties. Stepwise stress relaxation revealed 5 steps with high- and low-stress regions. For example, the highest points are (0.11N at 3410 Sec) and (0.210 N at 63480 Sec), and the lowest points are (0.09N at 11550Sec) and (0.171 N at 64210 Sec) for steps 1 and 5, respectively. Moreover, stress-bearing was increased from almost 3.3 KPa at 3410 Sec to 7 KPa at 71880 Sec[35]. The reason may be that incremental random coils opened in 20 hours, numerous hydrogen bonds formed between polymer chains placed in close vicinity to each other as a result of the drying effect, and the time sweep experiment suggested stronger force-bearing capacity. This behavior is especially appealing for applications that need a material to stay intact under constant strain. At around 16-17 hours, most of the excess free water was removed and a steep step increase in stress was obvious, indicating an increase in stress at constant strain due to the sudden increase in intermolecular hydrogen bonds.

### S7.2 Storage and Loss Modulus ( $G'$ and $G''$ )

Previous works[36, 37] have studied hydrogels' rheological properties. Dynamic mechanical analysis in shear mode reveals an increasing trend in storage modulus or  $G'$ , at frequencies above 10 Hz, and Fig. 74 depicts its strong elastic

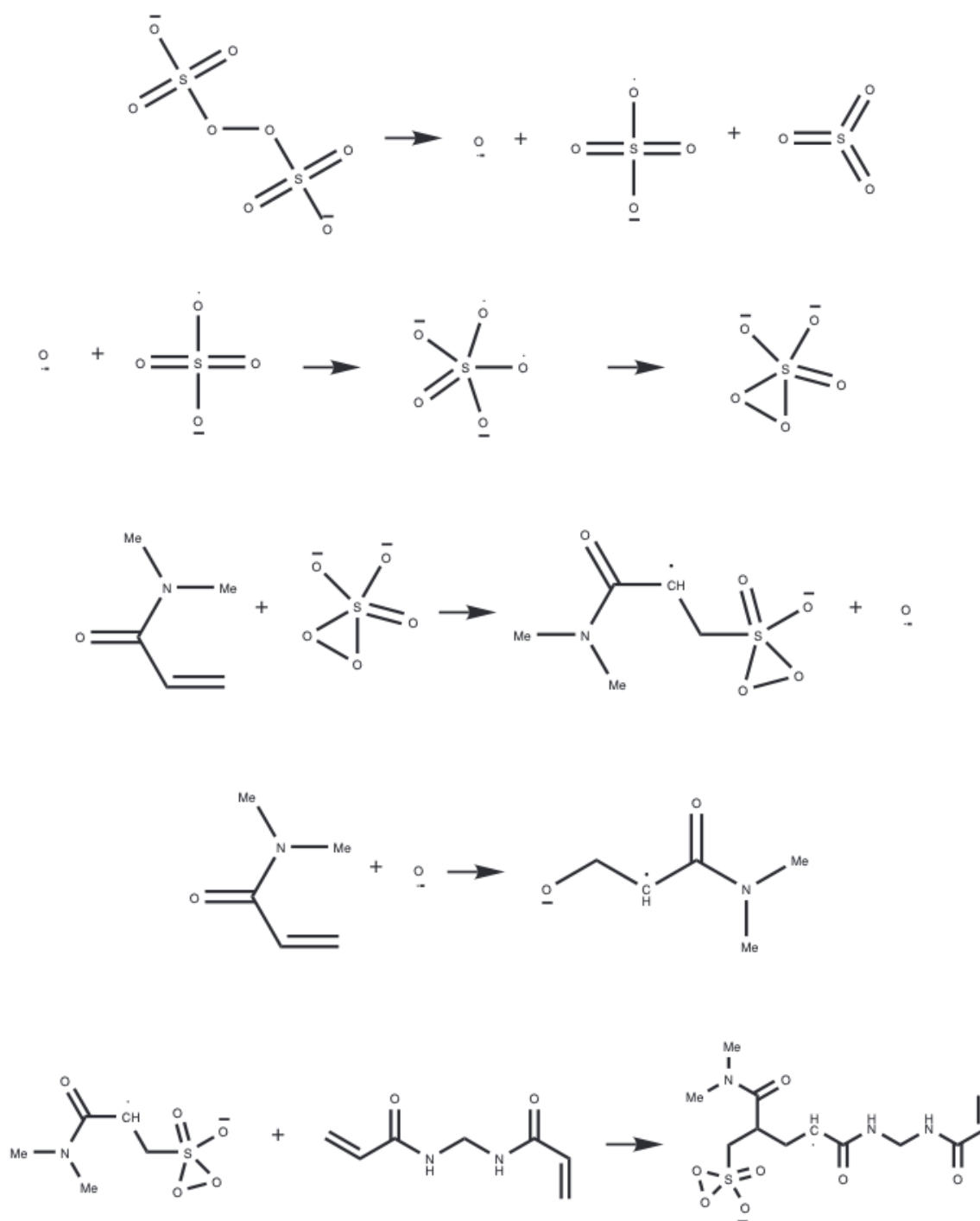


Figure 38: In an example from Group B, the initial decomposition of ammonium persulfate (APS) mirrors that of Group A. However, the subsequent reaction gives rise to a distinctive occurrence, as the sulfate radical anion ( $\text{SO}_4^{\cdot-}$ ) and oxygen radical anion combine to form a rarely reported  $\text{SO}_5$  structure. This  $\text{SO}_5$  species initiates the reaction by attacking the monomer's double bond head, setting in motion polymerization growth. Notably, this mechanism shows cases an unconventional pathway where the  $\text{SO}_5$  structure is instrumental in initiating reactions and can even engage with crosslinkers as the process advances.

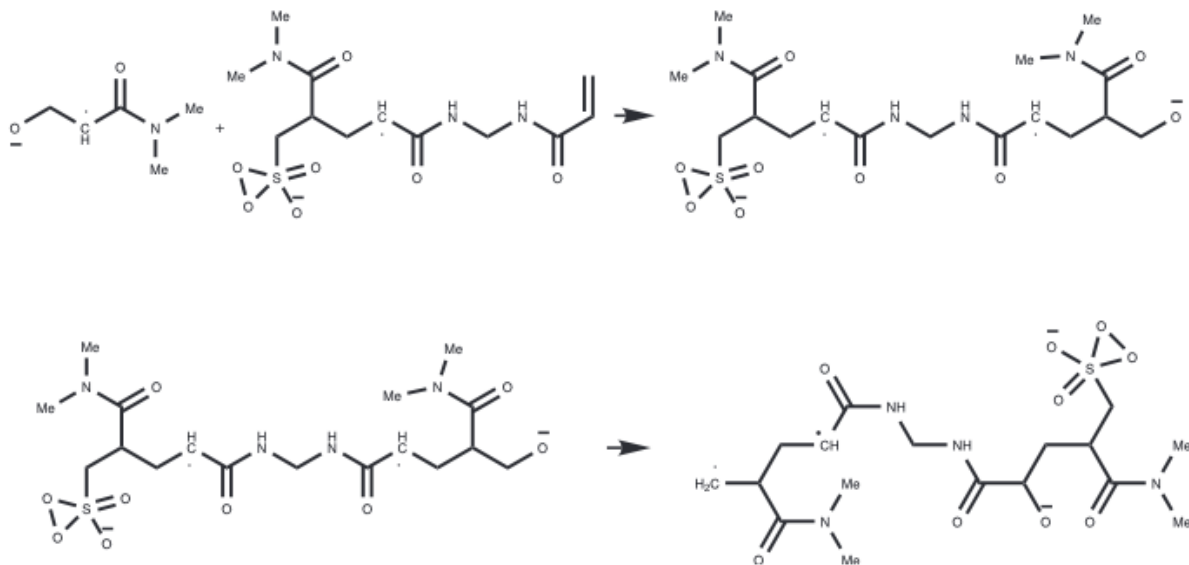


Figure 39: The final two reactions from the previous Group B example produce a unique scenario where two monomers, one activated by SO<sub>5</sub> and the other by Oxygen, interact with a crosslinker, resulting in the formation of a semi-gel structure. Importantly, this semi-gel structure contains two radicals, offering the potential for further growth. In the absence of additional monomers, the mechanism's final step rearranges radicals, optimizing their access to other components within the system.

behavior up to 2500 pa at around 20 Hz. The viscoelastic hydrogel sample at high frequency tends to behave more like an elastic material, and the disruption of physical crosslinks fails to give the slow-responding viscous components time to respond to fast-oscillating shear stress. At higher frequencies, disrupted molecular networks lag behind the physical crosslinks' elastic behavior and specifically intensify at around 10 Hz. This behavior may imply either the viscous components' large contribution at low frequencies or the extent of physical crosslink formation and microstructure rearrangement at high frequencies. Moreover, dynamic mechanical measurement in shear mode demonstrates that when  $G'$  is larger than  $G''$ , the applied force is smaller than the molecular forces. In other words, the material has some capacity to store energy and can return, to some extent, to its initial configuration and behave as an elastic solid, although not an ideal one since some of the mechanical energy is dissipated. However, at higher applied forces, the microstructure collapses and the mechanical energy given to the material is dissipated, so that the material flows, and  $G''$  becomes larger than  $G'$ . Furthermore, since the imaginary part,  $G''$ , represents rearrangements of deformed polymer segments to maximize entropy, this is a viscous response and dissipates some of the deformation energy. A small sinusoidal deformation is not large enough to impose a significant viscous response on PDMA hydrogel and dissipate some of the deformation energy. In contrast, at large deformations such as cyclic experiments, the response may not be in the linear viscoelastic region, so the rearrangement of polymer segments causes energy dumping to intensify.

### S7.3 Dynamic Mechanical in Axial Mode ( $E'$ and $E''$ )

Prior articles have reviewed dynamic mechanical analysis in axial mode for hydrogels, and Fig. 75 reveals a contrasting result compared to the shear mode experiment, reducing  $E'$  by increasing frequency[38, 39, 40]. The discrepancy in Figure 8 may well be explained by the unique structure of entangled chains that resist movement in dynamic shear force. In the axial direction, physical crosslinkers play a major role in the static mode's large extensibility. However, in axial dynamic mode, since PEO chains are physically bonded, they start to loosen drastically in response to a steep reduction in axial storage modulus at frequencies above 12 Hz. The loss modulus in both Figures 74 and 75 don't show significant values, but the storage modulus in  $G'$  and  $E'$  suggests polymer molecules' elastic behavior and storage of some of the deformation energy. This storage at 12 Hz is 2.5 and 59 KPa for  $G'$  and  $E'$ , respectively, indicating chain slippage in the shear mode as compared to the axial one.

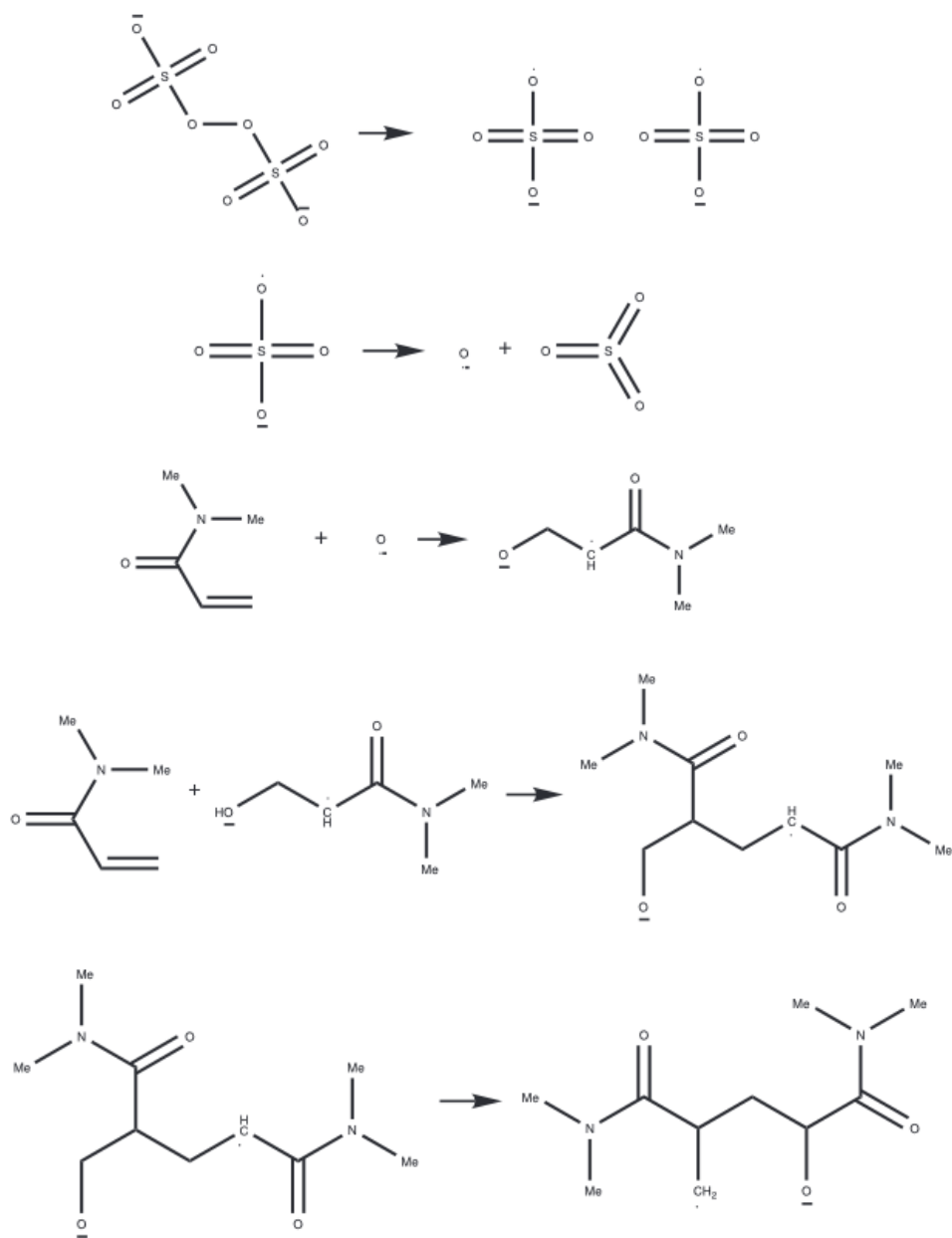


Figure 40: This example from Group C differs from the previous groups in its reaction sequence. In the initial reaction, the decomposition of ammonium persulfate (APS) yields two sulfate radical anions ( $\text{SO}_4^{\cdot-}$ ), leading to the formation of Sulfur trioxide and oxygen anion radicals. Notably, the oxygen anion radical serves as an activator, attacking the double bond and generating a radical monomer. This initiates the connection with another monomer, initiating the growth step. Importantly, the resulting dimer represents a head-to-tail configuration. In the real world, simultaneous conversion of radicals occurs among the two monomers and the crosslinker, allowing them to connect. However, due to computational limitations restricting one reaction per depth, this system emulates the real-world process by having the radical monomer interact with another monomer or crosslinker. Remarkably, the dimer's presence signifies the potential for polymerization to take place, reinforcing this mechanism's feasibility.

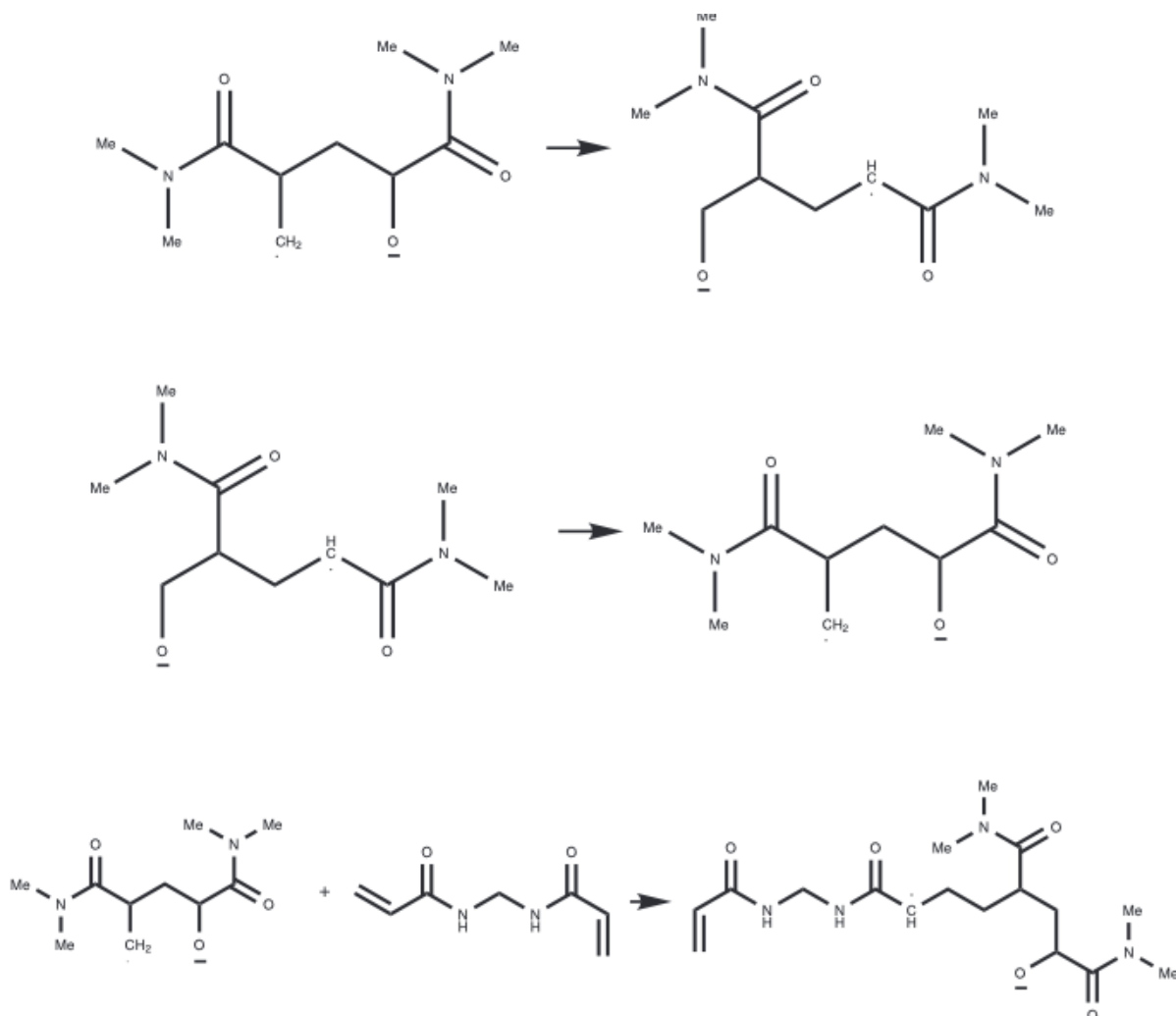


Figure 41: Concluding the previous example from Group C, this example focuses on the last three reactions. Following the rearrangement of radicals within the dimer, the crosslinker attaches to this dimer structure. Notably, the crosslinker exhibits structural symmetry, allowing initiators to potentially attach to both ends, either head or tail. This arrangement suggests the possibility of a symmetric structure forming on the other side of the crosslinkers, ultimately leading to gelation within the system.

#### S7.4 Additional Notes on Synthesis and Mechanical Test)

The monomer was polymerized at properly tuned low concentrations of initiator/crosslinker in the presence of linear polymer chains (PEO) at their excluded volume dilution to avoid either extremely soft or brittle premature breaking. A sample was drawn while the monomer was wrapped around the spatula from the hood surface to the laboratory floor; the sample showed extraordinary extensibility potential, to a magnitude that is nearly invisible (hypothetically, at their limit of extensibility a few fully elongated single chains are difficult to see by the naked eye) and left there for few weeks.

Random coil retraction to the original disordered equilibrium state confirmed the polymer chains' entropy transition: from order to disorder. The associated movies capture the unorthodox behaviors in the structure proposed above (supplemental movies). At extremely low concentrations, the carefully balanced amounts of initiator/crosslinker, linear polymer, and monomer create a narrow window where molecular interactions become highly precise. This precise control enables unique and unusual behaviors at the molecular level. For out-of-tune concentrations (either below or beyond values provided in the synthesis method), gradual thinning upon extension and collapsing demonstrates these effects at different angles, enabling one to grasp different aspects of molecular-level arrangement competence and its profound effect on macroscopic behaviors. Videos arranged sequentially illustrate samples of extensibility, low

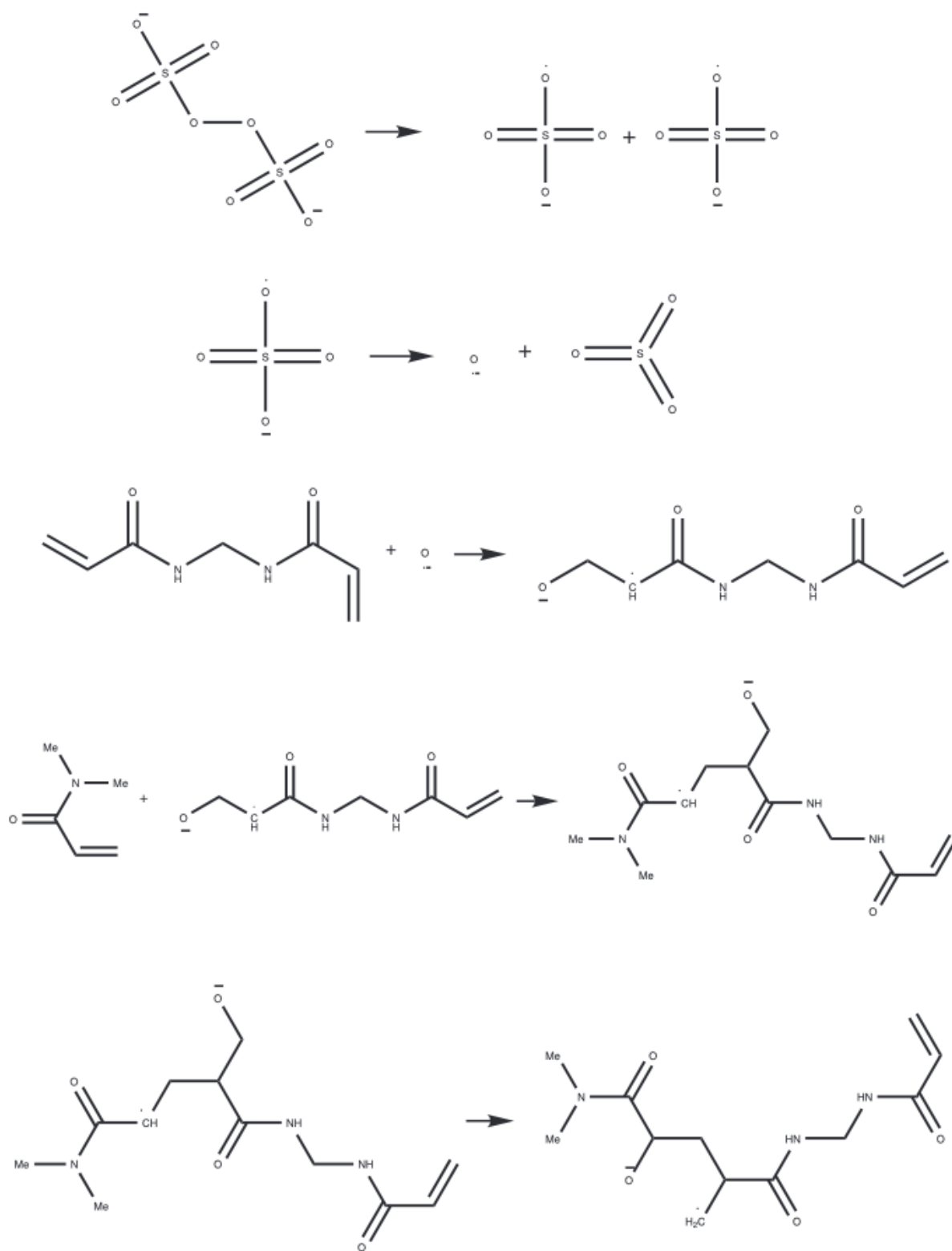


Figure 42: This third example from Group C undergoes the same decomposition reactions. In this scenario, the oxygen anion radical initiates the reaction by attacking the crosslinker, subsequently attaching to a monomer. This observation aligns with the observation discussed earlier: that initiators can simultaneously interact with other components. As a result, the other side of the crosslinker can connect to a different chain, culminating in the formation of a gel-like structure comprising two chains interconnected via the crosslinker.



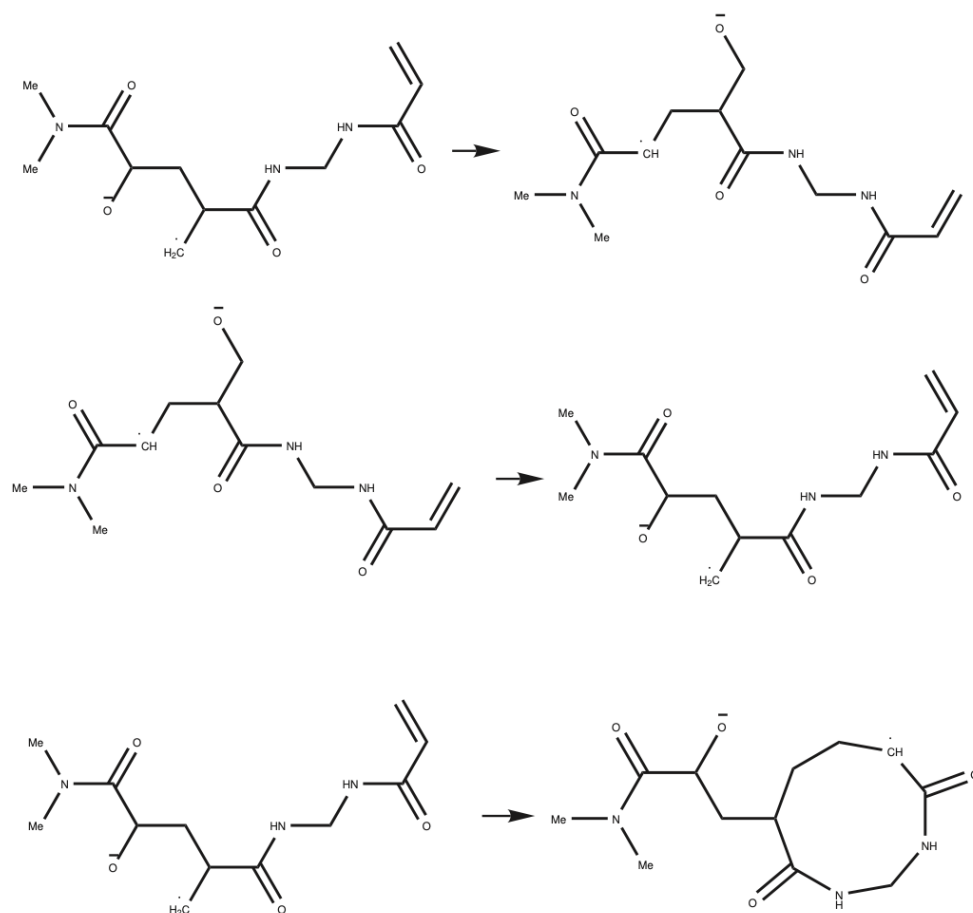


Figure 43: This example depicts the concluding three reactions from the previous example in Group C. The final step shows that in addition to the initiator attacking the tail of the crosslinker, an alternative mechanism becomes apparent. This mechanism transforms a radical from the head to the tail of the crosslinker structure, providing an opportunity for connection to another chain. However, due to the absence of added monomers in the final step, the radical can revert to the other side of the crosslinker, potentially leading to the formation of a ring structure, which is considered a feasible outcome.

extensibility, and non-extensibility (for deviation from a narrow range of concentration implemented in the synthesis method). Retraction at a slow pace confirms thermodynamically driven phenomena.

## References

- [1] Jeong-Yun Sun, Xuanhe Zhao, Widusha RK Illeperuma, Ovijit Chaudhuri, Kyu Hwan Oh, David J Mooney, Joost J Vlassak, and Zhigang Suo. Highly stretchable and tough hydrogels. *Nature*, 489(7414):133–136, 2012.
- [2] Anthony Atala, Robert Lanza, Tony Mikos, and Robert Nerem. *Principles of regenerative medicine*. Academic press, 2018.
- [3] Wen Zhao, Xing Jin, Yang Cong, Yuying Liu, and Jun Fu. Degradable natural polymer hydrogels for articular cartilage tissue engineering. *Journal of Chemical Technology & Biotechnology*, 88(3):327–339, 2013.
- [4] Takashi Iizawa, Hatsumi Taketa, Makoto Maruta, Takashi Ishido, Takehiko Gotoh, and Shuji Sakohara. Synthesis of porous poly (n-isopropylacrylamide) gel beads by sedimentation polymerization and their morphology. *Journal of applied polymer science*, 104(2):842–850, 2007.
- [5] Libo Yang, James S Chu, and Joseph A Fix. Colon-specific drug delivery: new approaches and in vitro/in vivo evaluation. *International journal of pharmaceuticals*, 235(1-2):1–15, 2002.

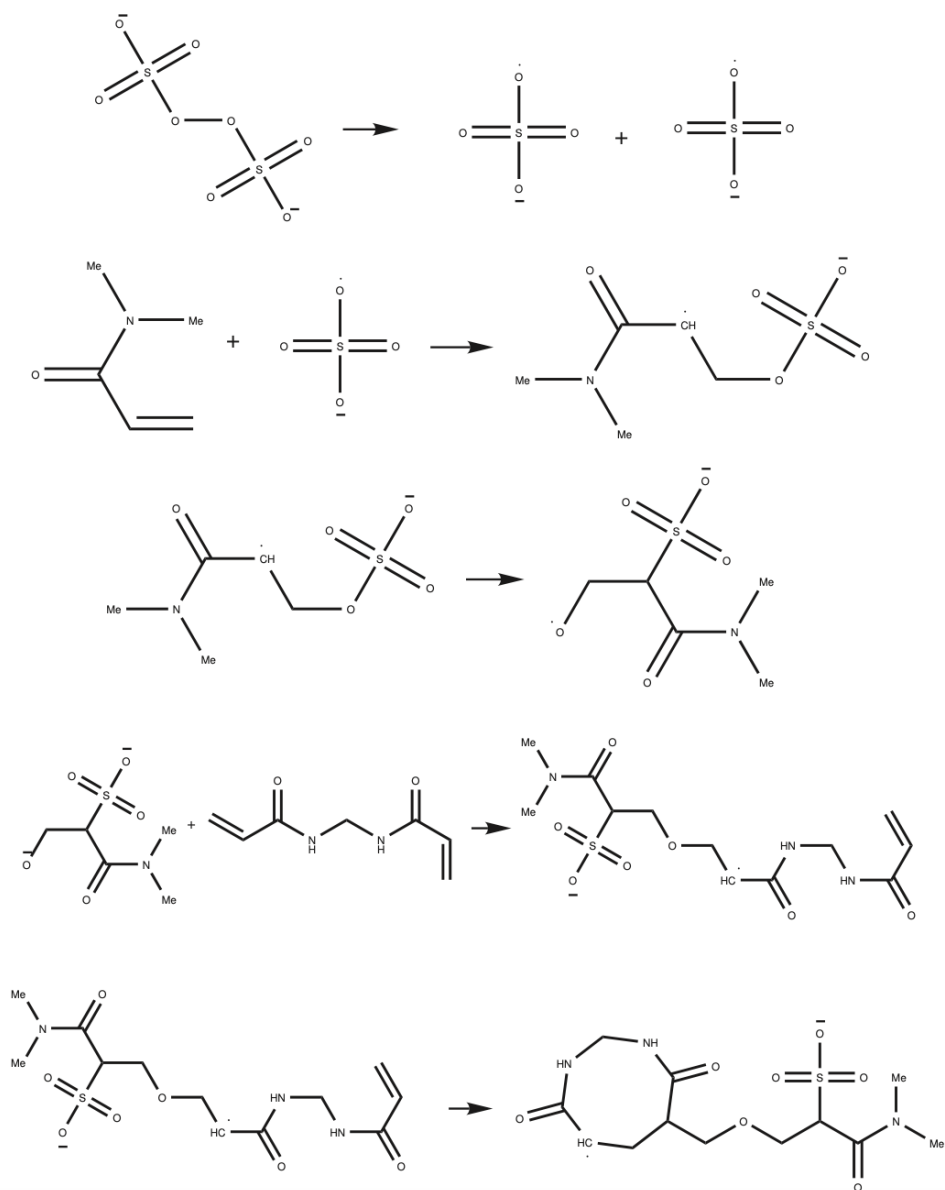


Figure 44: In this example from Group D, the initial reaction decomposes ammonium persulfate (APS) to produce two sulfate radical anions ( $\text{SO}_4^{\cdot-}$ ). Notably, in contrast to previous mechanisms, sulfate radical anion ( $\text{SO}_4^{\cdot-}$ ) directly attacks the monomer. However, in the third reaction, a distinct occurrence unfolds as sulfate radical anion ( $\text{SO}_4^{\cdot-}$ ) on the monomer interacts with two radicals on one end and  $\text{SO}_3$  on the other. This unique connection between two monomers results in the incorporation of oxygen (O) into the main chain as an ether group. Importantly, incorporation of this ether group, as indicated, does not align with the findings from FTIR (Fourier-transform infrared) spectroscopy results, suggesting a deviation from real-world behavior.

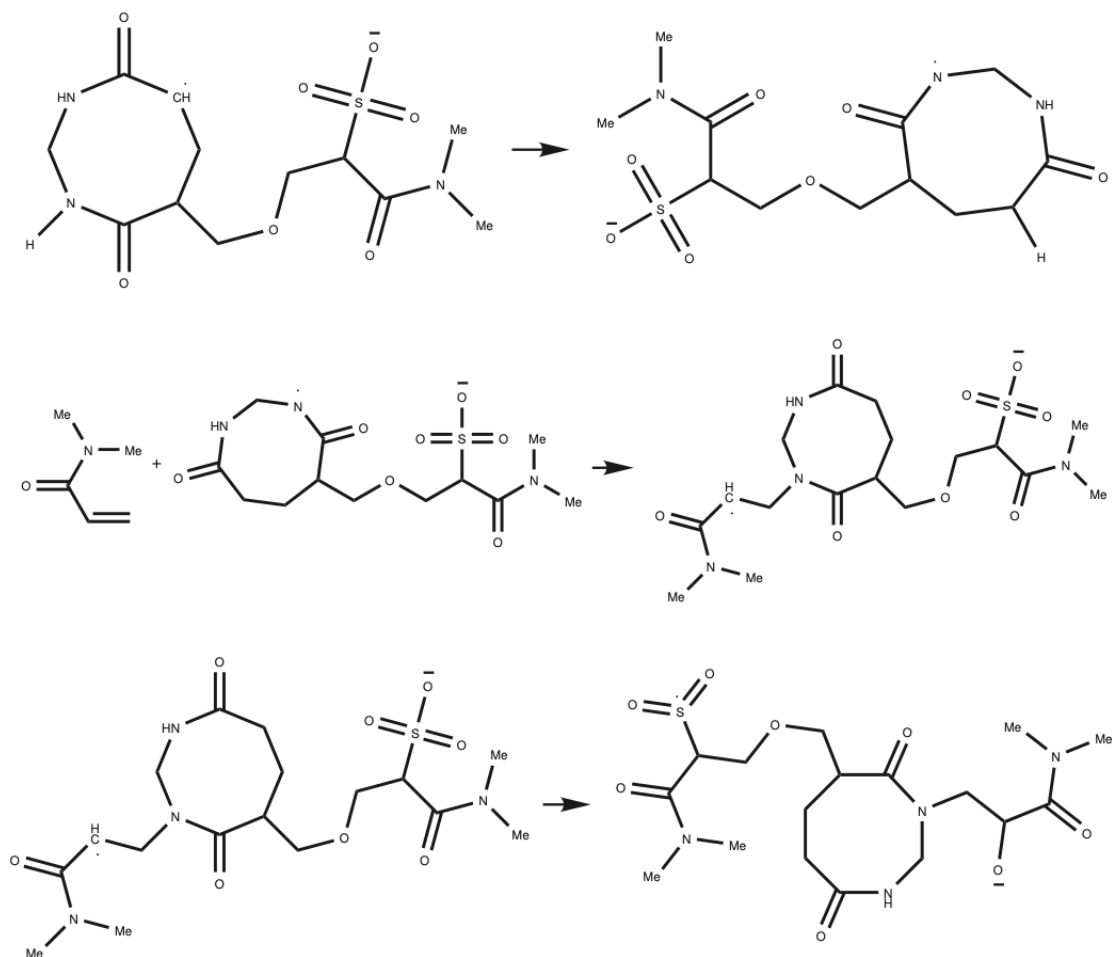


Figure 45: Here, the final three reactions within the previous example from Group D demonstrate an attempt to connect two monomers using a ring crosslinker. However, due to the presence of an ether group within the crosslinker, this connection proves infeasible, deviating from the expected outcome.

- [6] Zhai Maolin, Li Jun, Yi Min, and Ha Hongfei. The swelling behavior of radiation prepared semi-interpenetrating polymer networks composed of polynipaaam and hydrophilic polymers. *Radiation Physics and Chemistry*, 58(4):397–400, 2000.
- [7] Ecaterina Stela Dragan, Maria Marinela Lazar, Maria Valentina Dinu, and Florica Doroftei. Macroporous composite ipn hydrogels based on poly (acrylamide) and chitosan with tuned swelling and sorption of cationic dyes. *Chemical engineering journal*, 204:198–209, 2012.
- [8] Ecaterina Stela Dragan. Design and applications of interpenetrating polymer network hydrogels. a review. *Chemical Engineering Journal*, 243:572–590, 2014.
- [9] David Myung, Dale Waters, Meredith Wiseman, Pierre-Emile Duhamel, Jaan Noolandi, Christopher N Ta, and Curtis W Frank. Progress in the development of interpenetrating polymer network hydrogels. *Polymers for advanced technologies*, 19(6):647–657, 2008.
- [10] Leslie H Sperling. Interpenetrating polymer networks: an overview. 1994.
- [11] Jing Jing Wang and Fang Liu. Enhanced adsorption of heavy metal ions onto simultaneous interpenetrating polymer network hydrogels synthesized by uv irradiation. *Polymer bulletin*, 70:1415–1430, 2013.
- [12] Padmanabh Chivukula, Karel Dušek, Dong Wang, Mirka Dušková-Smrčková, Pavla Kopečková, and Jindřich Kopeček. Synthesis and characterization of novel aromatic azo bond-containing ph-sensitive and hydrolytically cleavable ipn hydrogels. *Biomaterials*, 27(7):1140–1151, 2006.

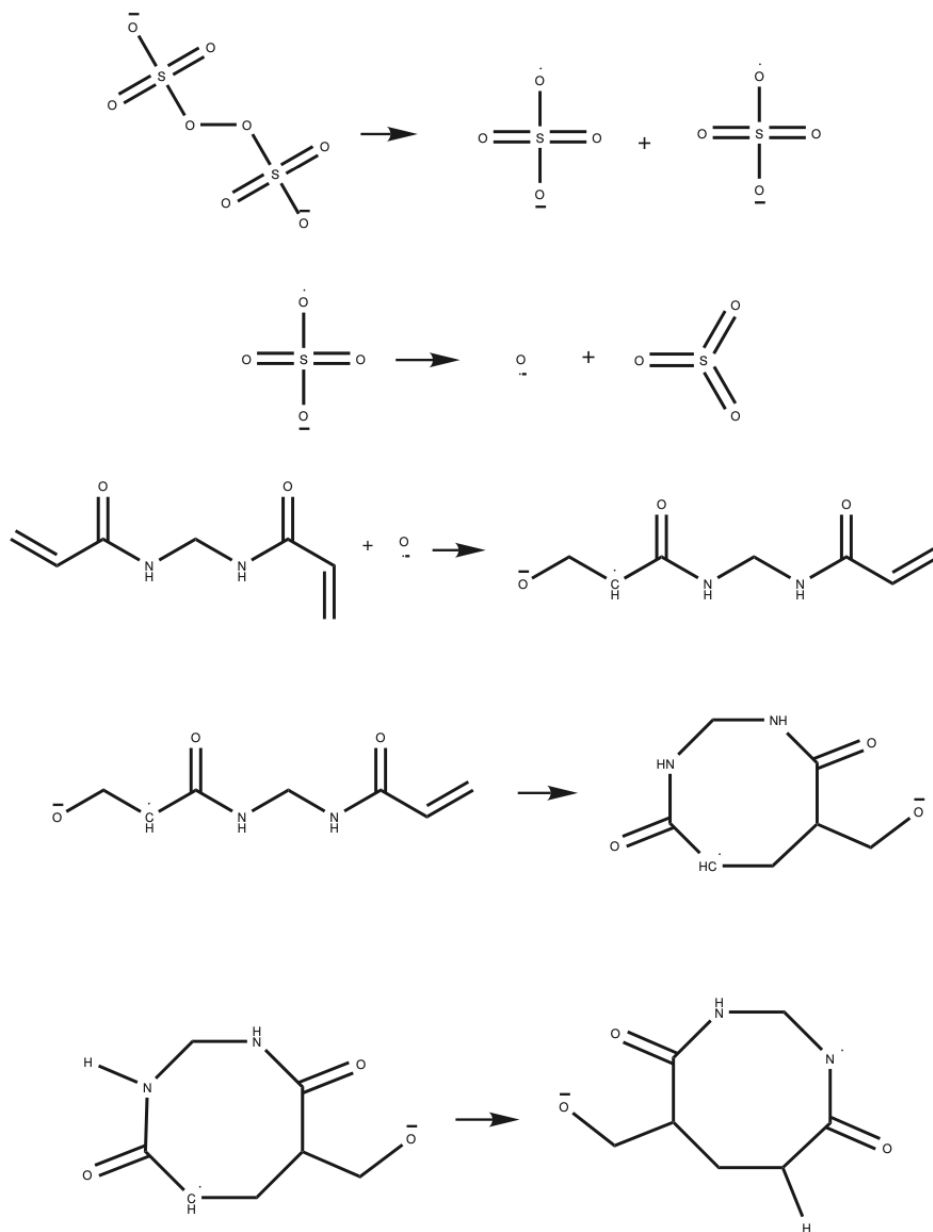


Figure 46: In a remarkable case from Group C, an intriguing sequence of reactions unfolds. Initially, the oxygen radical anion attacks the crosslinker, leading to subsequent interactions between the crosslinker and a monomer. Notably, this unique scenario results in the formation of a ring structure, an outcome that adds an interesting dimension to the reaction mechanisms.

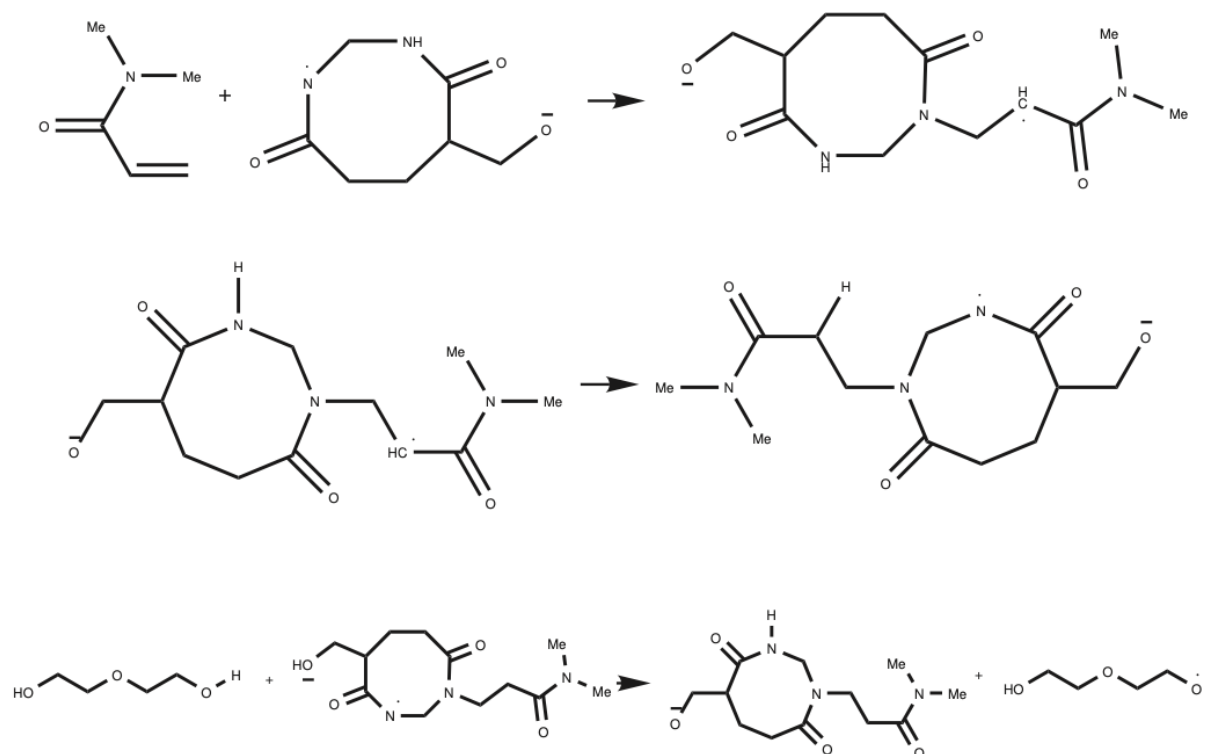


Figure 47: The final three reactions of the previously observed rare mechanism demonstrate that after attacking the monomer, the radical on the head of the monomer may transfer to one of the crosslinker's nitrogen atoms. This nitrogen atom, being unstable, can acquire a hydrogen (H) atom from the end group of Polyethylene Oxide (PEO). It's noteworthy that among the 188 possible mechanisms investigated in this run, PEO rarely participated in the reactions. This reaction highlights a rare instance in which PEO becomes involved by providing a hydrogen atom for activation. Across all groups, radicals are located primarily within the main chain or crosslinker, subsequently enabling interactions with PEO.

- [13] Mohammadamin Tavakoli, Pierre Baldi, Ann Marie Carlton, Yin Ting Chiu, Alexander Shmakov, and David Van Vranken. Ai for interpretable chemistry: Predicting radical mechanistic pathways via contrastive learning. *Advances in Neural Information Processing Systems*, 36, 2024.
- [14] Mohammadamin Tavakoli, Yin Ting T Chiu, Pierre Baldi, Ann Marie Carlton, and David Van Vranken. Rmechdb: A public database of elementary radical reaction steps. *Journal of Chemical Information and Modeling*, 63(4):1114–1123, 2023.
- [15] IM Borisov, RS Luksha, and ST Rashidova. Kinetic features of ammonium persulfate decomposition in aqueous medium. *Russian Chemical Bulletin*, 64:2512–2513, 2015.
- [16] Ahmedy Abu Naim, Abdulganiyu Umar, Mohd Marsin Sanagi, and Noraimi Basaruddin. Chemical modification of chitin by grafting with polystyrene using ammonium persulfate initiator. *Carbohydrate polymers*, 98(2):1618–1623, 2013.
- [17] Francisco HA Rodrigues, Cristiane Spagnol, Antonio GB Pereira, Alessandro F Martins, André R Fajardo, Adley F Rubira, and Edvani C Muniz. Superabsorbent hydrogel composites with a focus on hydrogels containing nanofibers or nanowhiskers of cellulose and chitin. *Journal of Applied Polymer Science*, 131(2), 2014.
- [18] JM Liegeois. The influence of oxygen on the decomposition of ammonium persulfate. *Bulletin des Sociétés Chimiques Belges*, 81(1):393–403, 1972.
- [19] Jorge Herrera-Ordóñez. The role of sulfate radicals and ph in the decomposition of persulfate in aqueous medium: A step towards prediction. *Chemical Engineering Journal Advances*, 11:100331, 2022.
- [20] Richard L Johnson, Paul G Tratnyek, and Reid O'Brien Johnson. Persulfate persistence under thermal activation conditions. *Environmental science & technology*, 42(24):9350–9356, 2008.

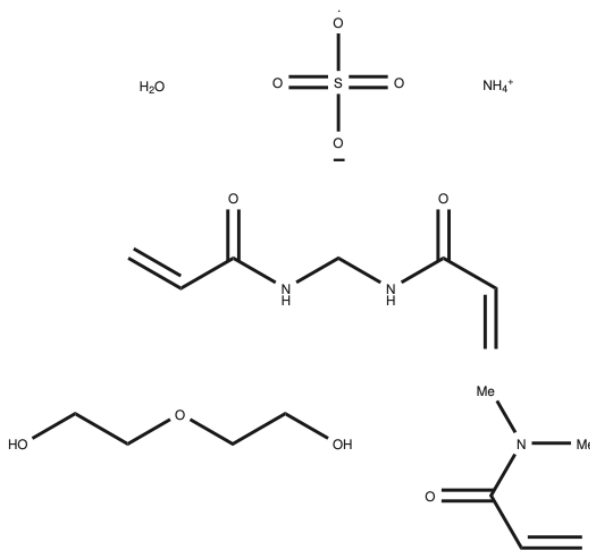


Figure 48: This figure outlines the configuration for the most probable structure run. The experimental conditions involve the presence of water as a conditioning agent, with sulfate radical anion (SO<sub>4</sub>·<sup>-</sup>) serving as the primary initiator radical. The reactants in this scenario include polyethylene oxide (PEO), N, N-Dimethylacrylamide as a monomer, and N, N'- Methylenebisacrylamide as the crosslinker. These components collectively contribute to the exploration of the most likely reaction pathways and resultant structures.

- [21] Ahmed A Oun and Jong-Whan Rhim. Effect of oxidized chitin nanocrystals isolated by ammonium persulfate method on the properties of carboxymethyl cellulose-based films. *Carbohydrate polymers*, 175:712–720, 2017.
- [22] Si-Hyun Do, Yong-Jae Kwon, Su-Jin Bang, and Sung-Ho Kong. Persulfate reactivity enhanced by fe<sub>2</sub>o<sub>3</sub>–mno and cao–fe<sub>2</sub>o<sub>3</sub>–mno composite: identification of composite and degradation of ccl<sub>4</sub> at various levels of ph. *Chemical Engineering Journal*, 221:72–80, 2013.
- [23] GR Mahdavinia, A Pourjavadi, H Hosseinzadeh, and MJ Zohuriaan. Modified chitosan 4. superabsorbent hydrogels from poly (acrylic acid-co-acrylamide) grafted chitosan with salt-and ph-responsiveness properties. *European Polymer Journal*, 40(7):1399–1407, 2004.
- [24] Yusuf Khan, Shahid Bashir, Maryam Hina, S Ramesh, K Ramesh, and Indranil Lahiri. Effect of salt concentration on poly (acrylic acid) hydrogel electrolytes and their applications in supercapacitor. *Journal of The Electrochemical Society*, 167(10):100524, 2020.
- [25] Shahid Bashir, Maryam Hina, S Ramesh, and K Ramesh. Flexible and self-healable poly (n, n-dimethylacrylamide) hydrogels for supercapacitor prototype. *Colloids and Surfaces A: Physicochemical and Engineering Aspects*, 617:126377, 2021.
- [26] Jorge Herrera-Ordóñez. New insights on the kinetics of persulfate-initiated itaconic acid free-radical polymerization. *Macromolecular Reaction Engineering*, page 2300022, 2023.
- [27] Yunxiao Liu, Lehuan Liu, Kuntao Wang, Hui Zhang, Yuan Yuan, HongXiu Wei, Xin Wang, Yongxin Duan, Lijuan Zhou, and Jianming Zhang. Modified ammonium persulfate oxidations for efficient preparation of carboxylated cellulose nanocrystals. *Carbohydrate Polymers*, 229:115572, 2020.
- [28] Gülru Kayık and Nurcan Ş Tüzün. Stereoselective propagation in free radical polymerization of acrylamides: A dft study. *Journal of Molecular Graphics and Modelling*, 49:55–67, 2014.
- [29] Jaesang Lee, Urs Von Gunten, and Jae-Hong Kim. Persulfate-based advanced oxidation: critical assessment of opportunities and roadblocks. *Environmental science & technology*, 54(6):3064–3081, 2020.
- [30] Shahriar H Emami, Ronald Salovey, and Thieo E Hogen-Esch. Peroxide-mediated crosslinking of poly (ethylene oxide). *Journal of Polymer Science Part A: Polymer Chemistry*, 40(17):3021–3026, 2002.
- [31] Baldomero Gómez-Reyes and Anatoly K Yatsimirsky. Kinetics of amide and peptide cleavage by alkaline hydrogen peroxide. *Organic Letters*, 5(25):4831–4834, 2003.

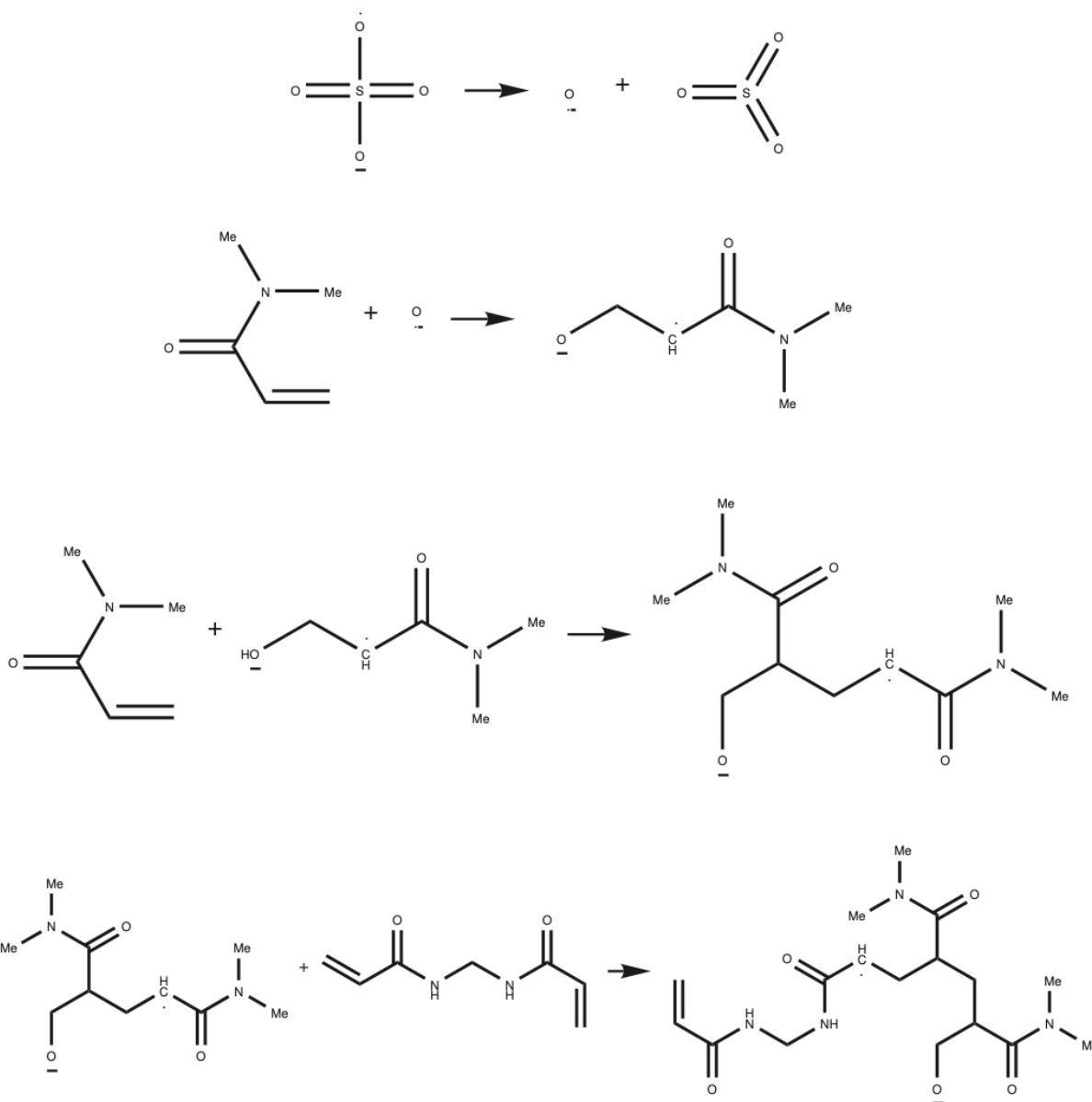


Figure 49: One of the system's most likely structural formations begins with ammonium persulfate (APS) decomposition, yielding sulfate radical anions ( $\text{SO}_4^{\cdot-}$ ). Subsequently, these  $\text{SO}_4^{\cdot-}$  radicals decompose into sulfur trioxide and oxygen anion radicals. The oxygen anion radical initiates the reaction by attacking a monomer, leading to the formation of a radical monomer. This radical monomer subsequently attaches head-to-tail to another monomer, followed by the attachment of a crosslinker to these monomers. As previously demonstrated, radicals within this structure can transfer to the crosslinker's tail and then engage with other chains. Notably, polymerization growth can occur either on these radicals or via the oxygen anion side group. The structure's symmetry enables other chains to potentially attach, contributing to the formation of a complex polymerization network.

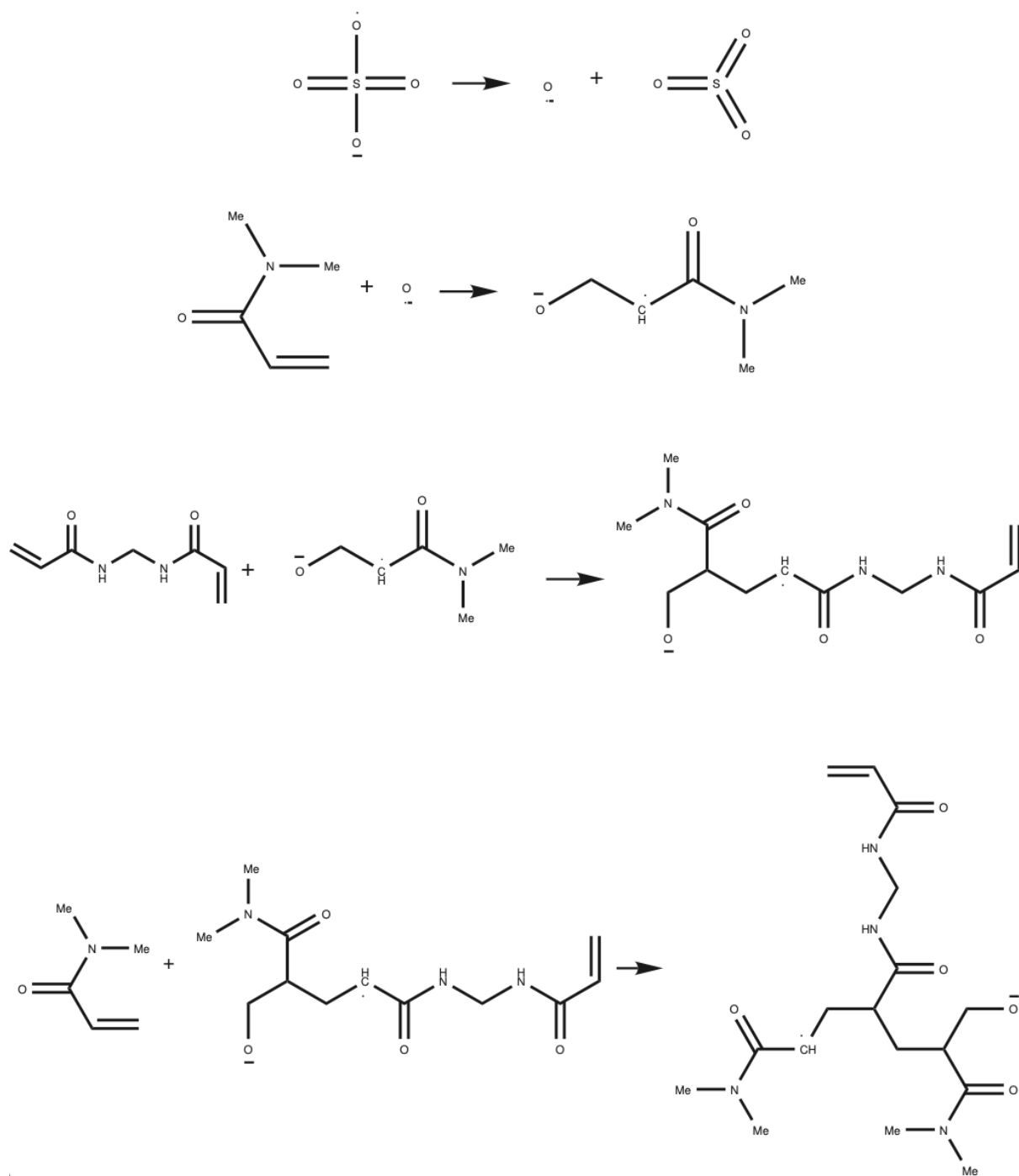


Figure 50: In the second-most likely structure based on the predictor system, the overall setup and conditions mirror those in Fig. 49. However, in this scenario, the radical monomer initiates the reaction by attacking the crosslinker. Subsequently, the reaction progresses analogously to Fig. 49, resulting in a similar complex polymerization structure. This figure illustrates the potential for multiple pathways leading to the formation of such intricate polymer networks within the system.



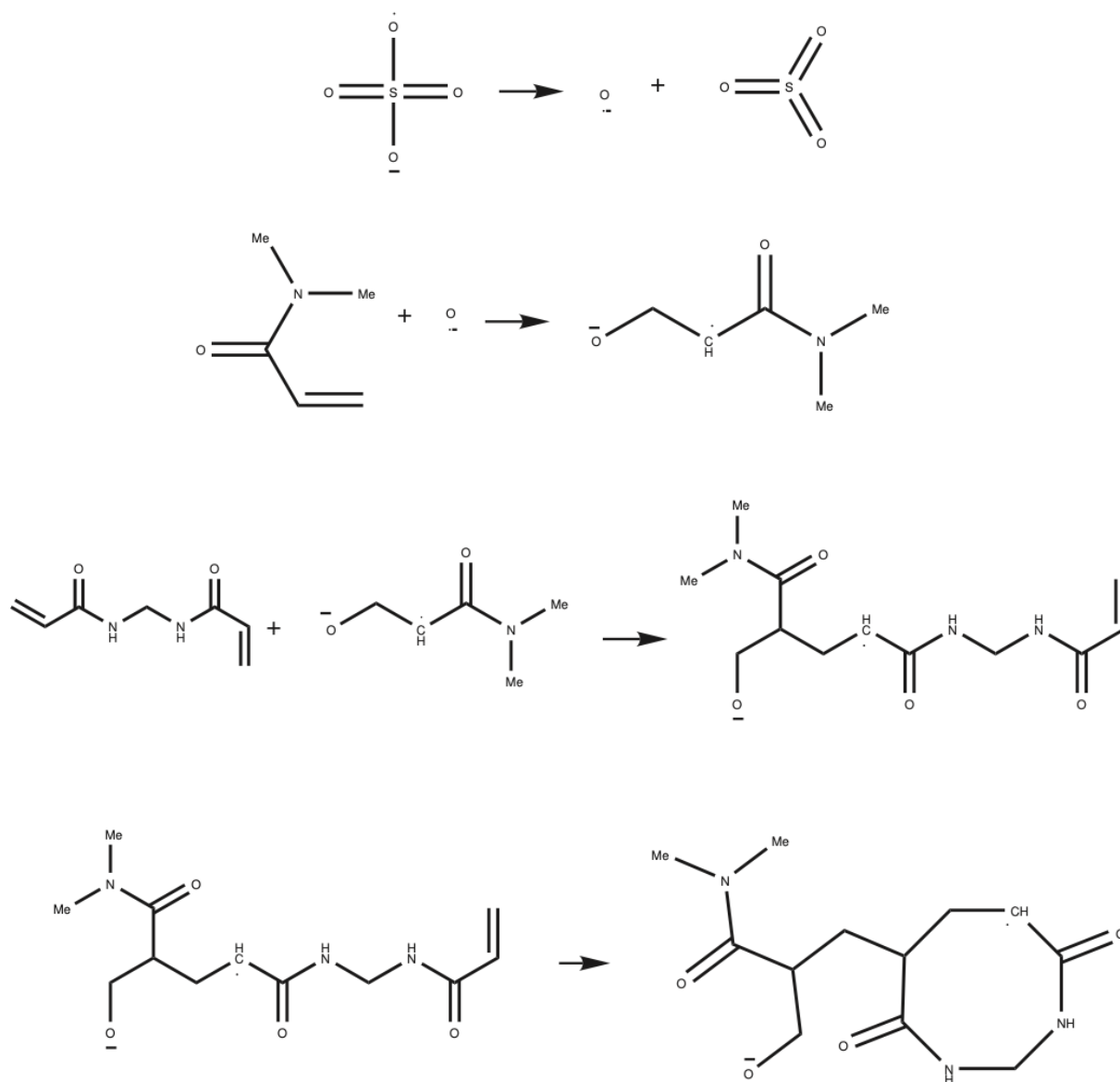


Figure 51: The third plausible mechanism begins by generating a radical monomer, which then attacks the crosslinker. In this scenario, the crosslinker subsequently reverses its attachment and forms a ring structure. This illustration emphasizes that by not advancing to the next step in the reaction, when available monomers are absent, the system has the capability to build rings rather than simply attaching radicals to each chain.

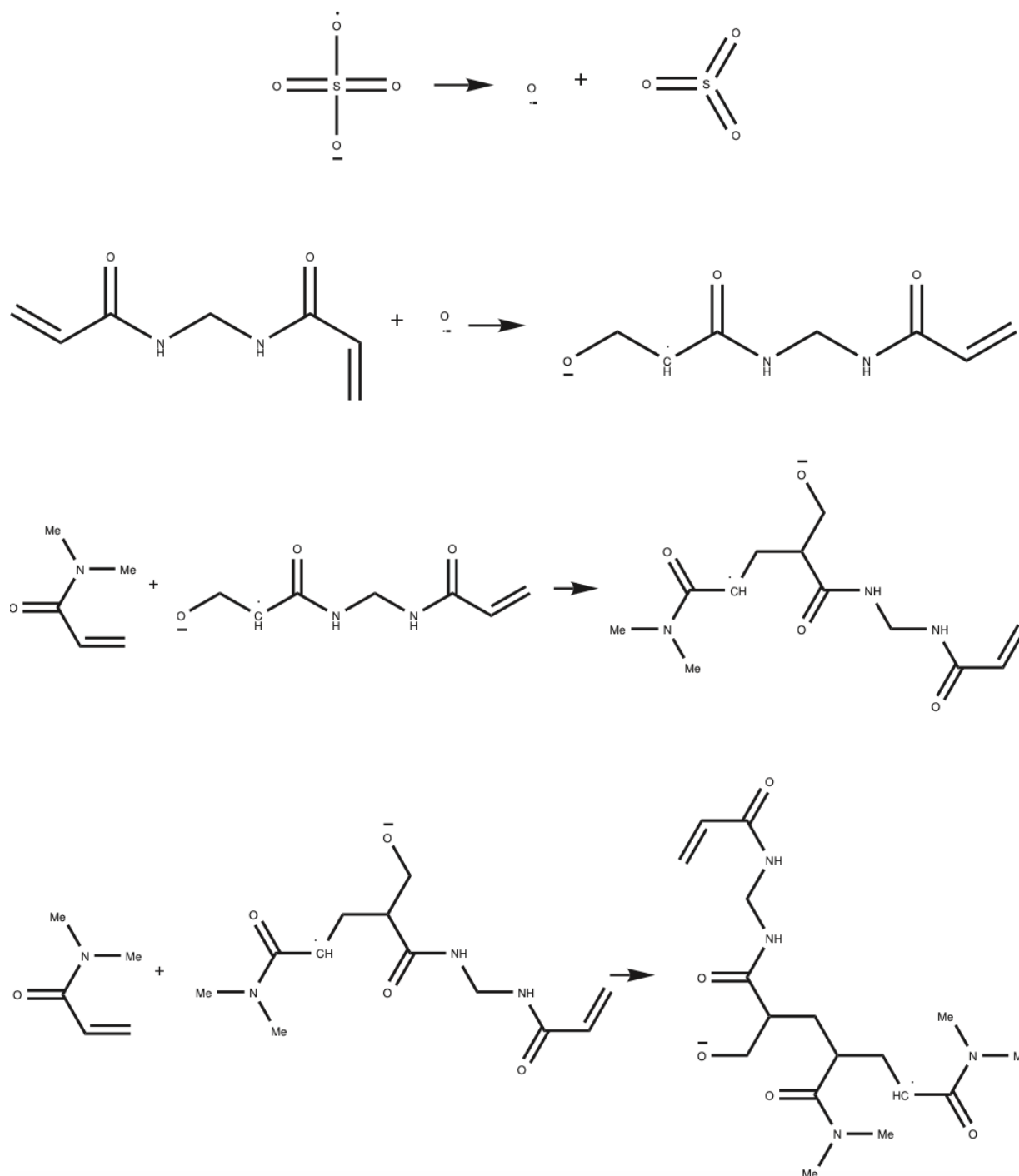


Figure 52: The other most possible final structure shares similarities with the three previous mechanisms. However, the key distinction lies in the initiation step, where the oxygen radical anion directly attacks the crosslinker instead of the monomer. This illustration highlights the system's dynamic nature, where initiator radicals can simultaneously attack both monomers and crosslinkers. Such parallel reactions within these mechanisms contribute to the formation of a three-dimensional (3D) network, exemplifying the system's versatility in producing complex structures.

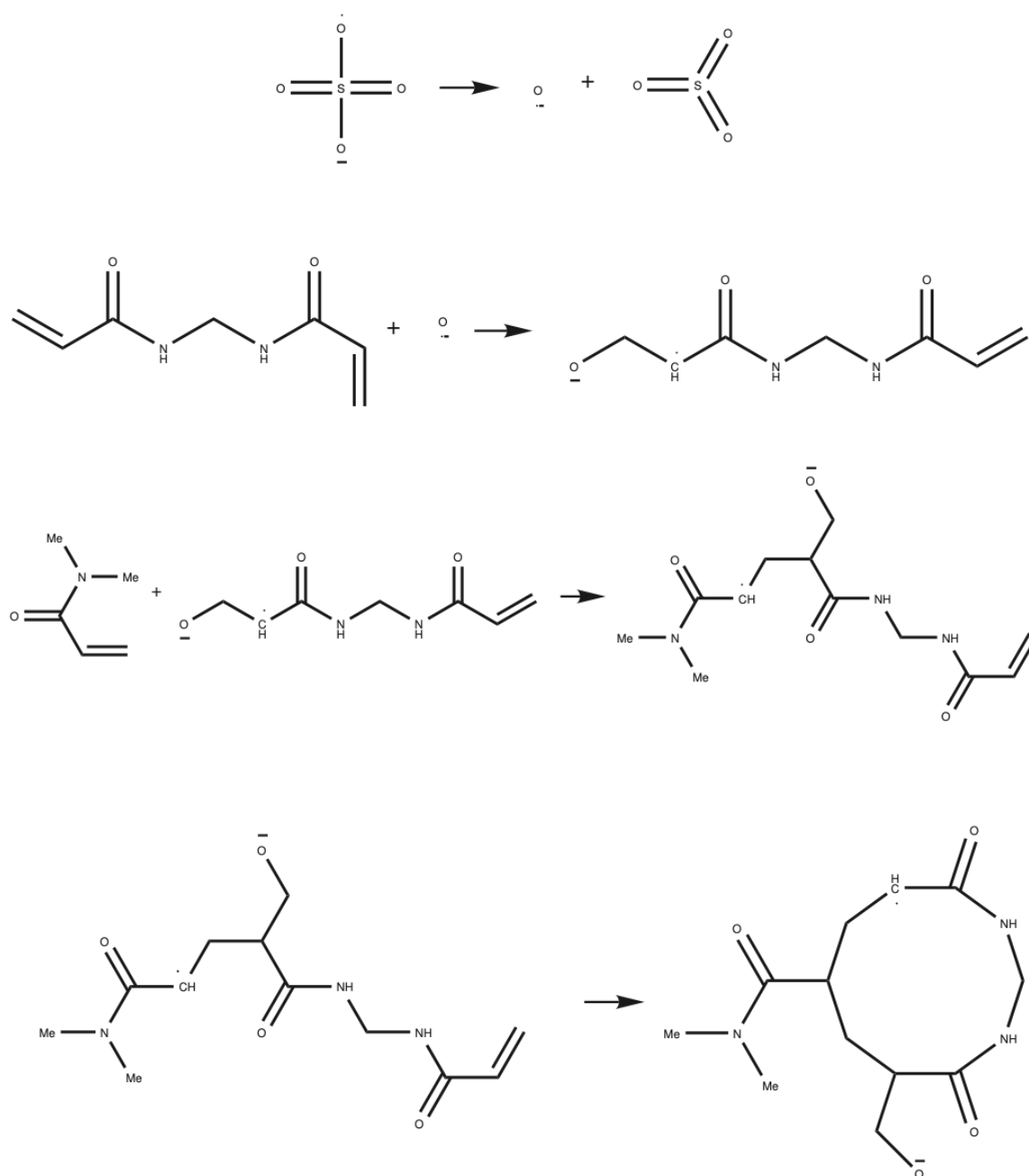


Figure 53: Another most likely mechanism shares similarities with Fig. 52. However, in this instance, the final step deviates from the previous mechanisms. Instead of the crosslinker attaching to another monomer, it forms a ring structure. This illustration emphasizes the system's ability to generate diverse structures based on slight variations in reaction pathways, showcasing its adaptability and complexity in producing intricate arrangements.

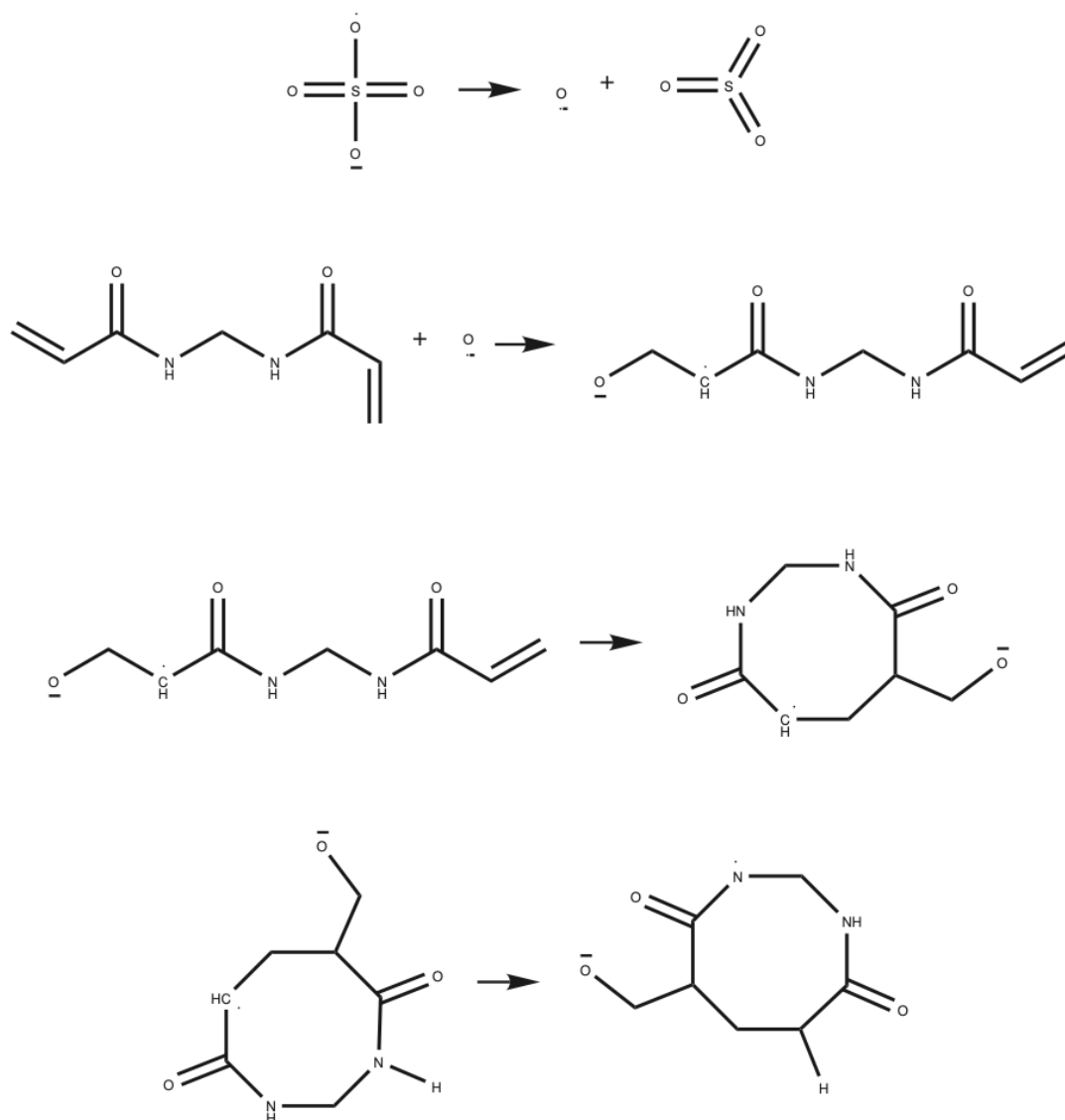


Figure 54: Here, in a distinctive prediction within the system, when the oxygen anion radical initiates by attacking the crosslinkers, the final two steps are primarily dedicated to rearrangement and the transfer of radicals on the crosslinkers. This depiction introduces a unique exception to the typical reaction pathways, highlighting the system's capacity to exhibit diverse and unexpected behaviors under specific conditions.

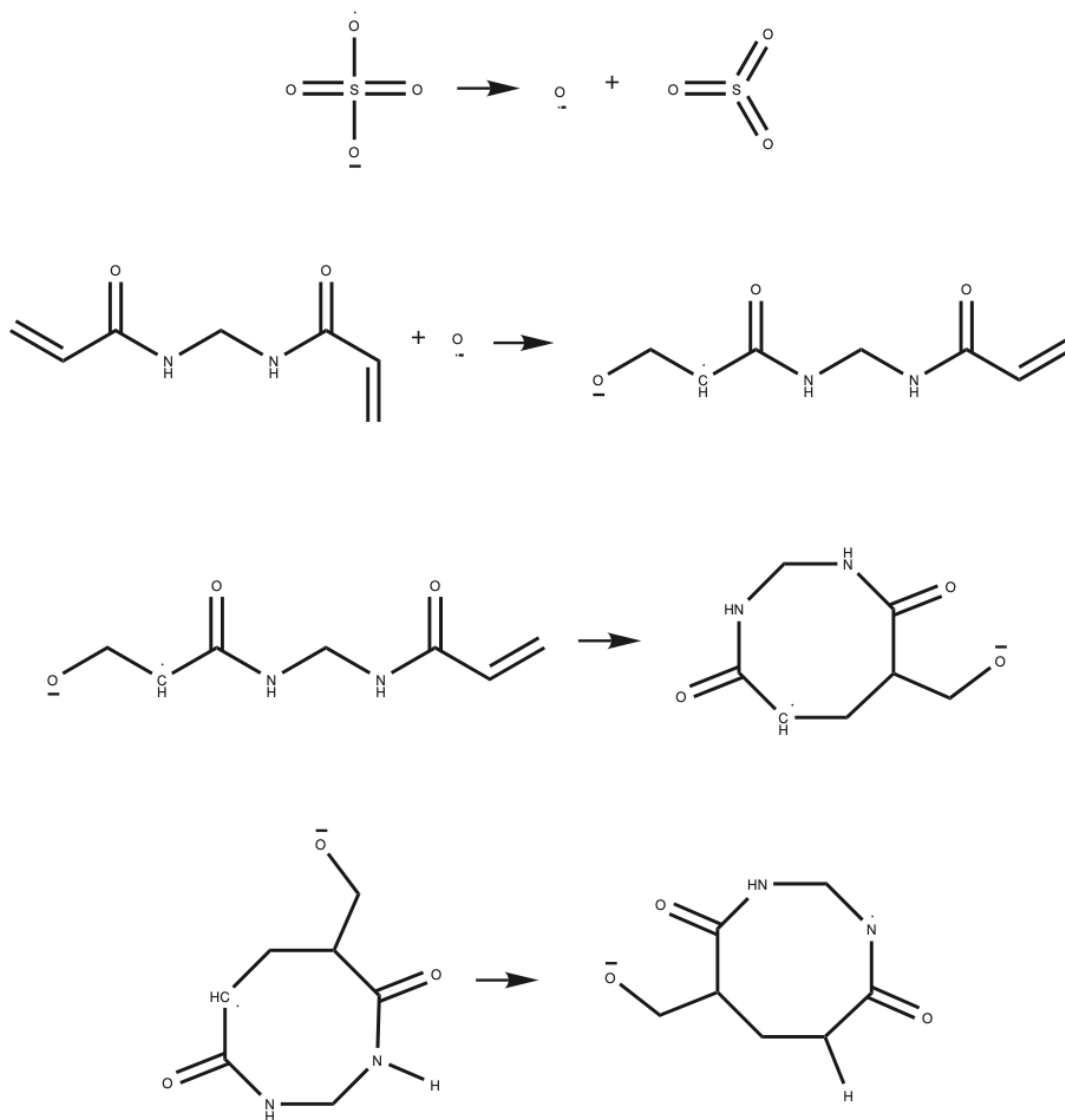


Figure 55: In a unique reaction pathway, radical transfer occurs within the crosslinker, differing from the scenario presented in Fig. 54. Specifically, the radical transfers to an alternate nitrogen atom within the crosslinker. This depiction underscores the system's potential for diverse and unexpected rearrangement patterns, adding complexity to the observed reactions.

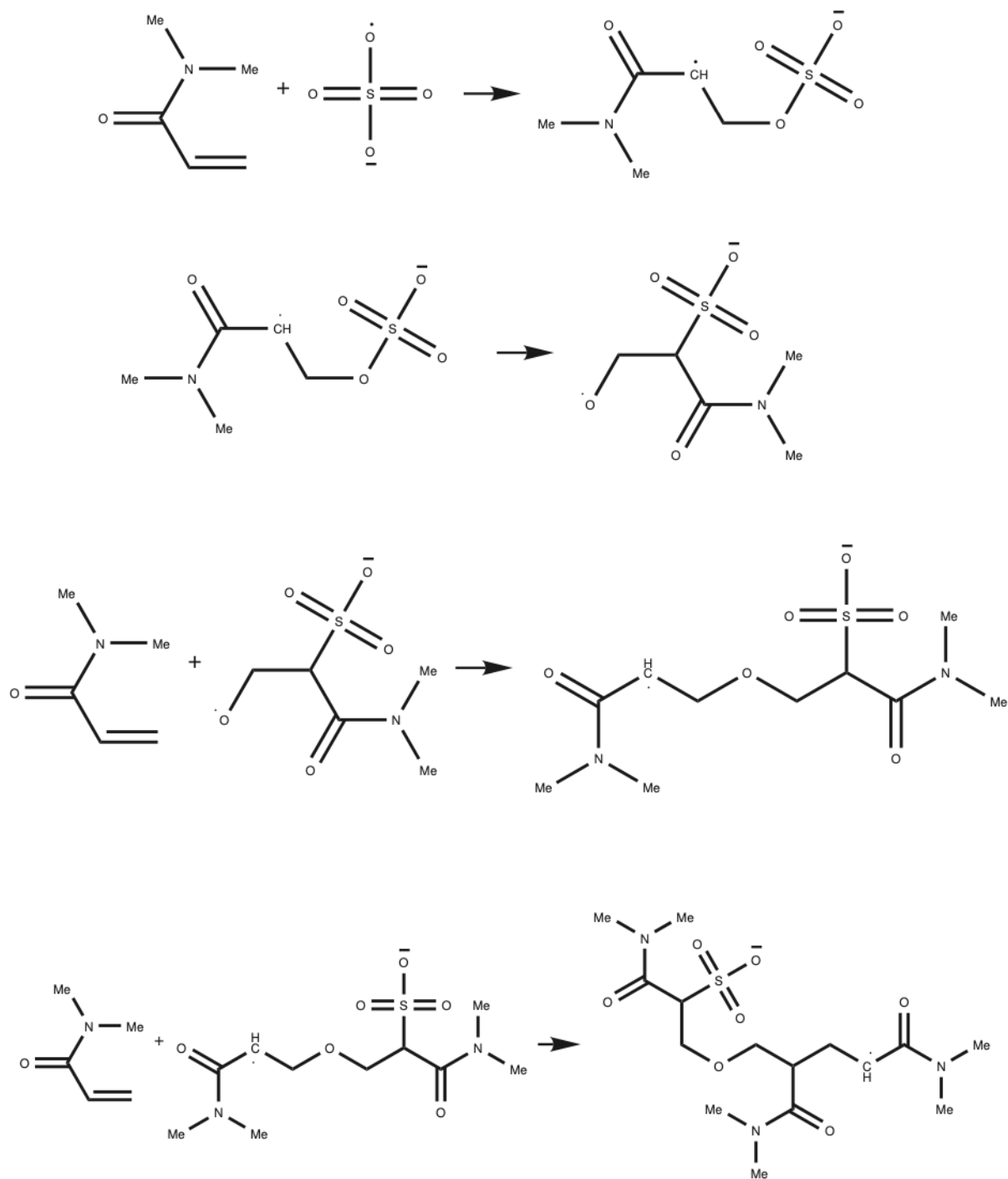


Figure 56: This unconventional reaction pathway is one of five similar cases that are mentioned in the next figures. In this instance, the sulfate radical anion ( $\text{SO}_4^{\bullet-}$ ) directly attacks the monomer, activating it in a manner that positions oxygen on the head and  $\text{SO}_3$  on the tail of the C-C double bond. Subsequently, polymerization occurs in a head-to-head fashion, accompanied by the incorporation of oxygen into the main chain, forming an ether group. This scenario leads to the formation of a trimer, where three monomers are interconnected.

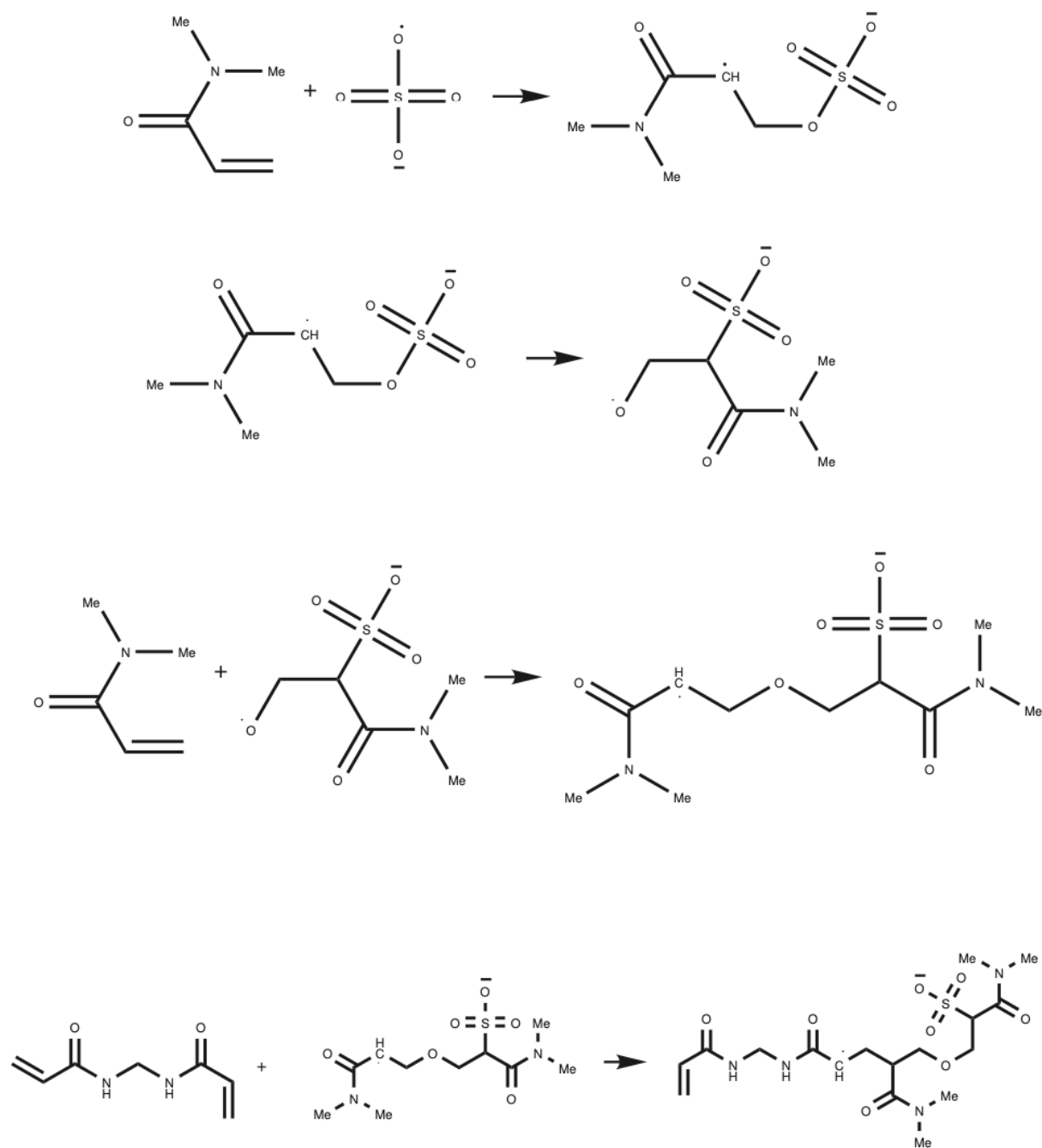


Figure 57: Here, in an atypical reaction mechanism similar to the previous case, the sulfate radical anion ( $\text{SO}_4^{\bullet-}$ ) directly attacks the monomer, initiating a chain of reactions. The radical monomer subsequently engages with another monomer, leading to the formation of a dimer, which represents a polymerization event. Importantly, this dimer includes an ether group incorporated into the main chain, although such an outcome is considered rare and may not align with observations from FTIR (Fourier-transform infrared) spectroscopy results. In the final step, the dimer further interacts with crosslinkers, adding complexity to the overall reaction pathway.

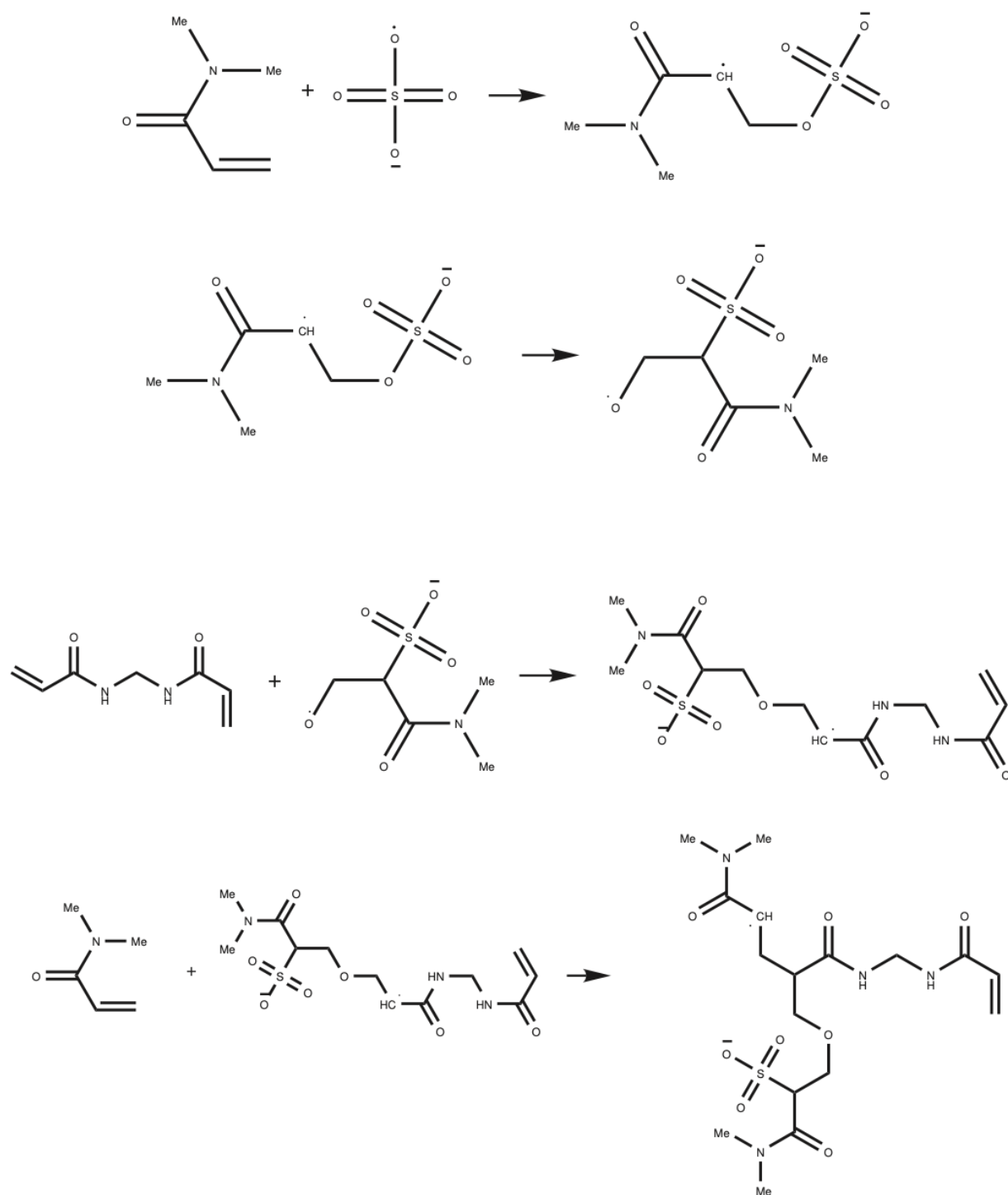


Figure 58: This unconventional mechanism is comparable to the previous cases. In this scenario, the radical monomer initiates the reaction by attacking the crosslinker. Subsequently, this activated crosslinker interacts with a monomer, resulting in a dimer formation. Notably, the connection between the monomer and the crosslinker introduces an ether group into the reaction pathway. This mechanism adds another layer of complexity, where the involvement of the crosslinker, monomer, and ether group shapes the overall reaction outcome.



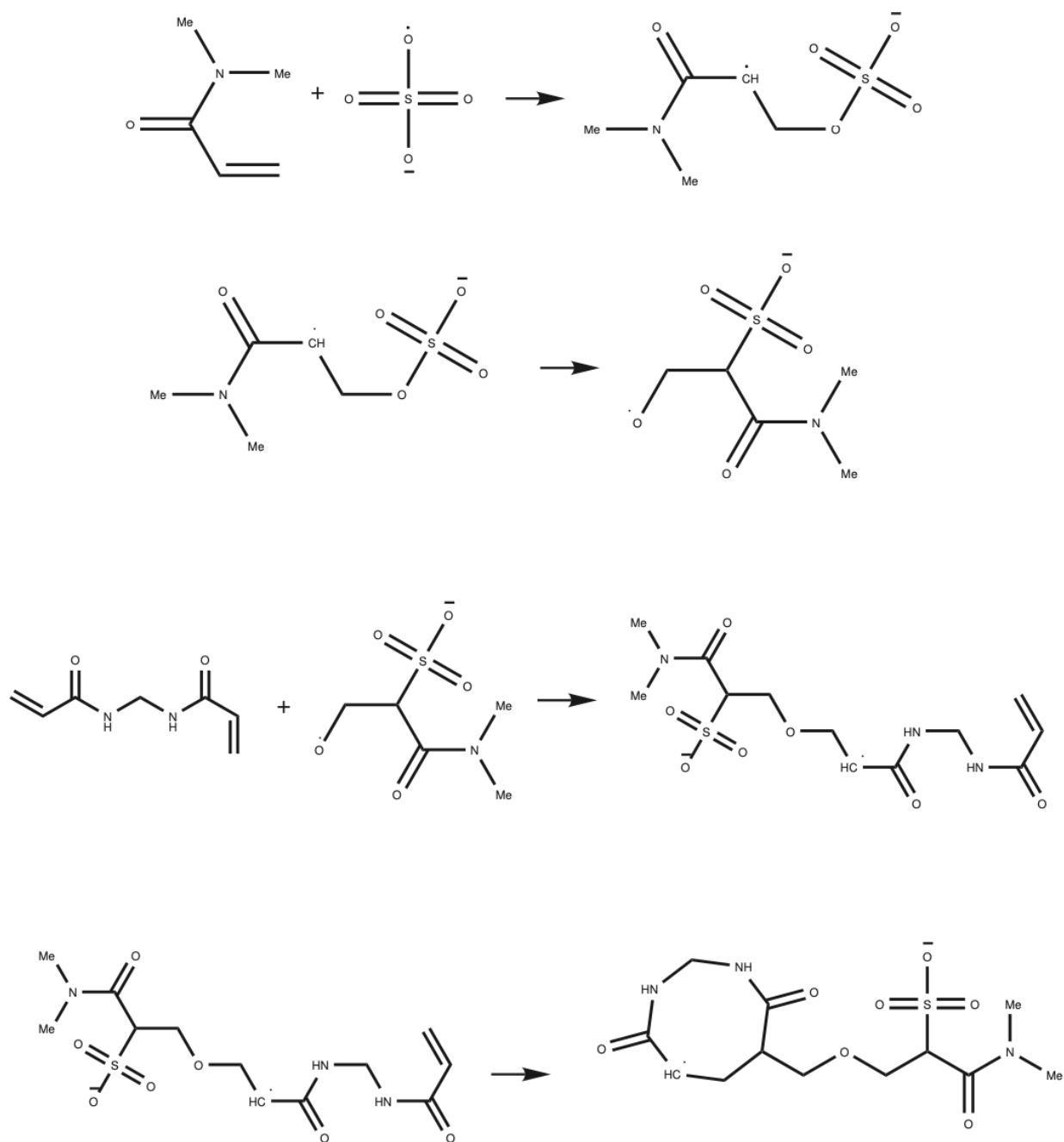


Figure 59: In this unique reaction pathway, following the monomer radical's attack on the crosslinker, the crosslinker forms a ring structure. Importantly, the presence of an ether group is a notable feature of this mechanism. This depiction highlights the system's potential to generate complex structures, including ring formations and the incorporation of ether groups, under specific conditions and pathways.

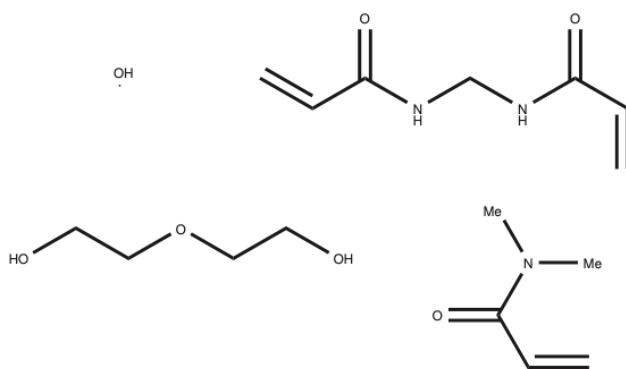


Figure 60: In this illustration of the configuration for Run Data 7, the initiation of reactions is facilitated by hydroxyl radical as the activated center. The reactants involved in this specific run include Polyethylene Oxide (PEO) as polymer, N, N-Dimethylacrylamide as a monomer, and N, N'- Methylenebisacrylamide as the crosslinker. This arrangement serves as the foundation for exploring the unique pathways and structures that arise when hydroxyl radicals initiate the reactions within this system.

- [32] Martha M Fitzgerald, Katherine Bootsma, Jason A Berberich, and Jessica L Sparks. Tunable stress relaxation behavior of an alginate-polyacrylamide hydrogel: comparison with muscle tissue. *Biomacromolecules*, 16(5):1497–1505, 2015.
- [33] Aline Bauer, Luo Gu, Brian Kwee, Weiwei Aileen Li, Maxence Dellacherie, Adam D Celiz, and David J Mooney. Hydrogel substrate stress-relaxation regulates the spreading and proliferation of mouse myoblasts. *Acta biomaterialia*, 62:82–90, 2017.
- [34] Ovijit Chaudhuri, Luo Gu, Darinka Klumpers, Max Darnell, Sidi A Bencherif, James C Weaver, Nathaniel Huebsch, Hong-pyo Lee, Evi Lippens, Georg N Duda, et al. Hydrogels with tunable stress relaxation regulate stem cell fate and activity. *Nature materials*, 15(3):326–334, 2016.
- [35] Bernard Drouin, Lucie Lévesque, Audrey Lainé, Erica Rosella, Caroline Loy, and Diego Mantovani. Viscoelastic properties of collagen hydrogels.
- [36] Lihui Weng, Xuming Chen, and Weiliam Chen. Rheological characterization of in situ crosslinkable hydrogels formulated from oxidized dextran and n-carboxyethyl chitosan. *Biomacromolecules*, 8(4):1109–1115, 2007.
- [37] Congqi Yan and Darrin J Pochan. Rheological properties of peptide-based hydrogels for biomedical and other applications. *Chemical Society Reviews*, 39(9):3528–3540, 2010.
- [38] Michael Gasik, Ana Gantar, Saša Novak, et al. Viscoelastic behaviour of hydrogel-based composites for tissue engineering under mechanical load. *Biomedical materials*, 12(2):025004, 2017.
- [39] Longxiang Zhu, Jianhui Qiu, and Eiichi Sakai. A high modulus hydrogel obtained from hydrogen bond reconstruction and its application in vibration damper. *RSC advances*, 7(69):43755–43763, 2017.
- [40] Tom KL Meyvis, Barbara G Stubbe, Mies J Van Steenbergen, Wim E Hennink, Stefaan C De Smedt, and Joseph Demeester. A comparison between the use of dynamic mechanical analysis and oscillatory shear rheometry for the characterisation of hydrogels. *International journal of pharmaceutics*, 244(1-2):163–168, 2002.

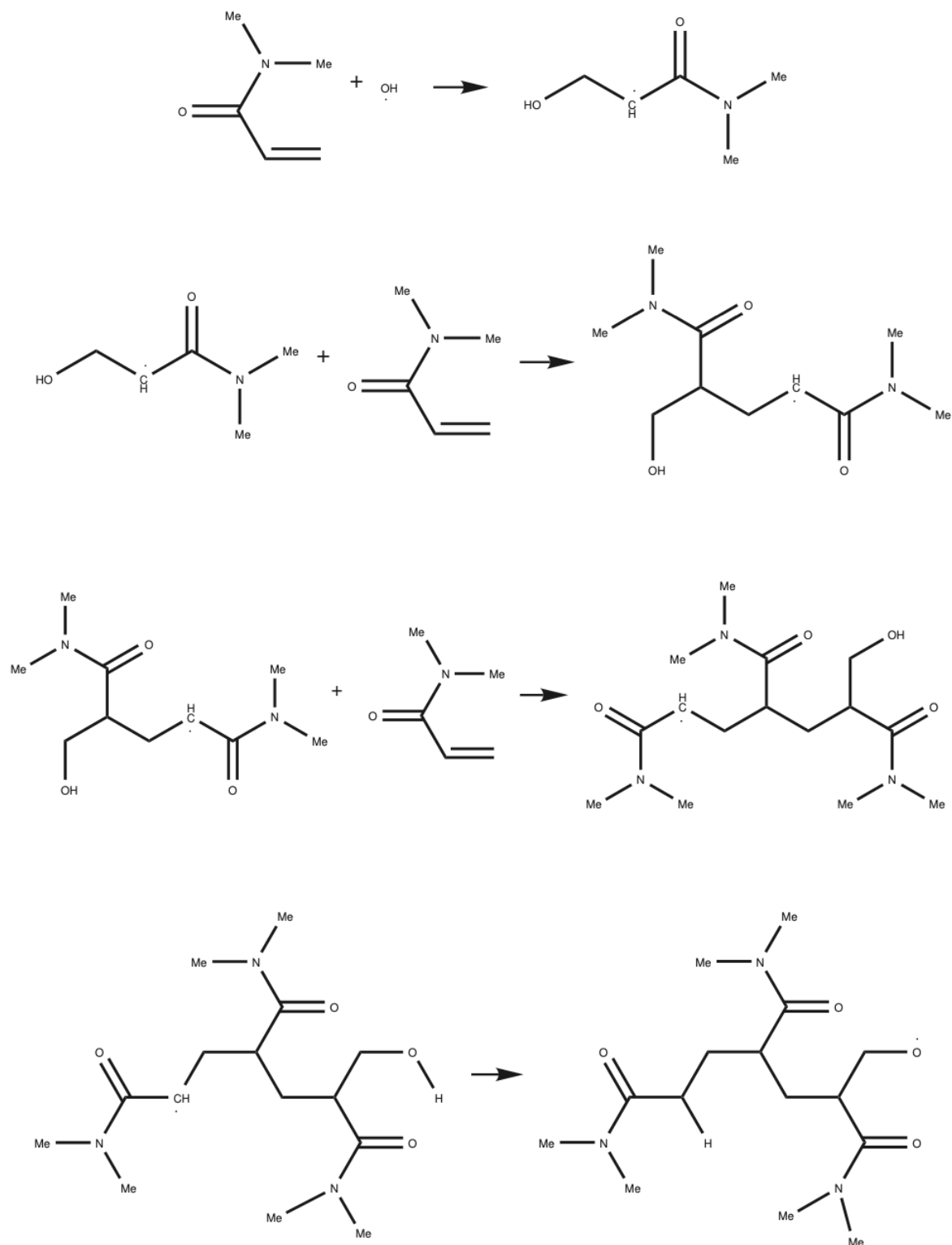


Figure 61: In one case, the hydroxyl radical initiates the reaction by attacking the double bond, leading to its breakage and the generation of a radical monomer. Subsequently, this radical monomer engages in polymerization with other monomers, extending the chain growth, and even progressing to involve three monomers. This illustration underscores the repeatability and reproducibility of polymerization within the system. The final step shows that the radical within the structure may separate hydrogen (H) from the hydroxyl (OH) group, potentially leading to further reactions.

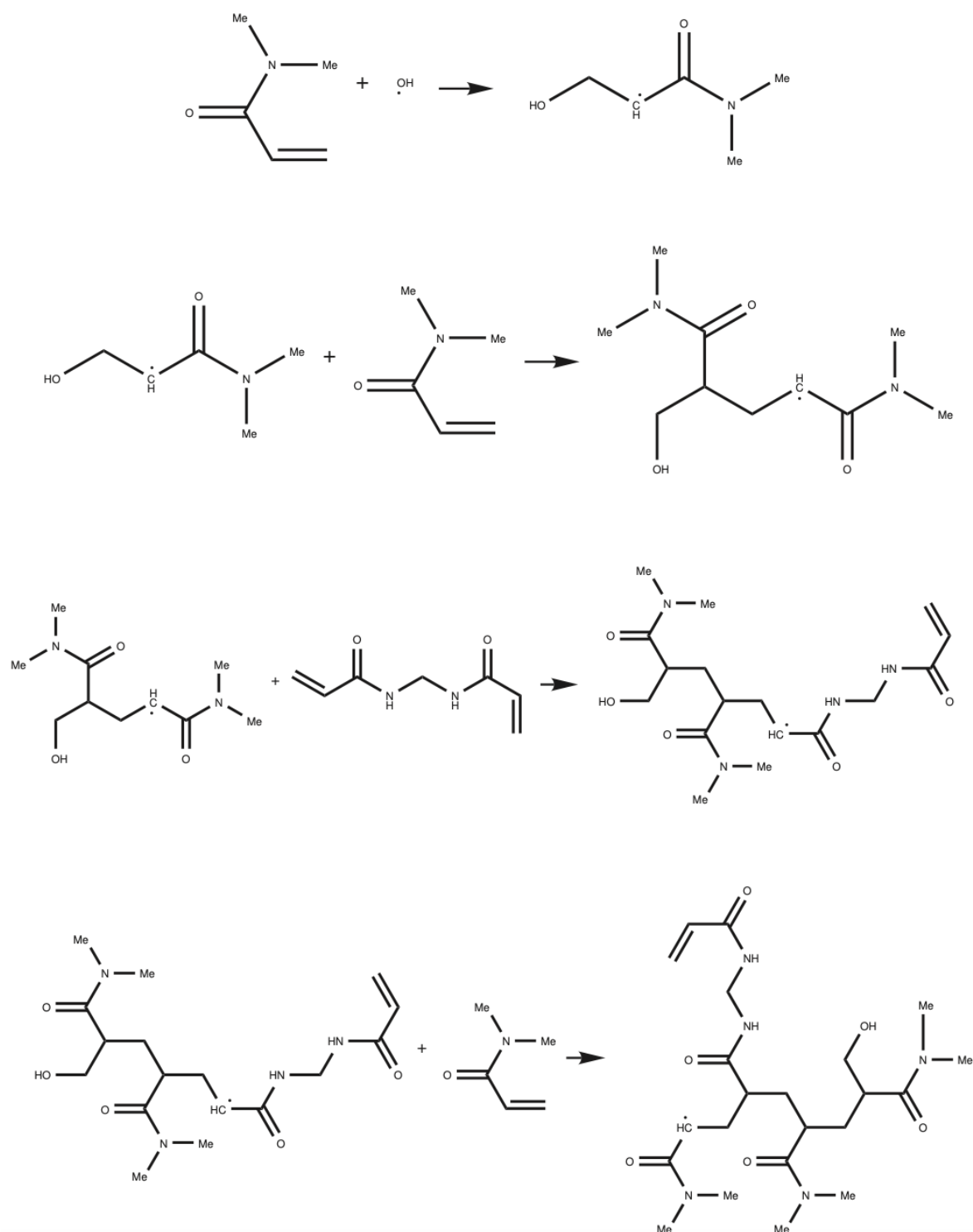


Figure 62: In an alternative mechanism, where the hydroxyl radical initiates the reaction by attacking the double bond of a monomer's double bond. Subsequently, polymerization occurs, with one monomer attaching head-to-tail with another. Additionally, the crosslinker is introduced into the reaction, connecting to the junction of the dimer. However, with the addition of another monomer, the chain growth continues, showcasing the system's flexibility of the system. Notably, the symmetry in the crosslinker's structure and the potential transfer of radicals contribute to the ability to connect to other chains in these plausible mechanisms.

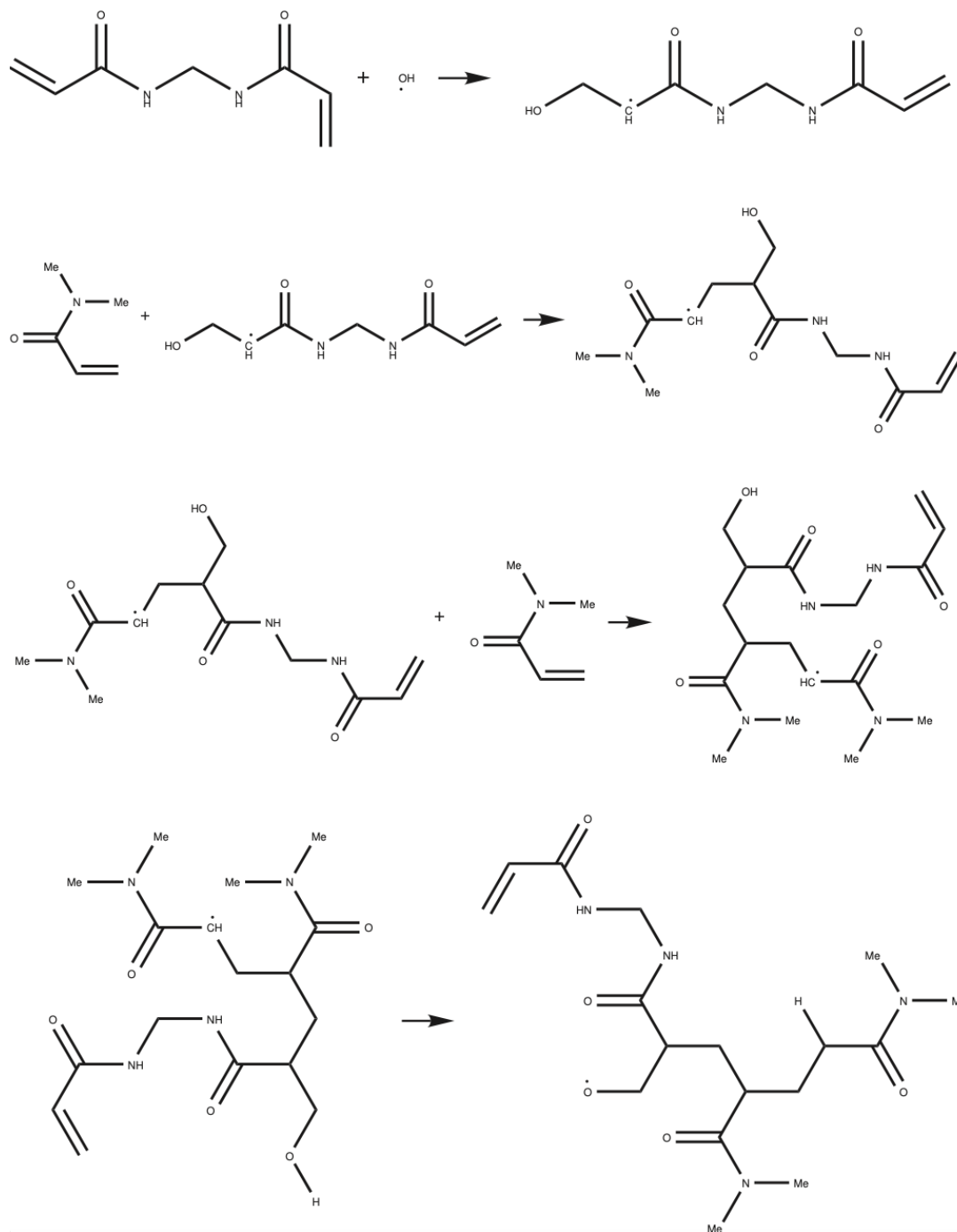


Figure 63: In this illustrative case the hydroxyl radical initiates the reaction by attacking the crosslinker, demonstrating the system's capacity for simultaneous initiation of reactions involving multiple components. Following the radical crosslinker, two monomers engage and connect, representing a polymerization process facilitated by a single crosslinker. This scenario underscores the system's versatility in accommodating diverse reaction pathways and mechanisms.

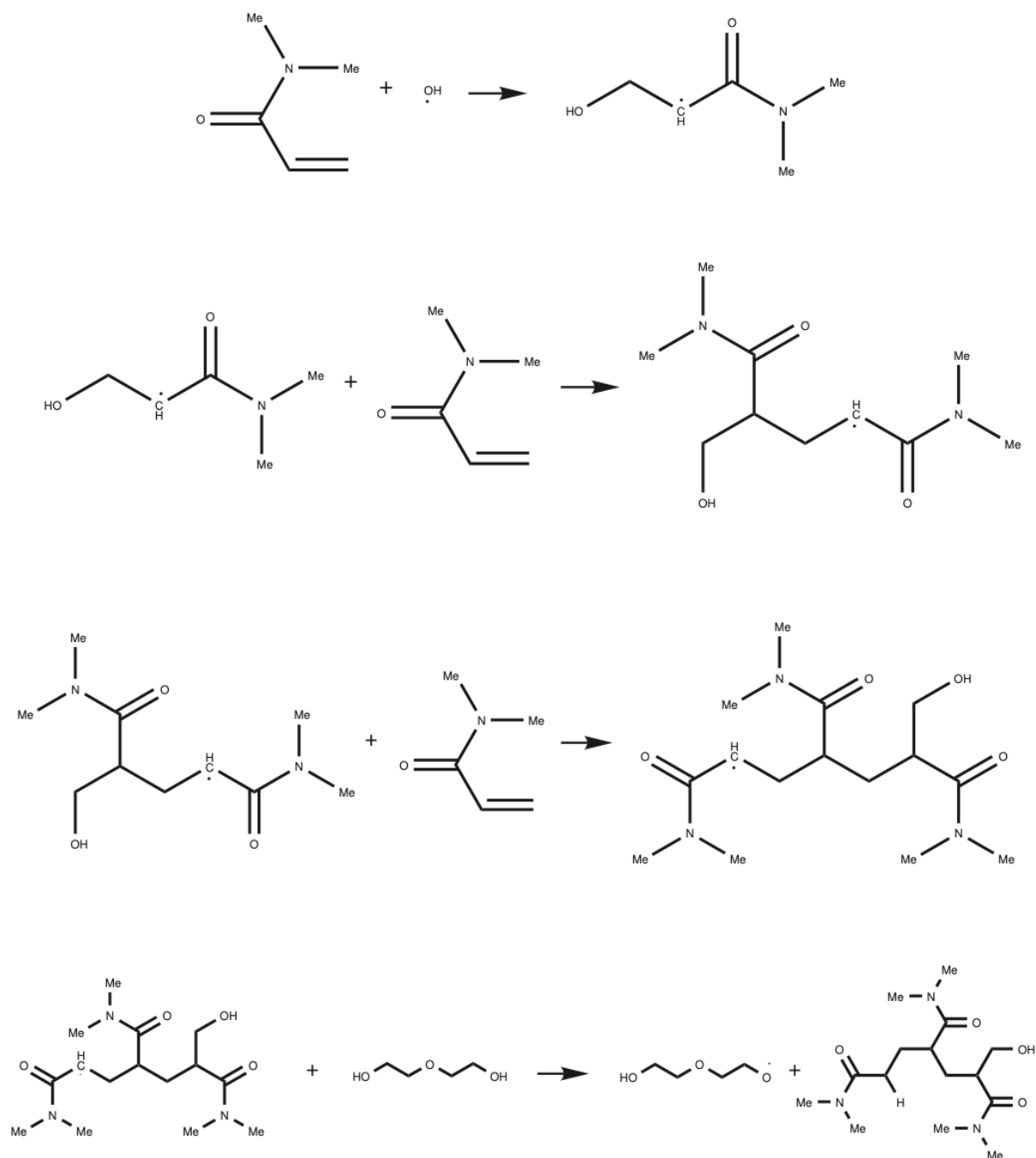


Figure 64: In this unique scenario, following the hydroxyl radical's attack on the monomer and the subsequent formation of a dimer and trimer, a backbiting mechanism occurs. In this instance, the structure may capture a hydrogen atom (H) from PEO, suggesting a possible pathway for incorporating PEO into the final structures. This illustration raises the possibility that the system's reaction products include PEO, highlighting its potential role in shaping the final structures.

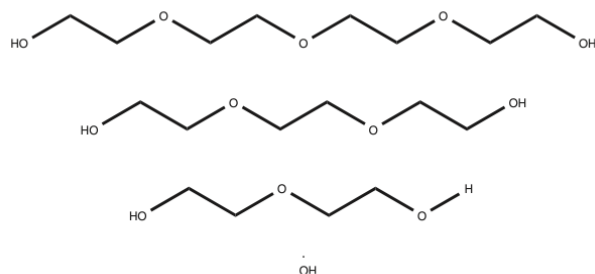


Figure 65: Setup for Run Data 8, where the hydroxyl radical initiates the reactions. This run involves the presence of three Polyethylene Oxide (PEO) chains of different lengths: short, medium, and long. Including various PEO chain lengths allows for the exploration of how different chain lengths may impact the reaction pathways and final structures within the system.

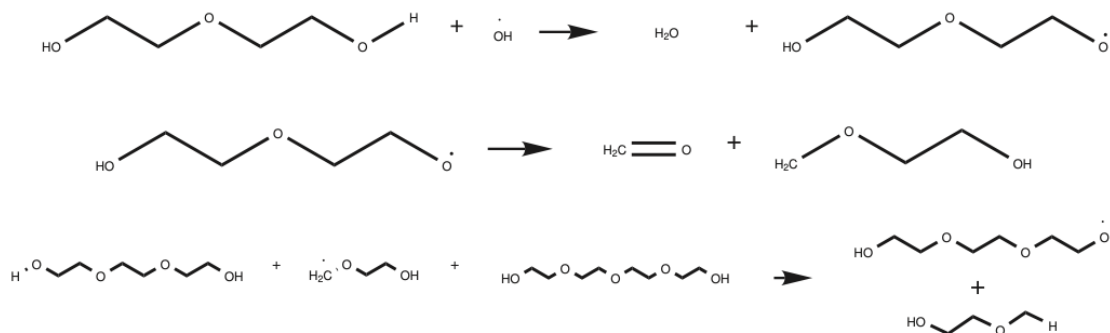


Figure 66: This chain session involves a medium-length Polyethylene Oxide (PEO) chain. During this session, a CH<sub>2</sub> group with a double bond and oxygen (O) is formed, suggesting the potential for chain disruption and session occurrence across chains within a given range. This outcome hints at the system's potential for intricate reactivity and structural diversity.

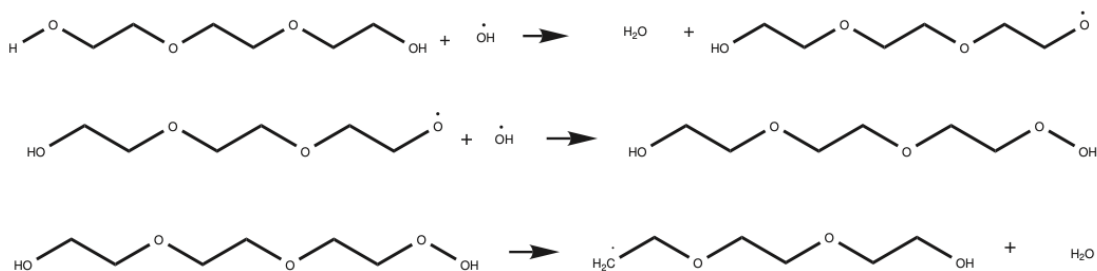


Figure 67: This chain session involves a medium-length polyethylene oxide (PEO) chain, accompanied by the release of water molecules. This illustration highlights the recurrent nature of chain sessions, which occur across various cases within the system.

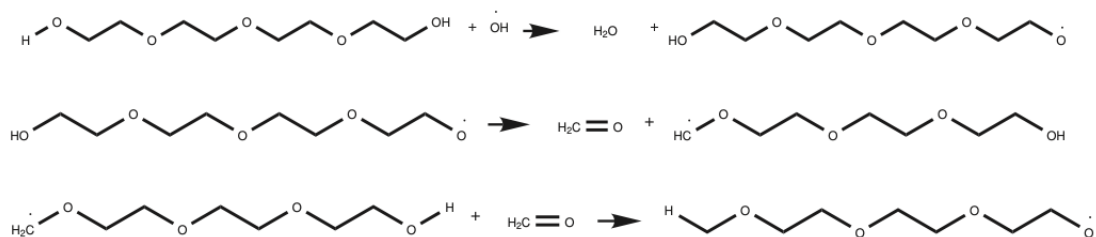


Figure 68: In this scenario, radicals are positioned on carbon atoms rather than oxygen. In a 3-depth simulation, each step of the depicted mechanism can occur individually. However, the noteworthy observation is that, if other components are simultaneously accessible in the system, chain sessions may be triggered, potentially leading to the incorporation of polyethylene oxide (PEO) or other components. This emphasizes the dynamic nature of the system's reactions and the potential for diverse outcomes.

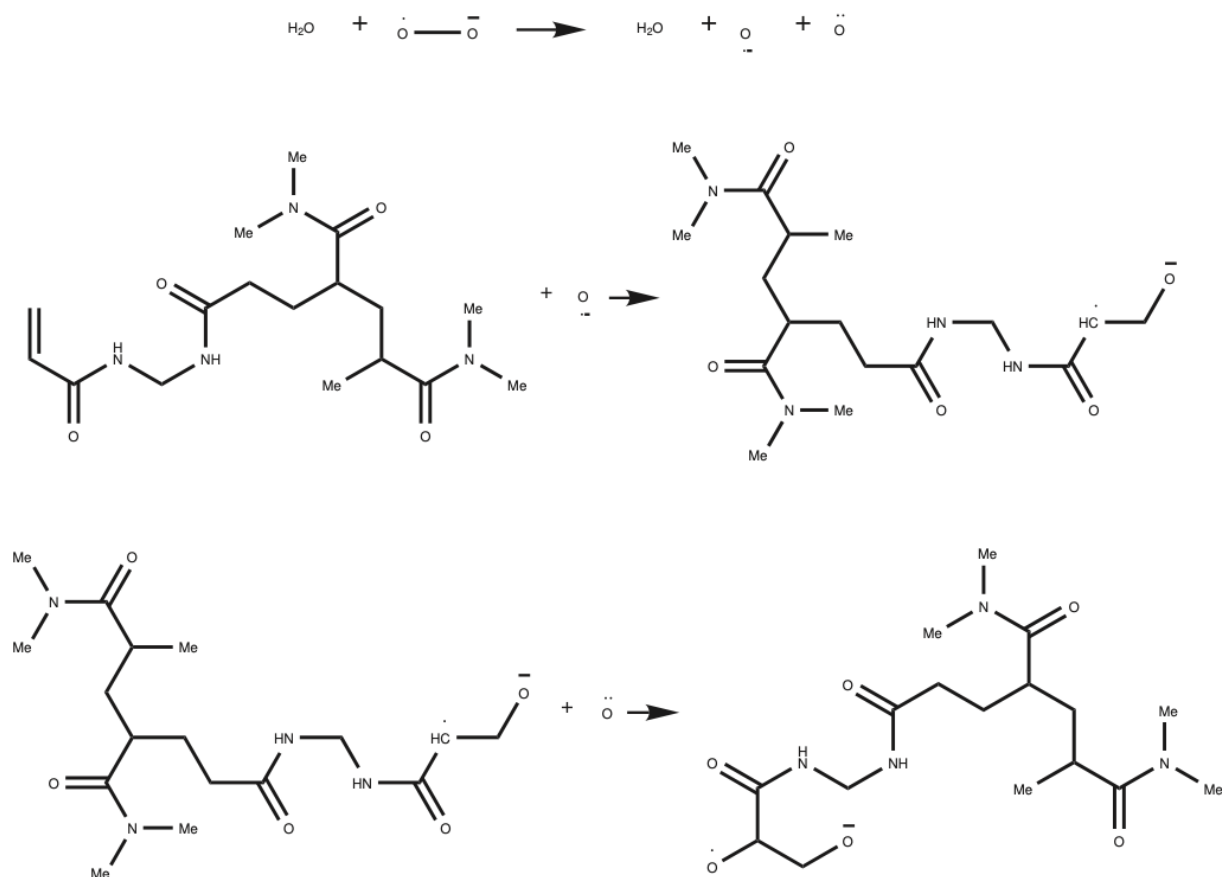


Figure 69: In this scenario a superoxide anion interacts with water, generating free oxygen and an oxygen radical anion. The oxygen radical anion then attacks the head of a monomer within the structure. Notably, in this illustration, other components or monomers were not added, but the oxygen radical anion's interaction with free oxygen showcases the system's capacity for reactivating the final structure. This observation underscores the repeatability and reactivation potential of the system's main chain.



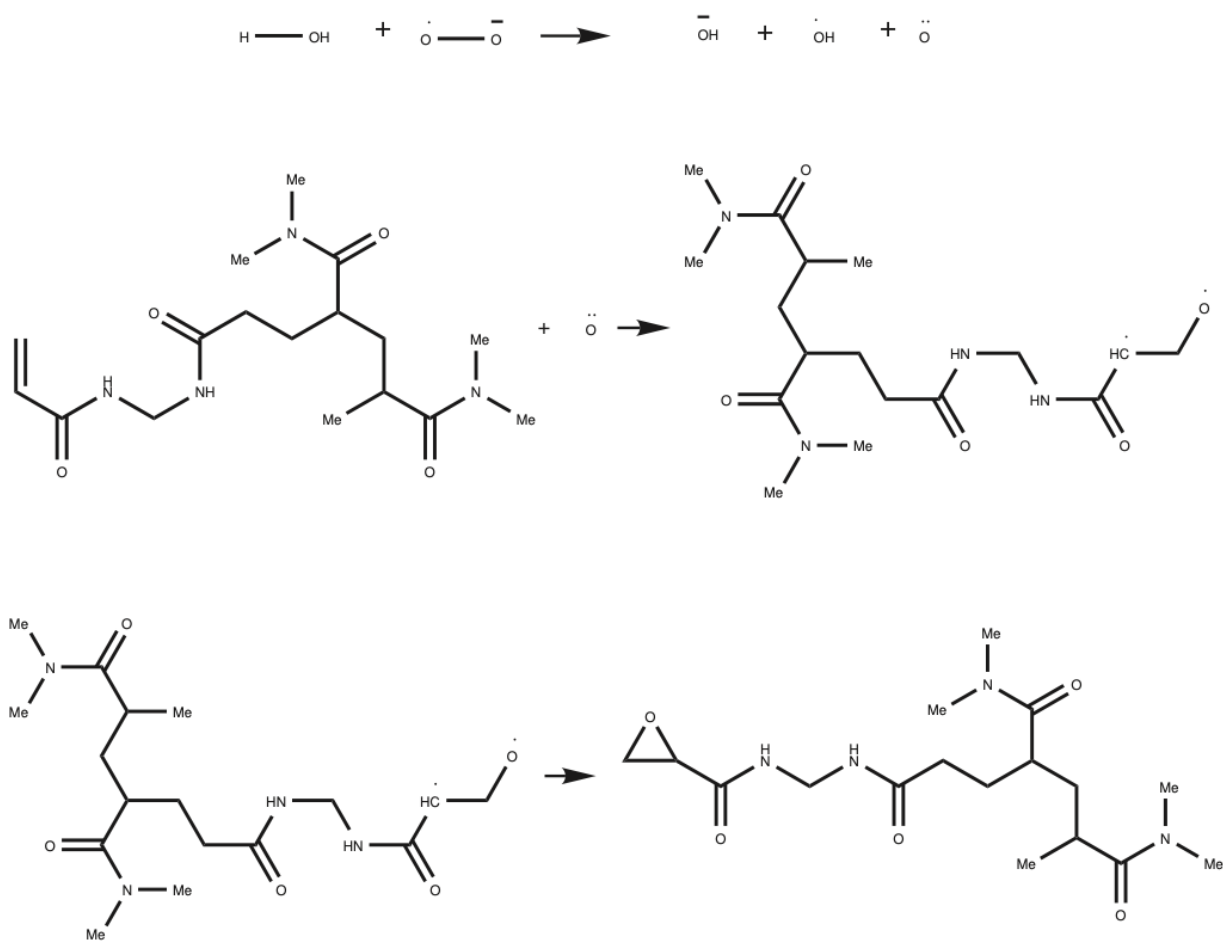


Figure 70: In this scenario free oxygen, rather than a superoxide anion, attacks. In the final step, due to the absence of additional components, a 3-point ring structure forms. This observation emphasizes that when other components, such as monomers and crosslinkers (which are typically present in real-world systems), are available in the system, the chain growth can continue beyond this point.

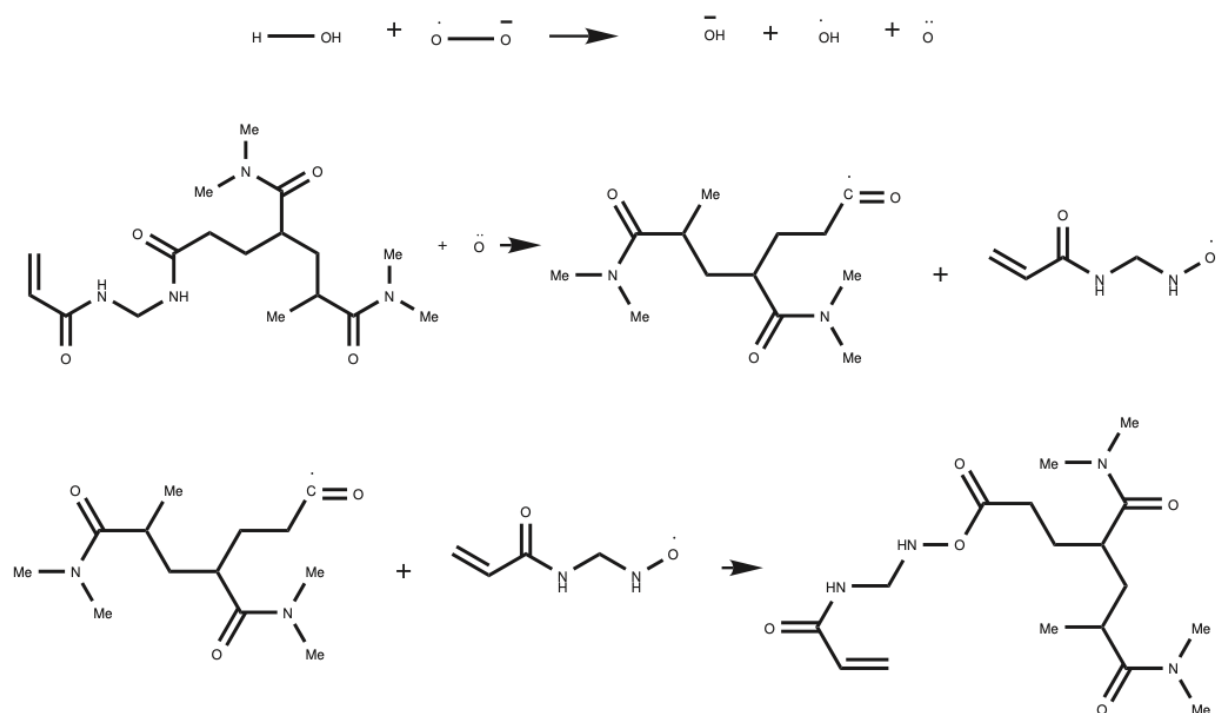


Figure 71: The interaction and reaction between water and a superoxide anion produces a hydroxyl radical, hydroxyl anion, free oxygen, and free oxygen's interaction with the final structure. This interaction leads to the breaking and rejoining of the crosslinker at the carbon double bond, forming ester groups. This mechanism highlights one of the processes that could potentially contribute to the formation of ester groups within the repeated crosslink structure. The presence of ester groups can be significant for the system's overall structure and properties and is reported in the FTIR results.

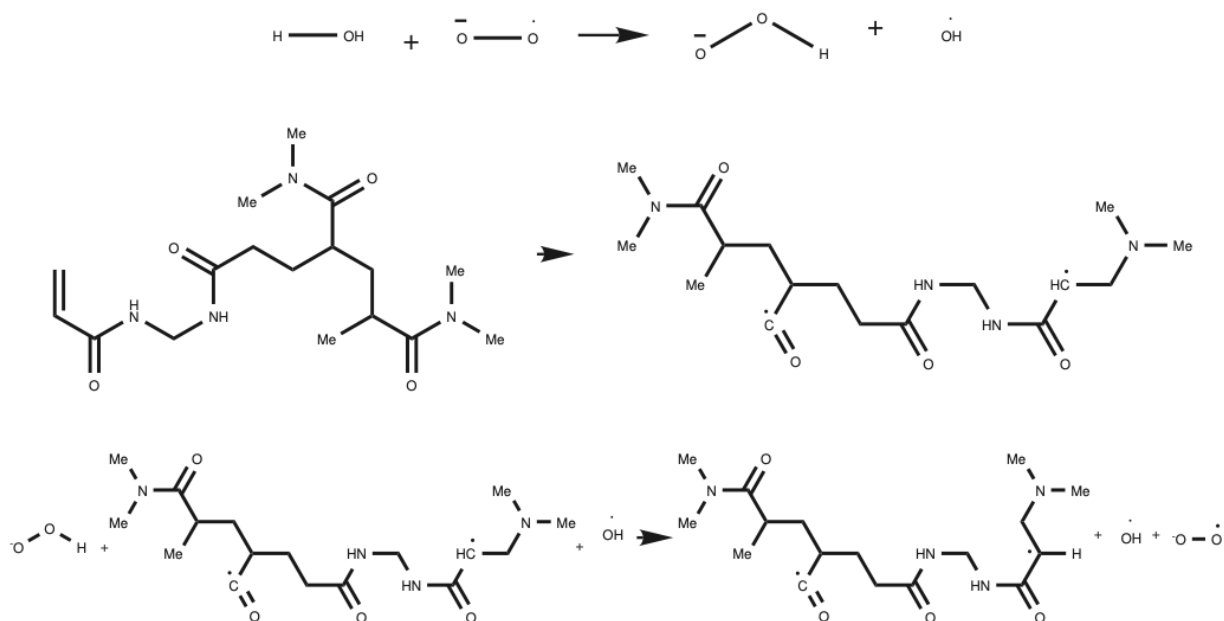


Figure 72: In an expected occurrence, the reaction between a superoxide anion and water generates OOH-. Of particular significance is the final structure's reaction in the presence of OOH-, which results in a rearrangement leading to the production of a radical c=O. This transformation suggests that the structure becomes poised for subsequent reactions. This observation raises the intriguing possibility that this point serves as a potential site for PEO, which has undergone chain scission and is ready for reaction, to interact with the newly formed radical c=O. Such interactions may lead to the formation of ester groups within the structure, highlighting their role in the system's reactivity and potential for further modifications[31].

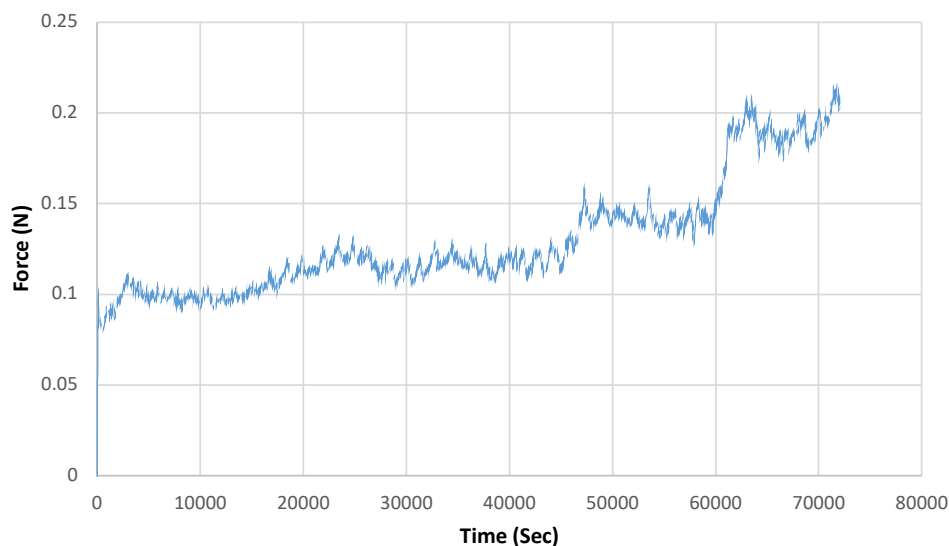


Figure 73: Relaxation experiment overnight for 20 hours at 150 mm extension with a gradual increase in stress under predetermined strain. The specimen is kept in that stretched position for a prolonged time. In typical materials, over time, a smaller amount of load is required to maintain that strain, also known as stress decay. Stress relaxation causes stress decay. In contrast to typical solids, stress flourishes as the sample dries up and more chains align in an axial direction.

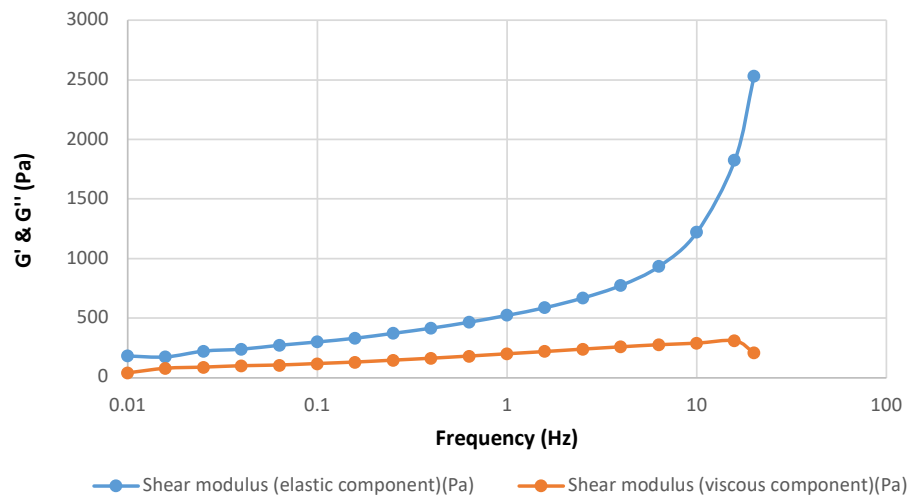


Figure 74: Dynamic mechanical analysis performed in parallel plates. Rheometer in shear mode and frequency sweep.

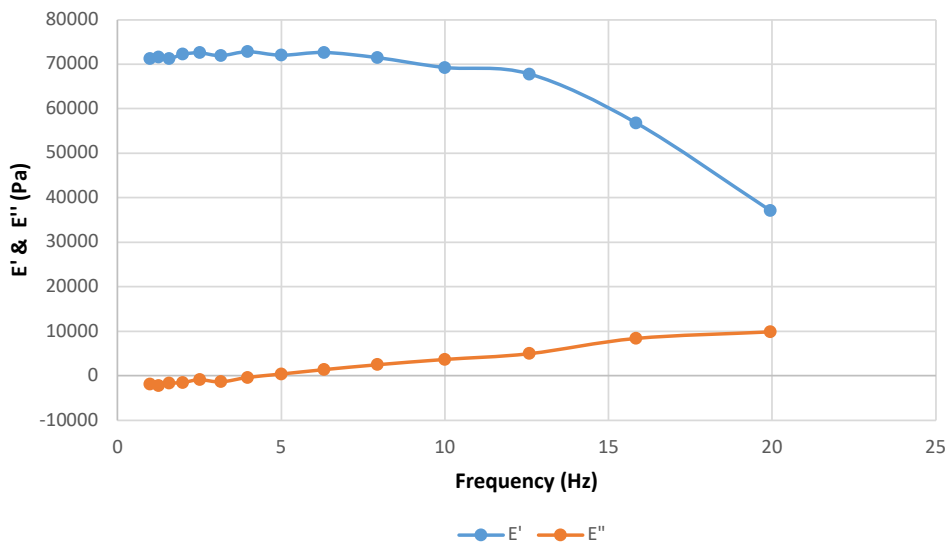


Figure 75: Dynamic mechanical analysis performed in the tensile fixture or axial geometry at frequency sweep mode.